



# Theory of polyelectrolytes in solutions and at surfaces

Andrey V. Dobrynin<sup>a,\*</sup>, Michael Rubinstein<sup>b,\*</sup>

<sup>a</sup>*Polymer Program, Institute of Materials Science and Department of Physics, University of Connecticut, Storrs, CT 06269-3136, USA*

<sup>b</sup>*Department of Chemistry, University of North Carolina, Chapel Hill, NC 27599-3290, USA*

Received 21 February 2005; received in revised form 7 July 2005; accepted 11 July 2005

Available online 8 September 2005

This review is dedicated to the memory of our dear friend, Claudine E. Williams, who made a significant contribution to our understanding of polyelectrolytes.

## Abstract

Polyelectrolytes are polymers carrying either positively or negatively charged ionizable groups. The properties of these polymers in solutions and at charged surfaces depend on the fraction of dissociated ionic groups, solvent quality for polymer backbone, solution dielectric constant, salt concentration, and polymer–substrate interactions. In this review, we summarize the current development of theoretical models describing properties of polyelectrolyte solutions and adsorption of charged polymers at surfaces and interfaces. We discuss in detail the conformational properties of polyelectrolyte chains in dilute and semidilute solutions, the phenomenon of counterion condensation, the necklace structure of polyelectrolytes in poor solvent conditions for polymer backbone, the dynamics of polyelectrolyte solutions, the surface overcharging by adsorbed polyelectrolytes and its implication for assembled polyelectrolyte multilayers.

© 2005 Elsevier Ltd. All rights reserved.

*Keywords:* Polyelectrolytes; Ion-containing polymers; Counterions; Distribution of counterions; Condensation of counterions; Hydrophobic polyelectrolytes; Polyelectrolyte solutions; Dynamics of polyelectrolytes; Rheology of polyelectrolytes; Adsorption of charged polymers

## Contents

1. What are polyelectrolytes? . . . . .	1050
2. Polyelectrolytes in dilute solutions . . . . .	1053
2.1. Flory theory and scaling model of a polyelectrolyte chain . . . . .	1053
2.1.1. Flory theory . . . . .	1053
2.1.2. Scaling model . . . . .	1055
2.2. Non-uniform stretching of polyelectrolyte chains . . . . .	1055

\* Corresponding authors. Tel.: +1 860 486 9061; fax: +1 860 486 4745 (A.V. Dobrynin), Tel.: +1 919 962 3544; fax: +1 919 843 3698 (M. Rubinstein).

*E-mail addresses:* [avd@ims.uconn.edu](mailto:avd@ims.uconn.edu) (A.V. Dobrynin), [mr@unc.edu](mailto:mr@unc.edu) (M. Rubinstein).

2.3.	Polyelectrolyte chain in a poor solvent for polymer backbone	1058
2.4.	Polyelectrolyte chains at finite concentrations and counterion condensation	1063
2.4.1.	Two-state model of counterion condensation	1064
2.4.2.	Counterion distribution and osmotic pressure in dilute polyelectrolyte solutions.	1065
2.4.3.	Ion-binding and ion localization models for counterion condensation	1069
2.4.4.	Effect of counterion condensation on chain size and chain conformation	1071
2.5.	Effects of added salt on chain conformations and electrostatic persistence length	1072
3.	Semidilute polyelectrolyte solutions	1075
3.1.	Overlap concentration	1075
3.2.	Scaling model of semidilute polyelectrolyte solutions	1076
3.2.1.	Correlation length	1076
3.2.2.	Persistence length and chain size	1078
3.2.3.	Semidilute polyelectrolyte solutions with added salt	1080
3.2.4.	Osmotic pressure and scattering function	1082
3.2.5.	Dynamics of polyelectrolyte solutions	1085
3.2.6.	Semidilute polyelectrolyte solutions in a poor solvent for polymer backbone	1088
3.3.	Phase separation in polyelectrolyte solutions	1091
3.3.1.	Mean-field approach	1091
3.3.2.	Microphase separation	1093
3.3.3.	Necklace model of phase separation	1094
3.4.	PRISM and self-consistent field methods	1095
4.	Adsorption of polyelectrolytes	1097
4.1.	A brief historic overview of theoretical models of polyelectrolyte adsorption	1097
4.2.	Why self-consistent field method based on Poisson–Boltzmann approach does not work for polyelectrolyte adsorption	1099
4.3.	Two-dimensional adsorbed layers	1100
4.3.1.	Dilute regime	1100
4.3.2.	Semidilute adsorbed layers	1102
4.4.	Three-dimensional self-similar adsorbed layers	1103
4.5.	Effect of the image forces and short-range interactions on polyelectrolyte adsorption	1105
4.6.	Comparison with experiments	1108
5.	Conclusions and outlook	1110
	Acknowledgements	1112
	References	1112

## 1. What are polyelectrolytes?

Polyelectrolytes are polymers with ionizable groups [1–7]. In polar solvents such as water, these groups can dissociate, leaving charges on polymer chains and releasing counterions in solution. Examples of polyelectrolytes include polystyrene sulfonate, polyacrylic and polymethacrylic acids and their salts, DNA and other polyacids and polybases (see Fig. 1).

Electrostatic interactions between charges lead to the rich behavior of polyelectrolyte solutions

qualitatively different from those of uncharged polymers [8–10]. For example:

- (1) The crossover from dilute to semidilute solution regime occurs at much lower polymer concentrations than that in solutions of neutral chains.
- (2) There is a well-pronounced peak in the scattering function of the homogeneous polyelectrolyte solutions. The magnitude of the wave vector corresponding to this peak increases with concentration as  $c^{1/2}$ . There is no such peak in solutions of neutral polymers.

**Nomenclature**

$B$	second virial coefficient	$n_b$	number of beads on a necklace
$b$	bond length	$R_{\text{glob}}$	size of a polymer globule
$C$	third virial coefficient	$R_e$	end-to-end distance
$c$	polymer concentration	$R_e^{\text{blob}}$	end-to-end distance of a polyelectrolyte chain from scaling approach
$c^*$	polymer overlap concentration	$R_e^{\text{F}}$	end-to-end distance of a polyelectrolyte chain from Flory-like minimization of the chain free energy
$c_{\text{Bead}}$	crossover concentration between string and bead controlled regimes	$r_0$	radius of a rod-like polyion
$c_b$	polymer concentration for overlap of electrostatic blobs	$r_D$	Debye screening length
$c_e$	entanglement concentration	$T$	absolute temperature
$c_s$	salt concentration	$U$	interaction parameter defined as the ratio of the Bjerrum length $l_B$ to the bond size $b$
$e$	elementary charge	$\beta$	fraction of condensed counterions
$D_b$	bead size in the necklace model of a polyelectrolyte chain in a poor solvent	$\Gamma$	polymer surface coverage
$D_e^0$	electrostatic blob size	$\gamma_0$	Oosawa–Manning counterion condensation parameter, $\gamma_0 = l_B/N/L$
$D_e^*$	electrostatic blob size for the effective fraction of charged monomers $f^*$	$\delta\sigma$	surface overcharging
$D_e(z)$	electrostatic blob size in non-uniformly stretched chain	$\varepsilon$	dielectric constant of a medium
$D_{\text{self}}$	chain self-diffusion coefficient	$\varepsilon_{\text{LJ}}$	interaction parameter of the Lennard–Jones potential
$F_{\text{conf}}(R)$	conformational part of the chain free energy	$\eta$	solution viscosity
$f$	fraction of charged monomers on polymer backbone	$\eta_{\text{sp}}$	specific viscosity
$f^*$	effective fraction of charged monomers	$\Theta$	theta temperature
$G$	plateau modulus	$\kappa$	inverse Debye screening length, $r_D = \kappa^{-1}$
$g_e^0$	number of monomers in an electrostatic blob	$\xi$	correlation length of a semidilute polymer solution
$g_{\text{intra}}(r)$	intrachain monomer–monomer correlation function	$\xi_T$	thermal blob size
$g_T$	number of monomers in a thermal blob	$\pi$	polymeric osmotic pressure
$q$	charge valence	$\sigma$	monomer diameter in Sections 2 and 3 and surface number charge density in Section 4
$k_B$	Boltzmann constant	$\sigma^*$	surface number charge density at which adsorbed polyelectrolyte chains begin to overlap
$L$	length of a rod-like polyion	$\sigma_e$	crossover surface number charge density between 2D and 3D adsorbed layer
$L_{\text{nec}}$	end-to-end distance of a necklace	$\tau = 1 - \Theta/T$	effective temperature
$l_B$	Bjerrum length	$\tau_{\text{Rouse}}$	chain relaxation time in an unentangled regime
$l_0$	length of a polymeric strand with $m_{\text{str}}$ monomers	$\tau_{\text{rep}}$	chain relaxation time in an entangled regime
$l_p^{\text{OSF}}$	Odijk–Skolnick–Fixman electrostatic persistence length	$\tau_{\xi}$	relaxation time of a correlation blob
$l_{\text{str}}$	string length between the centers of two neighboring beads	$\phi$	polymer volume fraction, $\phi = cv$
$m_b$	number of monomers in a bead	$\varphi(r)$	reduced electrostatic potential
$m_{\text{str}}$	number of monomers in a string	$\phi_{\text{osm}}$	osmotic coefficient
$N$	degree of polymerization		

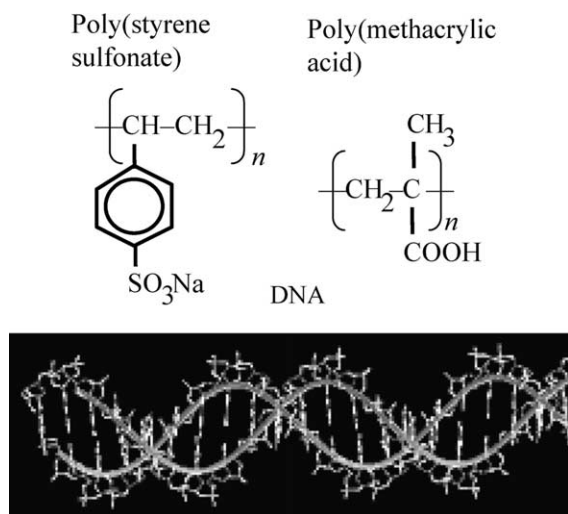


Fig. 1. Examples of polyelectrolytes.

- (3) The osmotic pressure of polyelectrolytes in salt-free solutions exceeds the osmotic pressure of neutral polymers at similar polymer concentrations by several orders of magnitude. It increases almost linearly with polymer concentration and is independent of the chain molecular weight in a wide range of polymer concentrations. This almost linear concentration dependence of the osmotic pressure together with its strong dependence on added salt demonstrates that osmotic pressure is mainly due to the counterion contribution.
- (4) The viscosity of polyelectrolyte solutions is proportional to the square root of polymer concentration  $\eta \sim c^{1/2}$  (Fuoss' law [11]), while for solutions of uncharged polymers at the same concentration the viscosity is proportional to polymer concentration. There is no concentration regime where reduced viscosity  $\eta/c$  of solutions of neutral polymers decreases with polymer concentration ( $\eta/c \sim c^{-1/2}$  for polyelectrolytes in the Fuoss regime).
- (5) Polyelectrolyte chains in semidilute regime follow unentangled dynamics in a much wider concentration range and the crossover to the entangled dynamics occurs further away from the chain overlap concentration than in solutions of uncharged polymers.

Polyelectrolyte chains at surfaces and interfaces represent an example of both two- and three-

dimensional polyelectrolyte solutions in which the local polymer concentration is controlled by interactions between adsorbing substrate and polyelectrolyte chains. As the surface charge density increases, the dilute solution of adsorbed chains transforms into a two-dimensional semidilute solution. If the surface charge density increases even further, the chains in the adsorbed layer form a concentrated polyelectrolyte solution with thickness increasing with surface charge density. The new and unusual phenomenon observed in the adsorbed layers is the surface overcharging (overcompensation of surface charge) by adsorbed polyelectrolyte chains. The amount of surface overcharging can be tuned by varying the solution ionic strength. The charge inversion plays a central role in the layer-by-layer deposition technique. This self-assembly method has been introduced for fabrication of the molecularly layered multicomposite films with a high degree of complexity (see for review [12,13] [14–17]). The film growth is achieved by alternating the deposition of polyanions and polycations from their aqueous solutions. The simplicity of the electrostatic assembly technique with practically no limitations on the shape of charge bearing species allows fabrication of multilayer films from synthetic polyelectrolytes, DNA, proteins, inorganic platelets, nanoparticles, and viruses.

Below we review modern theoretical approaches to polyelectrolyte solutions and to adsorption of charged polymers that ignore the atomistic details of solvent and polymers. In these theories, polyelectrolyte chains are modeled by charged bead-spring chains with beads representing groups of chemical monomers. The solvent molecules are replaced by a continuum with the same macroscopic physical properties such as dielectric constant  $\epsilon$  and solvent viscosity  $\eta_0$ . The counterions and salt ions are treated either explicitly or as an effective background leading to screening of the electrostatic interactions between ionized groups on the polymer backbone. Fig. 2 shows an example of such representation of polystyrene sulfonate in water by a chain consisting of charged beads (we will call them monomers) with counterions in a dielectric continuum. In the following sections we will show how this simplified model can be used to describe properties of charged polymers in solutions and at interfaces.

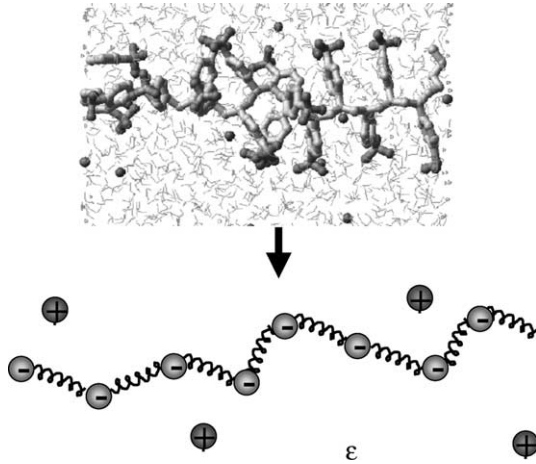


Fig. 2. Illustration of the mapping procedure of sodium polystyrene sulfonate (NaPSS) in water. The repeat units of NaPSS are replaced by spherical monomers (green circles) connected by springs and the solvent molecules are represented by a continuum with dielectric constant  $\epsilon$ . Counterions are represented by spherical beads (red circles) (For interpretation of the reference to colour in this legend, the reader is referred to the web version of this article.).

## 2. Polyelectrolytes in dilute solutions

In dilute solutions, the intrachain interactions dominate over the interchain ones. Thus, one can effectively consider a single polyelectrolyte chain with counterions surrounding it in a large unit cell with size equal to the distance between chains. Consider a polyelectrolyte chain with degree of polymerization  $N$  and with fraction  $f$  of charged groups on the polymer backbone in a medium with dielectric constant  $\epsilon$ . The potential energy of the polyelectrolyte chain  $U(\{\mathbf{r}_i\})$  with monomers located at positions  $\mathbf{r}_1, \mathbf{r}_2, \mathbf{r}_3, \dots, \mathbf{r}_N$  and carrying charges  $eq_1, eq_2, \dots, eq_N$  is

$$\begin{aligned} \frac{U(\{\mathbf{r}_i\})}{k_B T} &= \frac{3}{2b^2} \sum_{i=1}^{N-1} (\mathbf{r}_{i+1} - \mathbf{r}_i)^2 \\ &+ \sum_{i=1}^N \sum_{j<i} \frac{l_B q_i q_j}{|\mathbf{r}_i - \mathbf{r}_j|} \exp(-\kappa |\mathbf{r}_i - \mathbf{r}_j|) \\ &+ \frac{U_{sh}(|\mathbf{r}_i - \mathbf{r}_j|)}{k_B T} \end{aligned} \quad (2.1)$$

where the first term on the right-hand side of Eq (2.1) describes the entropic elasticity of harmonic bonds

with length  $b$  connecting monomers into a polymer chain, the second-term is the screened Coulomb (Yukawa) interaction between charged monomers,  $k_B$  is the Boltzmann constant,  $T$  is the absolute temperature, and  $l_B$  is the Bjerrum length

$$l_B = e^2 / (\epsilon k_B T), \quad (2.2)$$

the distance at which the electrostatic interaction between two elementary charges  $e$  in the medium with dielectric constant  $\epsilon$  is equal to the thermal energy  $k_B T$ . The electrostatic interactions between counterions and salt ions are not explicitly included in the chain potential energy; instead, their effect is taken into account through the concentration dependence of the Debye screening length  $r_D = \kappa^{-1}$

$$r_D^{-2} = \kappa^2 = 4\pi l_B \sum_s c_s q_s^2 \quad (2.3)$$

where  $c_s$  is the concentration of small ions of type  $s$  and  $q_s$  is their valence. Electrostatic interactions are exponentially screened on the length scales larger than the Debye screening length  $r_D$ . In a dilute salt-free solution, the concentration of counterions is very low (the Debye screening length is larger than the chain size) and therefore ionized groups on a chain interact with each other through the unscreened Coulomb potential.

The last-term on the right-hand side of Eq. (2.1),  $U_{sh}(r)$ , represents the short-range interactions between monomers, which are typically described in computer simulations [18,19] by the Lennard–Jones 6–12 potential

$$U_{LJ}(r) = 4\epsilon_{LJ} \left( \left( \frac{\sigma}{r} \right)^{12} - \left( \frac{\sigma}{r} \right)^6 \right) \quad (2.4)$$

where  $\epsilon_{LJ}$  is the interaction parameter and  $\sigma$  is the monomer diameter.

### 2.1. Flory theory and scaling model of a polyelectrolyte chain

#### 2.1.1. Flory theory

The Flory-like description of a polyelectrolyte chain without short-range interactions was first introduced over 50 years ago by Kuhn et al. [20]. A polyion is described in this model as a random coil with the restriction that the length  $R_e$  of its end-to-end

vector minimizes the sum of the configurational and electrostatic free energies. In this approach, the two terms associated with the chain connectivity and interactions are evaluated separately. The conformational part of the chain free energy is estimated neglecting the interactions between monomers

$$F_{\text{conf}}(R_e) \approx k_B T \frac{R_e^2}{b^2 N} \quad (2.5)$$

(Here and below we will present scaling analysis neglecting all numerical coefficients.)

The interaction part of the chain free energy is evaluated by neglecting the connectivity of the polymer chain and by assuming that monomers are uniformly distributed within the chain volume  $V_{\text{ch}}$ . Let us assume that electrostatic interactions lead to the unidirectional elongation of the chain, for instance along  $z$ -axis, while its size stays unperturbed in the directions perpendicular to the elongation axis. Thus, the polyelectrolyte chain has the shape of an ellipsoid with the longitudinal size equal to  $R_e$  and with the transverse size equal to that of an ideal chain  $bN^{1/2}$  (see Fig. 3).

The electrostatic energy of the uniformly charged ellipsoid [21] with the net charge  $efN$ , where  $f$  is the fraction of charged monomers, is proportional to

$$\frac{F_{\text{electr}}(R_e)}{k_B T} \approx \frac{l_B (fN)^2}{R_e} \ln \left( \frac{R_e}{bN^{1/2}} \right) \quad (2.6)$$

Combining conformational and interaction parts of the free energy (Eqs. (2.5) and (2.6)), we arrive at the free energy of a polyelectrolyte chain with a given value of the end-to-end vector  $R_e$  [20]

$$\frac{F_{\text{Flory}}(R_e)}{k_B T} \approx \frac{R_e^2}{b^2 N} + \frac{l_B (fN)^2}{R_e} \ln \left( \frac{R_e}{bN^{1/2}} \right) \quad (2.7)$$

The analysis of Eq. (2.7) shows that the conformational part of the chain free energy (the first-term on

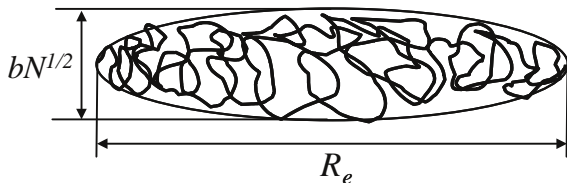


Fig. 3. Schematic representation of a polyelectrolyte chain in an elongated conformation.

the right-hand side of Eq. (2.7)) increases as the value of  $R_e$  increases. This increase in the conformational part of the chain free energy is associated with its entropic nature. The number of available conformations decreases with increasing end-to-end distance leading to a decrease in the chain conformational entropy and an increase in the conformational part of the free energy. On the contrary, the electrostatic part of the chain free energy (the second-term on the right-hand side of Eq. (2.7)) decreases with increasing chain size  $R_e$ . Charged monomers move further apart with increasing chain size leading to weaker electrostatic repulsion between them. Thus, the optimal chain size corresponds to the minimum of the chain free energy as a function of end-to-end distance  $R_e$ . Taking the derivative of Eq. (2.7) with respect to  $R_e$  and solving iteratively the resultant non-linear equation, we obtain the following expression for the chain size

$$R_e^F \approx bNu^{1/3} f^{2/3} [\ln(eN(uf^2)^{2/3})]^{1/3} \quad (2.8)$$

where  $u$  is the interaction parameter—the ratio of the Bjerrum length  $l_B$  (Eq. (2.2)) to the bond size  $b$

$$u = l_B/b \quad (2.9)$$

The chain size grows faster than linear as  $N[\ln(N)]^{1/3}$  with the degree of polymerisation. The onset of elongation of a polyelectrolyte chain is at the value of its electrostatic energy (see Eq. (2.6)) on the order of the thermal energy  $k_B T$

$$\frac{l_B (fN)^2}{bN^{1/2}} \approx 1 \quad (2.10)$$

This happens when the number of charged monomers on the chain  $fN$  is on the order of  $u^{-1/2} N^{1/4}$ . At stronger electrostatic interactions, the chain size monotonically increases with increasing fraction of charged monomers  $f$  on the polymer backbone. However, one has to keep in mind that Eq. (2.8) is only valid in the range of parameters for which the chain size  $R_e^F$  is smaller than the size of the fully stretched chain  $bN$ . This requirement leads to the upper bound on the chain degree of polymerization  $N < u^{-2/3} f^{-4/3} \exp(u^{-1/3} f^{-2/3})$ . For longer chains, quadratic dependence of the conformational part of the chain free energy on the end-to-end distance (the first term in Eq. (2.7)) is no longer valid and one has to take into account the non-linear effects in chain

elasticity [10,22]. In this case, the chain’s end-to-end distance  $R_e^F$  is proportional to the degree of polymerization  $N$ . For example, for polyelectrolyte chains with interaction parameter  $u \approx 2$  and fraction of charged monomers  $f=0.2$  the crossover degree of polymerization is about 50 Kuhn monomers.

The fluctuations of chain size near the optimal value  $R_e^F$  are on the order of  $bN^{1/2}$ . This can be shown by expanding Eq. (2.7) for the Flory free energy of a polyelectrolyte chain in the power series of  $\delta R_e = R_e - R_e^F$  up to the quadratic term. The energy fluctuations around the minimum are

$$\Delta F_{\text{Flory}}(\delta R_e) \approx k_B T \frac{\delta R_e^2}{b^2 N} \quad (2.11)$$

Typical energy fluctuations are on the order of the thermal energy  $k_B T$ , which leads to the typical value of the mean-square average fluctuations  $\langle \delta R_e^2 \rangle$  in the chain size to be on the order of  $b^2 N$ . The fluctuations of the chain size are small in comparison to the optimal chain size  $R_e^F$  above the chain deformation threshold and can be neglected when  $fN \gg u^{-1/2} N^{1/4}$ .

### 2.1.2. Scaling model

The scaling approach to the polyelectrolyte chain conformations in dilute solutions is based on the assumption of the separation of different length scales and the concept of an electrostatic blob [9,23–25]. The conformations of the chain inside the electrostatic blob are unperturbed by the electrostatic interactions. For a  $\Theta$ -solvent for uncharged polymer backbone, the relation between the blob size and the number of monomers in it is expected to be  $D_e^0 \approx b\sqrt{g_e^0}$ . (The good solvent conditions for polymer backbone can be taken into account by changing the relation between the blob size and the number of monomers in it to that for a swollen section of a chain,  $D_e^0 \approx b(g_e^0)^{3/5}$ , (see for details [9, 23–25])). The energy of the electrostatic interactions between all charged monomers inside a blob is on the order of the thermal energy  $k_B T$

$$\frac{l_B(fg_e^0)^2}{D_e^0} \approx uf^2(g_e^0)^{3/2} \approx 1 \quad (2.12)$$

(Note the similarity between Eq. (2.12) for the electrostatic blob and Eq. (2.10) for the onset of electrostatic effects of the whole chain.) Eq. (2.12)

leads to the following relations between the number of monomers in a blob  $g_e^0$ , its size  $D_e^0$  and the fraction of charged monomers  $f$

$$g_e^0 \approx (uf^2)^{-2/3} \quad (2.13a)$$

$$D_e^0 \approx b(uf^2)^{-1/3} \quad (2.13b)$$

Electrostatic interactions at the length scales larger than the blob size lead to the elongation of the polyelectrolyte chain into an array of blobs. The size of the polyelectrolyte chain is estimated as the number of blobs per chain  $N/g_e^0$  times the blob size  $D_e^0$

$$R_e^{\text{blob}} \approx \frac{N}{g_e^0} D_e^0 \approx bN(uf^2)^{1/3} \quad (2.14)$$

The difference between expressions in Eqs. (2.14) and (2.8) appears to be in the logarithmic term. The origin of this difference lies in the assumption of linear additivity of the electrostatic energy adopted in the scaling approach—all electrostatic blobs were assumed to have the same size independently of their location along the polymer backbone. The blobs in the middle of the chain interact with the rest of the chain stronger than blobs at the chain ends. This additional contribution from larger length scales leading to the logarithmic correction is discussed in the next section.

### 2.2. Non-uniform stretching of polyelectrolyte chains

The main contribution to the free energy of a polyelectrolyte in the case of strong deformation with small fluctuation corrections comes from the chain conformation that minimizes its potential energy  $U(\{\mathbf{r}_i\})$  given by Eq. (2.1). Let us select the  $z$ -axis of our coordinate system along the chain’s end-to-end

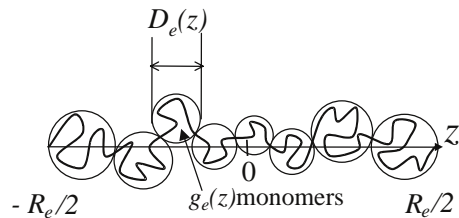


Fig. 4. Schematic sketch of a non-uniformly stretched polyelectrolyte chain in a dilute salt-free solution.

vector with its origin located in the middle of the polyelectrolyte chain (see Fig. 4).

The chain conformation corresponding to the minimum of its potential energy is given by the following expression

$$\frac{\partial}{\partial z_i} \frac{U(\{\mathbf{r}_i\})}{k_B T} = -\frac{3}{b^2} (z_{i+1} + z_{i-1} - 2z_i) + l_B q_i \frac{\partial}{\partial z_i} \sum_{j \neq i} \frac{q_j}{|\mathbf{r}_j - \mathbf{r}_i|} = 0, \quad \text{for } i \neq 1, N \quad (2.15)$$

where we neglected the effect of the short-range LJ-interactions. Let us consider index  $i$  as a continuous variable  $m$  and treat  $z_i$  as a continuous function  $z(m)$  of argument  $m$ . In the continuous limit Eq. (2.15) can be reduced to [26]

$$\frac{3}{b^2} \frac{d^2 z(m)}{dm^2} \approx f \frac{d\varphi(z)}{dz} \quad (2.16)$$

The reduced electrostatic potential  $\varphi(z)$  at position  $z$  along the deformation axis of a polyelectrolyte chain is defined as the sum of all the contributions from all charges along the chain

$$\varphi(z) = l_B \sum_j \frac{q_j}{|\hat{\mathbf{e}}_z - \mathbf{r}_j|} \quad (2.17a)$$

where  $\hat{\mathbf{e}}_z$  is a unit vector pointing along the deformation axis of the polyelectrolyte chain. The term on the left-hand side of Eq. (2.16) describes the elastic force acting on the  $m$ th monomer, balanced by the electrostatic force on the right-hand side of the equation. This equation is valid at any point along the chain except at chain ends where the tension  $v(m) = dz(m)/dm$  vanishes ( $v(0) = v(N) = 0$ ). Eq. (2.16) together with the boundary conditions is similar to Newton's equation of motion of the particle along the  $z$ -direction in the external potential  $\varphi(z)$ . The 'particle' starts its motion at time  $t=0$  from the point  $z = -R_e/2$  with zero initial velocity and arrives at point  $z = R_e/2$  at time  $t=N$  with zero final velocity.

The reduced electrostatic potential can be estimated by assuming one-dimensional charge

distribution

$$\varphi(z) \approx l_B \left( \int_{-R_e/2}^{z-D_e(z)/2} \frac{f g_e(z')}{D_e(z')} \frac{dz'}{z-z'} + \int_{z+D_e(z)/2}^{R_e/2} \frac{f g_e(z')}{D_e(z')} \frac{dz'}{z'-z} + \frac{f g_e(z)}{D_e(z)} \right) \quad (2.17b)$$

Here,  $R_e$  is the chain size along the direction of elongation, and  $g_e(z)$  and  $D_e(z)$  are the number of monomers in the electrostatic blob and the electrostatic blob size at position  $z$ , respectively (see Fig. 4). Assuming that the blob size  $D_e(z)$  in a  $\Theta$ -solvent for the uncharged backbone varies weakly with  $z$ , and taking into account the relation between the number of monomers  $g_e(z)$  in an electrostatic blob and its size  $D_e(z) = b g_e(z)^{1/2}$ , we can simplify expression (2.17b)

$$\varphi(z) \approx \frac{uf D_e(z)}{b} \left( \ln \left[ \frac{R_e^2 - 4z^2}{D_e(z)^2} \right] + 1 \right) \quad (2.18)$$

Eq. (2.18) is valid in the interval  $-R_e/2 + D_e^0/2 < z < R_e/2 - D_e^0/2$ , where  $D_e^0 \approx b(uf^2)^{-1/3}$  is the size of the electrostatic blobs at chain ends. We can self-consistently find the electrostatic blob size using the classical path approximation for a strongly stretched chain. The average position of a monomer along the chain can be uniquely described within the strong stretching approximation by its projection on the deformation direction  $z$ . In this case, the derivative  $d/dm$  can be transformed into the derivative with respect to  $z(d/dm = v(z)d/dz)$ . Defining the local tension  $v(z)$  in terms of the number of monomers  $g_e(z)$  in the electrostatic blob and its size  $D_e(z)$  ( $v(z) = D_e(z)/g_e(z)$ ), one can rewrite Eq. (2.16) for the electrostatic blob size

$$\frac{3b^2}{2} \frac{d}{dz} D_e(z)^{-2} \approx f \frac{d\varphi(z)}{dz} \quad (2.19)$$

The solution of this equation with the electrostatic potential  $\varphi(z)$  given by Eq. (2.18) can be approximated by

$$D_e(z) \approx D_e^0 \left[ \ln \left( \frac{R_e^2 - 4z^2}{2R_e D_e^0} \right) + 1 \right]^{-1/3} \quad (2.20)$$

Thus, the smallest electrostatic blob is in the middle of the chain. This result is not surprising since the center of the

chain experiences stronger electrostatic repulsion than sections closer to chain ends. The chain size is obtained from the monomers' conservation condition

$$N = 2 \int_0^{R_e/2 - D_e^0/2} \frac{g_e(z) dz}{D_e(z)} \approx \frac{R_e D_e^0}{b^2} \left( \ln \frac{e R_e}{D_e^0} \right)^{-1/3} \quad (2.21)$$

The logarithmic term on the right-hand side of Eq. (2.21) accounts for the non-uniform stretching of the polyelectrolyte chain. An iterative solution of Eq. (2.21) yields the following expression for the chain size [26–29]

$$R_e \approx b N u^{1/3} f^{2/3} [\ln(e N / g_e^0)]^{1/3} \quad (2.22)$$

This expression for the chain size is in agreement with the result obtained by the Flory-like calculations by balancing electrostatic and elastic energies of a polyelectrolyte chain (Eq. (2.8)).

The non-uniform stretching of polyelectrolyte chains was directly tested in the molecular dynamics simulations by Liao et al. [26]. Fig. 5 shows the test of Eq. (2.22) for the end-to-end distance in dilute solutions of fully charged chains ( $f=1$ ). The electrostatic blob size  $D_e$  for this plot was obtained from the linear monomer density distribution  $\rho(z) = g_e(z)/D_e(z)$  averaged along the

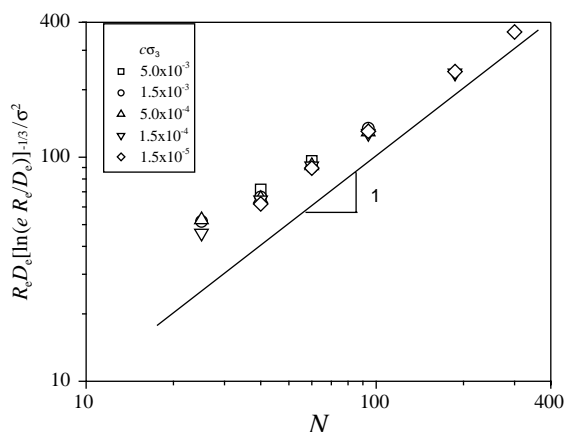


Fig. 5. Universal plot of root-mean-square end-to-end distances obtained using Eq. (2.22) approaches the solid line with slope 1 for the longest chains. Reproduced with permission from Liao, Q., Dobrynin, A.V., & Rubinstein, M. *Macromolecules* 36, 3386–3398 (2003). [26] Copyright 2003, American Chemical Society.

chain elongation direction. Data for different concentrations collapse on the universal curve that approaches a straight line with unit slope for longer chains. This is a confirmation of the non-uniform chain stretching and the applicability of the strong stretching approximation. The deviation from the straight line for short chains is due to the finite size effect. The fluctuations of the end-to-end distance for short chains are comparable with the average size of these chains.

Experimentally, the information about chain structure in dilute solutions is obtained from the analysis of the scattering function  $S(\mathbf{q})$ . In dilute solutions, the scattering function  $S(\mathbf{q})$  is proportional to the Fourier transform of the intrachain monomer–monomer correlation function

$$g_{\text{intra}}(r) = \frac{1}{cN} \sum_{i \neq j} \langle \delta(\mathbf{r} - \mathbf{r}_{ij}) \rangle \quad (2.23)$$

where  $c$  is the monomer concentration, brackets  $\langle \rangle$  correspond to the ensemble average over all chain conformations, and  $\mathbf{r}_{ij}$  is the vector between  $i$ th and  $j$ th monomers on the chain. The summation in Eq. (2.23) is carried out over all pairs of monomers on the chain. In the strong stretching limit, the fluctuations of the linear monomer density  $\delta\rho(z)$  along the chain stretching direction  $z$  can be neglected in comparison with the average linear monomer density  $\rho(z)$ . In this case, Eq. (2.23) can be written in terms of the average linear monomer density  $\rho(z)$

$$\begin{aligned} g_{\text{intra}}(r) &= \frac{1}{cN} \int_{-R_e/2}^{R_e/2} dz \\ &\times \int_{-R_e/2}^{R_e/2} dz' \rho(z) \rho(z') \langle \delta(\mathbf{r} - (z' - z) \hat{\mathbf{e}}_z) \rangle_{\text{orient}} \\ &= \frac{1}{2\pi c N r^2} \int_{-R_e/2}^{R_e/2} dz \rho(z) \rho(z+r) \end{aligned} \quad (2.24)$$

where brackets  $\langle \rangle_{\text{orient}}$  denote the averaging over all orientations of the unit vector  $\hat{\mathbf{e}}_z$ . In the case of uniformly stretched chain with the average linear monomer density  $\rho(z) = N/R_e$ , Eq. (2.24) can be

further simplified

$$g_{\text{intra}}(r) = \frac{N}{2\pi cr^2} \frac{R_e - r}{R_e^2} \theta(R_e - r) \quad (2.25)$$

where  $\theta(x)$  is the step function ( $\theta(x)=1$  for  $x \geq 0$  and  $\theta(x)=0$  for  $x < 0$ ). The intrachain pair correlation function  $g_{\text{intra}}(r)$  follows the simple scaling law  $r^{-2}$  for distances  $r \ll R_e$ . In the case of non-uniformly stretched polyelectrolyte chain, the average linear monomer density  $\rho(z)$  varies logarithmically along the elongation axis ( $\rho(z) = g_e(z)/D_e(z) \approx D_e(z)/b^2$  where  $D_e(z)$  is given by Eq. (2.20)). The intrachain correlation function  $g_{\text{intra}}(r)$  counts the number of monomer pairs separated by distance  $r$ . The summation over all monomer pairs leads to additional averaging of the linear monomer density  $\rho(z)$  along the chain deformation direction. Both the end and the middle chain sections contribute to the function  $g_{\text{intra}}(r)$  (see Eq. (2.24)). Because of such averaging of the logarithmic function, one can expect the intrachain correlation function  $g_{\text{intra}}(r)$  to be close to that for uniformly stretched chains (see Fig. 6). For comparison, we fit the simulation result of  $cg_{\text{intra}}(r)$  using the analytical form (Eq. (2.25)) obtained for the stepwise monomer density distribution as well as by direct numerical integration (Eq. (2.24)) of the linear

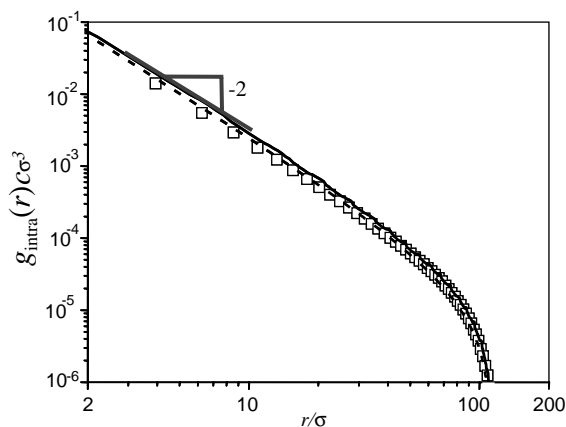


Fig. 6. Comparison of the simulation results (squares) with predictions of Eqs. (2.24) (solid line) and (2.25) (dashed line) for intrachain monomer–monomer correlation function in dilute solutions for fully charged chains with  $f=1$  and  $N=187$  at concentration  $c = 1.5 \times 10^{-5} \sigma^{-3}$  (see text for details). Reproduced with permission from Liao, Q., Dobrynin, A.V., & Rubinstein, M. *Macromolecules* 36, 3386–3398 (2003). [26] Copyright 2003, American Chemical Society.

monomer density  $\rho(z)$  obtained during simulations. The results of MD simulations [26] for the fully charged chains ( $f=1$ ) with the number of monomers  $N=187$  at polymer concentration  $c = 1.5 \times 10^{-5} \sigma^{-3}$  are shown in Fig. 6. One can see that the agreement between simulation data and both analytical results is excellent. In addition, it demonstrates that the intrachain correlation function is not very sensitive to the non-uniform chain stretching. A good approximation of this correlation function can be obtained from the uniform density profile.

### 2.3. Polyelectrolyte chain in a poor solvent for polymer backbone

In poor solvents for polymer backbone there is an effective attraction between monomers, which causes neutral polymer chain without charged groups to collapse into dense spherical globules in order to maximize the number of favorable polymer–polymer contacts and minimize the number of unfavorable polymer–solvent contacts [22]. Upon charging, polymeric globules change their shape and size. This phenomenon was observed over 50 years ago by Katchalsky and Eisenberg [30] in their study of the viscosity of aqueous solutions of poly(methacrylic acid) (PMA). The viscosity of dilute PMA solution stayed almost constant at a low pH and then abruptly increased as solution pH reached some critical value, indicating a dramatic change in the chain dimensions. This dramatic change in solution viscosity of PMA is qualitatively different from that observed in solutions of poly(acrylic acid) (PAA) for which viscosity grows smoothly with increasing neutralization, indicating smooth expansion of polymer chains. The difference in behavior of PMA and PAA is due to the fact that water is a poor solvent for PMA that has hydrophobic methyl groups while it is a good solvent for PAA. (For a historical overview of this subject see the paper by Morawetz [31].)

We begin our discussion of polyelectrolytes in a poor solvent by briefly reviewing the theory of the globular state in neutral polymers. In the globular state close to the transition point, the interaction part of the chain free energy  $F_{\text{int}}(R)$  can be expanded into a power series of the number density of monomers  $\rho \approx N/R_{\text{glob}}^3$  ( $R_{\text{glob}}$  is the size of the globule). This expansion is similar to the virial expansion in

the theory of real gases [32]. Thus, the interaction part of the free energy can be written as

$$\frac{F_{\text{int}}}{k_{\text{B}}T} \approx NB\rho + NC\rho^2 \quad (2.26)$$

where  $B$  and  $C$  are the second and third virial coefficients. These coefficients are determined by the functional form of the effective short-range interaction potential between monomers in a given solvent. For the Lennard–Jones potential, the second virial coefficient can be estimated as

$$B(T) = \frac{1}{2} \int d\mathbf{r} \left( 1 - \exp\left(-\frac{U_{\text{LJ}}(r)}{k_{\text{B}}T}\right) \right) \approx \sigma^3 \left( 1 - \frac{\Theta}{T} \right) \approx \sigma^3 \tau \quad (2.27)$$

where  $\Theta$  is the theta temperature and  $\tau = 1 - \Theta/T$  is the relative deviation from the theta temperature, called effective temperature. At  $\Theta$ -point, the second virial coefficient is equal to zero. Below the  $\Theta$ -temperature, the second virial coefficient  $B(T)$  is negative, corresponding to the effective attraction between monomers—poor solvent conditions for polymer backbone. The third virial coefficient  $C$  is always positive and is proportional to  $\sigma^6$ . For simplicity, we will assume that the bond length between monomers  $b$  is on the order of the monomer diameter  $\sigma$ . The equilibrium size of the globule is

obtained by minimizing the interaction part of the free energy  $F_{\text{int}}$  of the globule (Eq. (2.26)) with respect to its size  $R_{\text{glob}}$ . The optimal size of the globule [10,22] is equal to

$$R_{\text{glob}} \approx b|\tau|^{-1/3}N^{1/3} \quad (2.28)$$

There is an important length scale—the correlation length  $\xi_{\text{T}}$  of the density fluctuations inside a globule (thermal blob size). At length scales smaller than the thermal blob size  $\xi_{\text{T}}$ , the chain statistics are unperturbed by monomer–monomer attractive interactions and are that of an ideal chain of  $g_{\text{T}}$  monomers ( $\xi_{\text{T}} \approx bg_{\text{T}}^{1/2}$ ) (see Fig. 7(a)). At length scales larger than the thermal blob size, the attraction between monomers wins (the attractive interaction between two blobs is on the order of the thermal energy  $k_{\text{B}}T$ ) and thermal blobs in a globule are densely packed,  $\rho \approx g_{\text{T}}/\xi_{\text{T}}^3$ . The polymer density  $\rho$  inside the globule scales linearly with the absolute value of the effective temperature  $\tau$

$$\rho \approx b^{-3}|\tau|$$

Thus, the number of monomers in a thermal blob is

$$g_{\text{T}} \approx |\tau|^{-2}$$

and its size is

$$\xi_{\text{T}} \approx b|\tau|^{-1}.$$

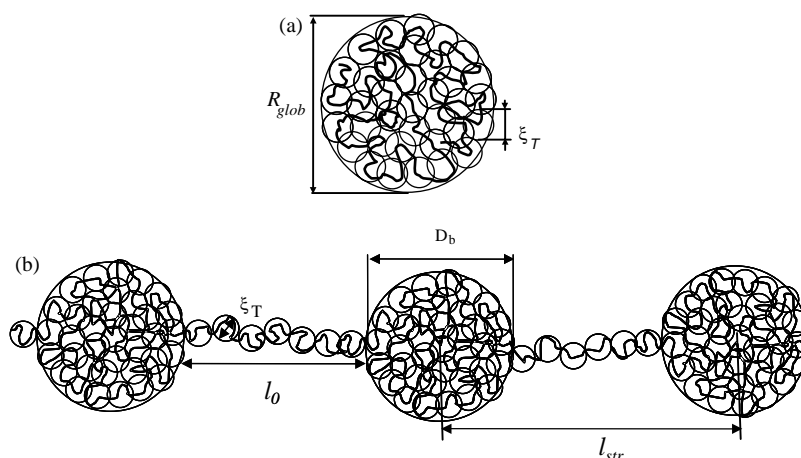


Fig. 7. (a) Schematic representation of a polymeric globule of size  $R_{\text{glob}}$  consisting of dense packing of thermal blobs of size  $\xi_{\text{T}}$ . (b) Schematic representation of a necklace-like polyelectrolyte chain.

The free energy of the globule is on the order of the thermal energy  $k_B T$  per thermal blob

$$\frac{F_{\text{int}}}{k_B T} \approx -\frac{N}{g_T} \approx -N\tau^2 \quad (2.29)$$

In addition to this bulk contribution to the free energy of a globule, there is also a surface energy contribution. The origin of the surface energy is the difference in the number of nearest neighbors for thermal blobs at the surface of the globule and those in the bulk. It requires extra energy to bring a blob to the surface. The surface energy of a globule can be estimated as the number of blobs at the globule surface  $S/\xi_T^2$  times  $k_B T$  because any two blobs inside the globule attract each other with the energy on the order of the thermal energy  $k_B T$  and blobs at the surface are missing part of this attraction energy because they have fewer neighbors

$$F_{\text{surf}} \approx k_B T S / \xi_T^2 \approx \gamma S \quad (2.30)$$

where  $\gamma$  is the surface tension of the globule ( $\gamma \approx k_B T / \xi_T^2$ ). In fact, a polymeric globule can be envisioned as a liquid droplet in the air.

The problem of the shape of a charged globule bears similarity with the classical problem of the instability of a charged droplet, considered by Lord Rayleigh over 100 years ago [33]. In his classical experiments, Rayleigh showed that a charged droplet is unstable and breaks into smaller droplets if its electric charge exceeds some critical value. The value of the critical charge is controlled by the electrostatic energy,  $Q^2 / (\epsilon R_{\text{drop}})$ , of the droplet of size  $R_{\text{drop}}$  with charge  $Q$ , and its surface energy  $\gamma R_{\text{drop}}^2$  where  $\gamma$  is the surface tension of the air–water interface. Balancing these two energies, one finds that the critical charge  $Q_{\text{crit}}$  scales with the size of the droplet as  $R_{\text{drop}}^{3/2}$ . The equilibrium state of the charged droplet with  $Q > Q_{\text{crit}}$  is a set of smaller droplets with charge on each of them smaller than the critical one and placed at an infinite distance from each other. For a polyelectrolyte chain in the globular state, its surface energy  $k_B T R_{\text{glob}}^2 / \xi_T^2$  becomes on the order of its electrostatic energy  $k_B T l_B (fN)^2 / R_{\text{glob}}$  at the critical fraction of charged monomers per chain  $f_{\text{crit}}$  equal to

$$f_{\text{crit}} \approx \left( \frac{|\tau|}{uN} \right)^{1/2} \quad (2.31)$$

(In the derivation of Eq. (2.31) we used Eq. (2.28) for the globular size  $R_{\text{glob}}$ .)

What are the conformations of the polymer chain after this transition? The Rayleigh's experiments give a hint to what happens with polyelectrolytes in a poor solvent when the fraction of charged monomers  $f$  exceeds the critical value  $f_{\text{crit}}$ . Similar to a charged droplet, a polyelectrolyte chain in a poor solvent reduces its energy by splitting into a set of smaller charged globules—beads connected by strings [34]. To show that, let us consider a necklace-like polyelectrolyte chain that has  $n_b$  ( $n_b > 1$ ) beads of size  $D_b$  with  $m_b$  monomers in each. These beads are connected by strings, each having  $m_{\text{str}}$  monomers. (See Fig. 7(b) for the definitions of different length scales.) Each bead is a collapsed charged globule with the size

$$D_b \approx b |\tau|^{-1/3} m_b^{1/3} \quad (2.32)$$

The total contribution to the necklace free energy due to bead interface is equal to the number of beads  $n_b$  per chain times the surface energy of a bead

$$\frac{F_b^s}{k_B T} \approx n_b \frac{D_b^2}{\xi_T^2} \approx n_b |\tau|^{4/3} m_b^{2/3} \quad (2.33)$$

Pulling monomers into a string requires extra energy  $k_B T$  per thermal blob or  $k_B T / g_T$  per monomer that is the difference between the average interaction energy of a monomer in a string and that in the interior (or even at the surface) of a bead. Thus, each string has an additional positive contribution to the necklace free energy of  $k_B T m_{\text{str}} / g_T$  due to the loss of favorable attractive interactions between monomers. The combined contribution of the surface energy of  $n_b - 1$  strings to the free energy of a necklace is

$$\frac{F_{\text{str}}^s}{k_B T} \approx (n_b - 1) \frac{m_{\text{str}}}{g_T} \approx (n_b - 1) \tau^2 m_{\text{str}} \quad (2.34)$$

In addition to the surface free energy term, the free energy of a string has an elastic contribution due to the stretching of the polymer backbone between beads. Combining elastic and surface free energy contributions to the string free energy we can write

$$\frac{F_{\text{str}}}{k_B T} = (n_b - 1) \left( \frac{l_0^2}{b^2 m_{\text{str}}} + \tau^2 m_{\text{str}} \right) \quad (2.35)$$

where  $l_0$  is the length of a strand with  $m_{\text{str}}$  monomers (see Fig. 7(b)). Minimization of Eq. (2.35) with respect to  $m_{\text{str}}$  at fixed length  $l_0$  of the strand results in the linear relation connecting the distance between surfaces of the two neighboring beads and the number of monomers in a string  $m_{\text{str}}$

$$m_{\text{str}} = \frac{l_0}{|\tau|b} \quad (2.36)$$

Substitution of this relation into Eq. (2.34) leads to the linear dependence of the string free energy on its length  $l_0$

$$\frac{F_{\text{str}}}{k_{\text{B}}T} = (n_{\text{b}} - 1)|\tau| \frac{l_0}{b} \quad (2.37)$$

The electrostatic contribution to the necklace free energy includes the electrostatic energy of beads, the electrostatic interaction between beads, and the electrostatic energy of strings. There are three different regions with different symmetry of the electrostatic potential in dilute solutions of necklaces. At distances from the center of a bead smaller than half the distance between the centers of mass of two neighboring beads,  $l_{\text{str}} = l_0 + D_{\text{b}}$ , the distribution of the electrostatic potential has almost spherical symmetry that is slightly perturbed by the strings of charged monomers. The contribution of a bead to the necklace electrostatic energy can be estimated as

$$\frac{U_{\text{b}}^{\text{elec}}}{k_{\text{B}}T} \approx \frac{l_{\text{B}}(fm_{\text{b}})^2}{D_{\text{b}}} \approx \frac{l_{\text{B}}|\tau|^{1/3}f^2m_{\text{b}}^{5/3}}{b} \quad (2.38)$$

By multiplying the last equation by the number of beads per chain  $n_{\text{bead}}$ , one obtains the combined electrostatic self-energy of all beads. At the length scales larger than half the string length, the distribution of electrostatic potential has a cylindrical symmetry. The self-energy of the cylinder with the diameter equal to  $l_{\text{str}}$  and total length  $(n_{\text{b}} - 1)l_{\text{str}}$  is estimated as

$$\frac{U_{\text{neck}}^{\text{elec}}}{k_{\text{B}}T} \approx \frac{l_{\text{B}}(fN)^2}{(n_{\text{b}} - 1)l_{\text{str}}} \ln(n_{\text{b}}) \quad (2.39)$$

Combining all the terms together, we can write the total energy of a necklace as the function of the number of monomers in a bead,  $m_{\text{b}}$ , the number of

beads on a chain,  $n_{\text{b}}$ , and the string length

$$\begin{aligned} \frac{F_{\text{neck}}}{k_{\text{B}}T} \approx & \frac{l_{\text{B}}(fN)^2}{(n_{\text{b}} - 1)l_{\text{str}}} \ln(n_{\text{b}}) + (n_{\text{b}} - 1)|\tau| \frac{l_0}{b} \\ & + n_{\text{b}}m_{\text{b}} \left( |\tau|^{4/3}m_{\text{b}}^{-1/3} + \frac{l_{\text{B}}f^2|\tau|^{1/3}m_{\text{b}}^{2/3}}{b} \right) \end{aligned} \quad (2.40)$$

where the first-term describes the electrostatic repulsion between beads, the second one—the surface energy of strings and finally the last two terms correspond to the surface energy of all beads and their electrostatic self-energy. Analyzing Eq. (2.40), one has to keep in mind that the total number of monomers in beads  $n_{\text{b}}m_{\text{b}}$  plus the number of monomers in all strings  $(n_{\text{b}} - 1)m_{\text{str}}$  should be equal to the degree of polymerization  $N$ .

The equilibrium distance between the centers of mass of two neighboring beads  $l_{\text{str}}$  is obtained by minimizing the first two terms of the free energy of a necklace Eq. (2.40) with respect to distance  $l_{\text{str}}$ . The distance between the centers of neighboring beads  $l_{\text{str}}$  is larger than the length  $l_0$  by the bead diameter  $D_{\text{b}}$  ( $l_{\text{str}} = l_0 + D_{\text{b}}$ ), thus on the scaling level both lengths  $l_{\text{str}}$  and  $l_0$  are on the same order of magnitude when  $l_{\text{str}} \gg D_{\text{b}}$ . Below we will call  $l_{\text{str}}$ —the length of a string. After minimization, we obtain

$$l_{\text{str}} \approx \frac{bfN}{n_{\text{b}}} \sqrt{\left(\frac{u}{|\tau|}\right) \ln(n_{\text{b}})} \quad (2.41)$$

where we assume that the number of beads per chain is large,  $n_{\text{b}} \gg 1$ . Eq. (2.41) shows the linear relation of the distance between the centers of mass of two neighboring beads and the charge per string  $fN/n_{\text{b}}$  for a given number of beads on a necklace.

In order to complete the optimization of the necklace structure, one has to minimize the free energy of a necklace with respect to the number of monomers in a bead  $m_{\text{b}}$  that leads to

$$m_{\text{b}} \approx \frac{|\tau|}{uf^2} \quad (2.42)$$

The number of monomers in a bead increases with increasing the absolute value of the effective temperature  $|\tau|$  and decreases with increasing fraction of charged monomers  $f$ . Eq. (2.42) is another form of

the Rayleigh's stability condition for a charged globule (Eq. (2.31)).

In the case  $m_b/m_{str} \gg 1$ , the number of beads  $n_b$  per chain is approximately equal to  $N/m_b$ . Since most of the length of the necklace is stored in the strings, the length of the necklace can be estimated as the number of beads  $n_b$  per chain times the distance between the centers of mass of two neighboring beads  $l_{str}$

$$L_{nec} \approx n_b l_{str} \approx b f N \sqrt{\frac{u}{|\tau|} \ln \left( \frac{N u f^2}{|\tau|} \right)} \quad (2.43)$$

The number of beads  $n_b$  ( $n_b \approx N/m_b$ ) in a necklace can only be an integer, therefore, Eq. (2.42) defines the set of boundaries

$$f \approx \left( \frac{|\tau|}{u} \frac{n_b}{N} \right)^{1/2} \quad (2.44)$$

between the states of the necklace globule with different number of beads. By changing the fraction of charged monomers  $f$  or solvent quality  $\tau$  the globule undergoes a cascade of transitions between states with different integer number of beads  $n_b$  per necklace.

Conformational transitions of polyelectrolyte chains in poor solvents for the polymer backbone were studied using molecular simulations by Hooper et al. [35] and by Higgs and Orland [36]. It was found that a polyelectrolyte chain undergoes an abrupt conformational transition from a collapsed to an extended state with increasing chain charge. As the strength of the segment–segment attraction decreases the transition becomes less pronounced [35].

The details of the transition and conformations of polyelectrolyte chains above the transition were described by Dobrynin et al. [34]. Performing Monte Carlo simulations of freely jointed uniformly charged polyelectrolyte chains with fractional charge on each monomer  $f$ , they showed that the critical number of charged monomers  $(fN)_{crit}$  on the chains at which charged globules becomes unstable is proportional to  $\sqrt{N}$  (see Fig. 8).

For the number of charged monomers on the chain  $fN$  above the critical value  $(fN)_{crit}$ , the polyelectrolyte chain first takes a dumbbell configuration (see Fig. 9(b)). At higher charge, the polymer forms a necklace with three beads joined by two strings (see Fig. 9(c)). These simulations have shown that there is a cascade of transitions between necklaces with

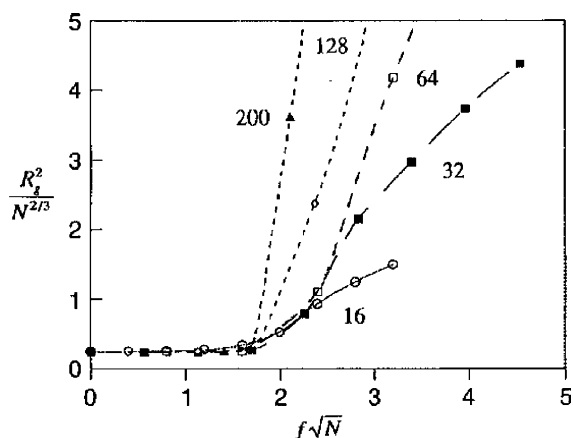


Fig. 8. Dependence of the reduced mean-square radii of gyration of polyelectrolyte chains in a poor solvent on the reduced chain valence  $fN^{1/2}$  for chains with degrees of polymerization  $N=16, 32, 64, 128, \text{ and } 200$ . Results of the Monte Carlo simulations of freely jointed chains interacting via Coulomb and Lennard–Jones potential ( $\epsilon_{LJ}=1.5$  and  $u=2$ ). Reproduced with permission from Dobrynin, A.V., Rubinstein, M., & Obukhov, S.P. *Macromolecules* 29, 2974–2979 (1996). [34] Copyright 1996, American Chemical Society.

different number of beads as the charge on the chain increases.

The effect of solvent quality on the cascade of transition between different pearl-necklace structures

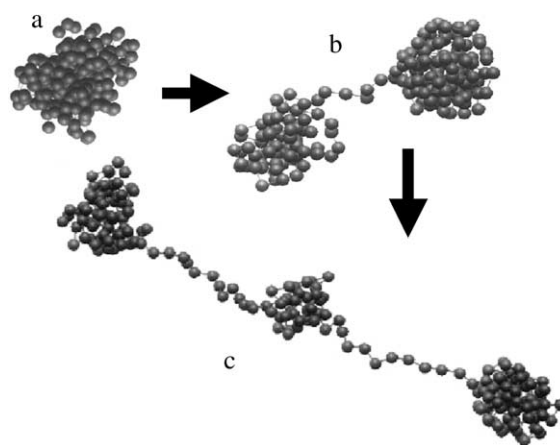


Fig. 9. Typical configurations of freely jointed uniformly charged chains in poor solvent conditions for three different charge fractions: (a) a spherical globule for  $f=0$ ; (b) a dumbbell for  $f=0.125$ ; and (c) a necklace with three beads for  $f=0.15$ . Reproduced with permission from Dobrynin, A.V., Rubinstein, M., & Obukhov, S.P. *Macromolecules* 29, 2974–2979 (1996). [34] Copyright 1996, American Chemical Society.

was investigated using Monte Carlo [37] and molecular dynamics [38] simulations. Chodanowski and Stoll [37] have found necklaces with up to 12 beads for a polyelectrolyte chain with degree of polymerization  $N=200$ . These results of computer simulations are in good qualitative agreement with theoretical models [34,39–41] of a polyelectrolyte chain in a poor solvent.

The transition between necklaces with different number of beads can be induced by applying an external force—stretching the necklace [40,42–44]. Since the necklaces with different numbers of beads coexist, the chain deformation will have a saw-tooth deformation curve. However, this mean-field picture of abrupt transitions between necklaces with different numbers of beads is smeared by fluctuations in the number of monomers in a bead as well as by fluctuations of the number of beads in a necklace [43,44]. The smooth deformation curve of a hydrophobic polyelectrolyte chain is confirmed by computer simulations [45,46].

#### 2.4. Polyelectrolyte chains at finite concentrations and counterion condensation

The electrostatic attraction between polyelectrolyte chains and counterions in solutions can result in condensation of counterions on polyelectrolytes. The counterion condensation appears to be due to a fine interplay between the electrostatic attraction of a counterion to a polymer chain and the loss of the translational entropy by counterions due to their localization in the vicinity of the polymer chain. In a very dilute polyelectrolyte solution the entropic penalty for counterion condensation is very high and almost all counterions leave polymer chains and stay ‘free’ in solution. However, as polymer concentration increases, the entropic penalty for counterion localization decreases resulting in a gradual increase in the number of condensed counterions. For polyelectrolyte solutions in a good or theta solvent for polymer backbone the fraction of free counterions decreases logarithmically with increasing polymer concentration.

A qualitatively different scenario is seen for polyelectrolyte chains in a poor solvent known as the avalanche-like counterion condensation [47–49]. By increasing polymer concentration or by decreasing

temperature one can cause a spontaneous condensation of counterions inside beads of necklace globules. The reduction of the effective charge of the beads by condensed counterions increases the mass of the beads, initiating further access of counterions that starts the avalanche-like counterion condensation process. At finite polyelectrolyte concentrations, this avalanche-like condensation results in a phase separation of polyelectrolyte solutions into dilute and concentrated phases.

There are several approaches to describe counterion condensation in polyelectrolyte solutions. In the first approach (Oosawa–Manning condensation theory), the counterions are separated into ‘free’ and ‘condensed’ [5,50–53]. Free counterions are able to explore the solution volume  $V$ . The condensed counterions are localized within a small volume surrounding polymer backbone. Modifications of the two-state counterion condensation model include ion-binding and ion localization models [48,54,55].

The two-state approximation for counterion distribution in a polyelectrolyte solution is an oversimplification of the real situation. A more rigorous description of the distribution of counterions can be obtained in the framework of the so-called Katchalsky’s cell model [56]. This model decouples the counterion and polymeric degrees of freedom providing the equilibrium counterion density profile for the fixed idealized polymer conformation. The mean-field approximation of the counterion density profile is obtained by solving the non-linear Poisson–Boltzmann equation describing the distribution of the electrostatic potential around a macroion. Unfortunately, the exact analytical solution of the non-linear Poisson–Boltzmann equation exists only for a rod-like polyelectrolyte [57–59] and for a planar charged surface. To avoid some of the limitations of the cell model and to describe the counterion distribution in dilute solutions, Deshkovski et al. [60] developed a two-zone model. In this model, the volume occupied by charged rods is divided into two types of regions. The inner regions are cylindrical zones around the charged rods with the diameter on the order of the length of rods  $L$ . The outer regions are spherical zones outside the cylindrical regions that extend up to the distance between chains. It turns out that this model also has an exact analytical solution of the non-linear Poisson–Boltzmann equation for the electrostatic

potential in the cylindrical regions around polyions [60]. In the limit when the outer (spherical) zone disappears, the solution of the two-zone model is reduced to that for the classical cell model.

#### 2.4.1. Two-state model of counterion condensation

According to the Oosawa–Manning two-state model [5,50], counterions in a polyelectrolyte solution can be classified into two categories: counterions localized inside potential valleys along polymer backbones (state 1) and counterions freely moving outside the region occupied by polyelectrolyte chains (state 2) (see Fig. 10). The total solution volume,  $V$ , is divided into two regions. One region surrounds polyelectrolyte backbone with volume  $v$  where counterions are localized. The total volume occupied by condensed counterions is equal to the total number of chains  $N_p$  in solution times the localization volume  $v$  ( $V_{\text{con}} = N_p v$ ). The outer region (state 2) is further away from polyions where free counterions are distributed. The volume of this region is  $V - N_p v$ . At equilibrium, the electrochemical potentials  $\mu_{\text{el}}$  of counterions in both states are equal

$$\frac{\mu_{\text{el}}}{k_B T} = \ln\left(\frac{n_1}{N_p v}\right) - \varphi_1 = \ln\left(\frac{n_2}{V - N_p v}\right) - \varphi_2 \quad (2.45)$$

where  $n_1$  is the number of condensed counterions,  $n_2$  is the number of free counterions, and  $\varphi_i$  is the reduced electrostatic potential of counterions in the  $i$ th state. Eq. (2.45) can be rewritten by introducing the

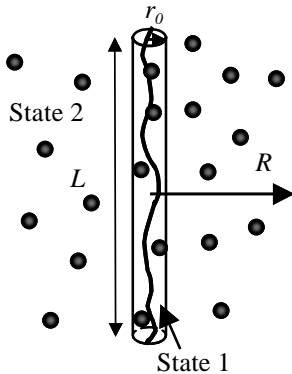


Fig. 10. Schematic sketch of a polyelectrolyte chain and the definition of different length scales for the two-state model.  $L$  is the length of rod-like polyion and  $R$  is the cell size ( $R \ll L$ ).

fraction of condensed counterions  $\beta = n_1/(n_1 + n_2)$  and polymer volume fraction  $\phi = N_p v/V$

$$\ln\left(\frac{\beta}{1-\beta}\right) = \ln\left(\frac{\phi}{1-\phi}\right) - \Delta\varphi \quad (2.46)$$

where  $\Delta\varphi = \varphi_2 - \varphi_1$  is the difference of the reduced electrostatic potentials between states 2 and 1. In the original Oosawa–Manning model, the polyelectrolyte chains were assumed to be rod-like with the distance  $2R$  between them smaller than their length  $L$ . In this case, the typical variations of the reduced electrostatic potential between two cylindrical regions occupied by counterions is approximately equal to

$$\Delta\varphi \approx 2(1-\beta)\frac{l_B f N}{L} \ln\left(\frac{r_0}{R}\right) \approx (1-\beta)\gamma_0 \ln(\phi) \quad (2.47)$$

where  $r_0$  is the radius of region 1 and  $\gamma_0$  is the so-called Oosawa–Manning counterion condensation parameter—product of the Bjerrum length  $l_B$  and the linear number density of ionized groups  $fN/L$  on the polymer backbone

$$\gamma_0 = \frac{l_B f N}{L} \quad (2.48)$$

Substituting expression for  $\Delta\varphi = \varphi_2 - \varphi_1$  from Eq. (2.47) into Eq. (2.46), we can rewrite Eq. (2.45) in the limit of low polymer volume fractions,  $\phi \ll 1$ , in the following form

$$\ln\left(\frac{\beta}{1-\beta}\right) = [1 - (1-\beta)\gamma_0] \ln(\phi) \quad (2.49)$$

There are two qualitatively different asymptotic regimes of Eq. (2.49) for the dependence of the fraction of condensed counterions  $\beta$  on the polymer volume fraction. For the small values of the counterion condensation parameter  $\gamma_0 \ll 1$ , the fraction of condensed counterions  $\beta$  is equal to  $\phi$  and decreases with decreasing polymer volume fraction  $\phi$ . The fraction of condensed counterions  $\beta$  eventually approaches zero at infinite dilution,  $\phi \rightarrow 0$ . In the opposite limit of large values of the Oosawa–Manning counterion condensation parameter  $\gamma_0 \gg 1$  the fraction of free counterions  $1 - \beta$  is equal to

$$1 - \beta \approx \gamma_0^{-1} [1 - \ln(\gamma_0)/\ln(\phi)] \quad (2.50)$$

and approaches  $1/\gamma_0$  at infinite dilution,  $\phi \rightarrow 0$ . Thus, there is the counterion condensation phenomenon that is associated with the value of the parameter  $\gamma_0$ .

The inverse reduced effective linear charge density  $(1-\beta)\gamma_0$  of the rod-like polyelectrolyte as ‘seen’ by a counterion in region 2 saturates at unity. In this regime, the distance between ionized charged groups on polyion,  $L/[(1-\beta)fN] \approx l_B[(1-\beta)\gamma_0]^{-1}$ , is of the order of the Bjerrum length  $l_B$ . Fig. 11 shows the dependence of the inverse reduced effective linear charge density  $(1-\beta)\gamma_0$  of the rod-like polyelectrolyte on its bare value  $\gamma_0$  with two qualitatively different regimes. The inverse reduced effective linear charge density  $(1-\beta)\gamma_0$  increases linearly for small values of the Oosawa–Manning condensation parameter  $\gamma_0$  and saturates as it becomes larger than unity.

The size of flexible polyelectrolytes increases with the fraction of ionized charged groups  $(1-\beta)f$  as  $L \approx bN(1-\beta)^{2/3}(uf^2)^{1/3}$  (see for example Eq. (2.14)). Substituting this expression for the chain size into the definition of the Oosawa–Manning counterion condensation parameter  $\gamma_0$  (Eq. (2.48)), we can rewrite Eq. (2.49) in the following form

$$\ln\left(\frac{\beta}{1-\beta}\right) = [1 - (1-\beta)^{1/3}u^{2/3}f^{1/3}]\ln(\phi) \quad (2.51)$$

The counterion condensation will occur in this case when the parameter  $u^2f$  becomes larger than unity. At the crossover value of the parameter  $u^2f \approx 1$ , the distance between two neighbouring charged groups along the polymer backbone,  $b/f^{1/2}$ , is comparable with the Bjerrum length  $l_B$ . The value of the parameter  $u^2f \approx 1$  separates two different classes of polyelectrolyte systems: weakly charged polyelectrolytes for

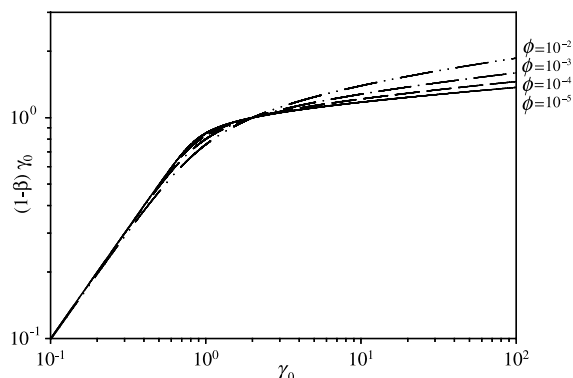


Fig. 11. Dependence of the inverse reduced effective linear charge density of the rod-like polyelectrolyte on the Oosawa–Manning condensation parameter  $\gamma_0$  at different polymer volume fractions  $\phi$ .

which the parameter  $u^2f$  is smaller than unity, and strongly charged polyelectrolytes with  $u^2f \gg 1$ . The counterion condensation phenomenon is expected only for strongly charged polyelectrolytes.

The counterion condensation phenomenon described above is a specific feature of the cylindrical symmetry of the system (even at the ‘infinite dilution’) for which the electrostatic potential varies logarithmically with distance  $r$  from the polyion. The original Oosawa–Manning treatment of counterion condensation corresponds to the case of semidilute polyelectrolyte solutions when the distance between chains is smaller than their length ( $L \gg R$ ). This relation between  $R$  and  $L$  is assumed even at ‘infinite dilution’ ( $L \gg R \rightarrow \infty$ ). Below we review a model [60] that releases this assumption.

#### 2.4.2. Counterion distribution and osmotic pressure in dilute polyelectrolyte solutions.

Consider a dilute solution of cylindrical polyions with radius  $r_0$ , length  $L$ , and the number of charged groups  $fN$  per polyion. A dilute solution can be modeled by placing each polyion at the center of a cell of size  $R_{\text{cell}} \sim c_{\text{pol}}^{-1/3}$ , where  $c_{\text{pol}}$  is the density of polyions (see Fig. 12). The cell volume is divided into two zones: a cylindrical zone (I) of length  $L$  and radius  $R=L/2$ , surrounding a rod-like polyion; and a spherical zone (II) with radius  $R_{\text{cell}}$ , outside the cylindrical region (see Fig. 12).

The reduced electrostatic potential  $\phi(r)$  in the cylindrical zone I satisfies the Poisson–Boltzmann equation

$$\left(\frac{\partial^2}{\partial r^2} + \frac{1}{r} \frac{\partial}{\partial r}\right)\phi(r) = 4\pi c(R)\exp[\phi(r)] \quad (2.52)$$

where  $r$  is the distance from the axis of the cylindrical polyion, and  $c(R)$  is the counterion concentration at the boundary of the cylindrical region where the electrostatic potential  $\phi(R)$  is set to zero. Here, we consider only systems with monovalent counterions. The inner boundary condition at the surface of the charged rod at  $r=r_0$  is determined by the reduced linear charge density  $\gamma_0=fNl_B/L$

$$\left.\frac{\partial\phi(r)}{\partial r}\right|_{r=r_0} = -2\frac{\gamma_0}{r_0} \quad (2.53)$$

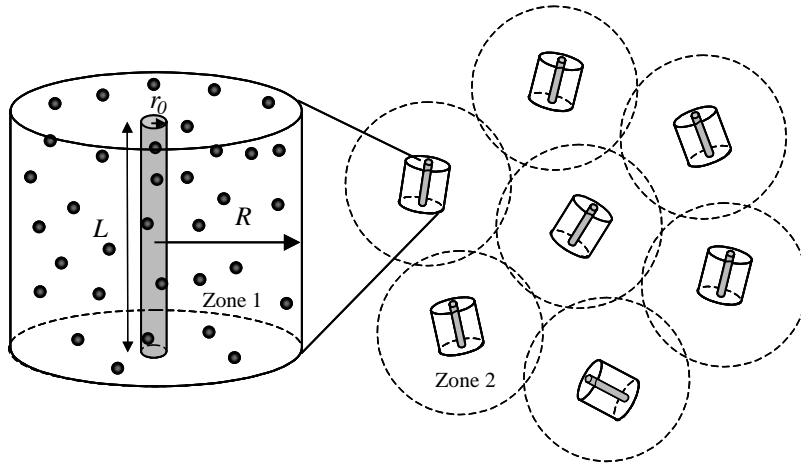


Fig. 12. Schematic sketch of a dilute solution of rod-like polyelectrolytes and the definition of different length scales for the two-zone model.

Note that the reduced linear charge density  $\gamma_0$  is the dimensionless Manning counterion condensation parameter (Eq. (2.48)) [50,51]. The outer boundary condition at  $r=R$  is determined by the effective linear charge density of the cylindrical region

$$\gamma_R = f_R N l_B / L, \tag{2.54}$$

where  $f_R N$  is the net charge within the cylindrical region, which is equal and opposite to the charge of the outer region due to the electroneutrality condition

$$\left. \frac{\partial \varphi(r)}{\partial r} \right|_{r=R} = -2 \frac{\gamma_R}{R} \tag{2.55}$$

The solution of the non-linear Poisson–Boltzmann equation (Eq. (2.52)) with the boundary conditions (Eqs. (2.53) and (2.55)) leads to the following counterion density profile in the cylindrical zone as a function of the distance  $r$  from the polyion axis [60]

$$c(r) = \frac{2}{\pi l_B} \frac{\alpha^2 \zeta^{2\alpha} r^{2\alpha-2}}{(r^{2\alpha} - \zeta^{2\alpha})^2} \tag{2.56}$$

where parameters  $\alpha$  and  $\zeta$  are defined by the following equations

$$r_0^{2\alpha} \frac{\gamma_0 - 1 - \alpha}{\gamma_0 - 1 + \alpha} = \zeta^{2\alpha} = R^{2\alpha} \frac{\gamma_R - 1 - \alpha}{\gamma_R - 1 + \alpha} \tag{2.57}$$

Eq. (2.57) represents the boundary conditions (Eqs. (2.53) and (2.55)) in terms of the model parameters.

The exact solution of the two-zone model predicts three qualitatively different regimes shown in Fig. 13 within the physical range  $\gamma_0 > \gamma_R$  of linear charge

densities  $\gamma_0$  and  $\gamma_R$ . These regions are separated by the line  $\alpha=0$  (thick solid line in Fig. 13)

$$\gamma_{0,\text{crit}}(\gamma_R) = \frac{\gamma_R + (1 - \gamma_R) \ln(R/r_0)}{1 + (1 - \gamma_R) \ln(R/r_0)} \tag{2.58}$$

Phase I ( $\gamma_R < \gamma_0 < \gamma_{0,\text{crit}}(\gamma_R) < 1$ ) corresponds to the real values of the parameter  $\alpha$  (parameter  $\alpha$  is proportional to  $1 - \gamma_0$  for large  $R$ ). In this regime, the electrostatic attraction is not strong enough to keep counterions adjacent to the polyion, and most of the counterions are outside the cylindrical region. The

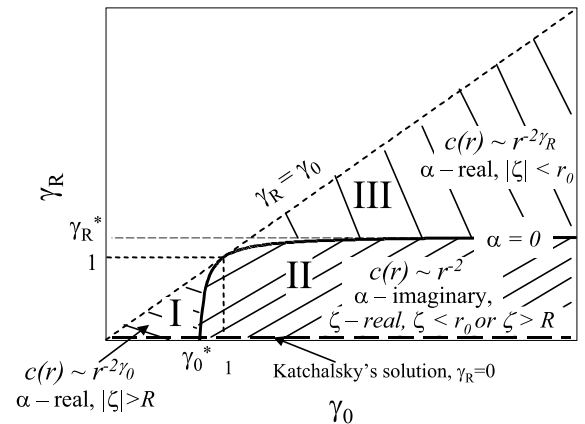


Fig. 13. Theoretical phase diagram of the two-zone model. Parameter  $\gamma_0$  is the bare linear charge density on polyion and  $\gamma_R$  is the effective linear charge density of the cylindrical region. Phase I—weakly charged polyions; Phase II—saturated condensation; Phase III—unsaturated condensation. See text for details.

counterion concentration in the cylindrical zone around the polyions has a power law dependence on the distance  $r$  from the polyion  $c(r) \propto r^{-2\gamma_0}$ . Phase II corresponds to  $\gamma_0 > \gamma_{0,\text{crit}}$  and to the pure imaginary values of the parameter  $\alpha$ . In this range of parameters the charge on the polyion is almost completely compensated by its counterions, and the counterion density profile is universal ( $c(r) \propto r^{-2}$ ) and independent of the linear charge density  $\gamma_0$  on the polyion. The line  $\alpha=0$  on this phase diagram (see Eq. (2.58)) is the line of second-order phase transitions that separates Phase II with the self-similar counterion density profile from Phases I and III. Phase III corresponds to the condition  $1(\gamma_R < \gamma_0 < \gamma_{0,\text{crit}}(\gamma_R) < 1)$ , and to the real values of the parameter  $\alpha$  (see Fig. 13). Here, the counterion density profile is  $c(r) \propto r^{-2\gamma_R}$ .

Experimentally the fraction of free counterions in salt-free polyelectrolyte solutions is believed to give the main contribution to the osmotic pressure. In order to obtain an expression for the osmotic pressure in the framework of the two-zone model, one has to know the counterion concentration at the outer boundary of the spherical region. This requires knowledge of the electrostatic potential within the spherical zone. However, we can avoid solving the non-linear Poisson–Boltzmann equation and use the relation between the pressure tensor  $P(r)\delta_{ij}$  and the Maxwell stress tensor [21]

$$T_{ij}(r) = \frac{\varepsilon}{4\pi} \left( E_i(r)E_j(r) - \frac{E^2(r)}{2} \delta_{ij} \right) \quad (2.59)$$

where  $\delta_{ij}$  is the unit tensor and  $E_i(r)$  is the  $i$ th component of the electric field vector. Since the system is in equilibrium, the mechanical and electrostatic forces are balanced at each point within a cell. This leads to the following relation between the pressure and the Maxwell stress tensor

$$\nabla_i P(r)\delta_{ij} - \nabla_i T_{ij}(r) = 0 \quad (2.60)$$

The integral of the last equation over the volume of the spherical zone reduces to the integral over the zone boundaries. The value of the electric field at the outer boundary of the spherical zone is equal to zero due to electroneutrality of the two zones,  $E(R_{\text{cell}}) = 0$ . The value of the pressure tensor at the outer boundary

of the spherical region is equal to the osmotic pressure

$$\begin{aligned} \pi &= P(R_{\text{cell}}) = k_B T c(R_{\text{cell}}) \\ &= k_B T c(R) - \frac{\varepsilon E^2(R)}{8\pi} \\ &= \frac{k_B T}{2\pi l_B R^2} ((\gamma_R - 1)^2 - \alpha^2 - \gamma_R^2) \end{aligned} \quad (2.61)$$

where parameter  $\alpha$  is the exponent related to the decay of the counterion density profile in the cylindrical zone and is given by Eq. (2.57).

Dividing the osmotic pressure by the ideal pressure of all counterions,  $k_B T f_N / V_{\text{cell}}$ , we obtain the prediction of the two-zone model for the osmotic coefficient

$$\phi^{\text{osm}} = \frac{V_{\text{cell}}}{2V_{\text{in}}\gamma_0} [(\gamma_R - 1)^2 - \alpha^2 - \gamma_R^2] \quad (2.62)$$

where  $V_{\text{cell}}$  and  $V_{\text{in}}$  are the total cell volume and volume of the cylindrical region, respectively. Eq. (2.62) for the osmotic coefficient reduces to that derived for the Katchalsky's cell model [56] in the case  $\gamma_R = 0$  corresponding to semidilute polyelectrolyte solutions with the length of the polyion larger than the distance between polyions ( $V_{\text{cell}} = V_{\text{in}}$ )

$$\phi_{\text{cell}}^{\text{osm}} = \frac{1 - \alpha^2}{2\gamma_0} \quad (2.63)$$

The osmotic coefficient in semidilute solutions (see Eq. (2.63)) is proportional to the fraction of 'free counterions'  $1/\gamma_0$  [5,50,56].

Eq. (2.62) can be simplified in the limit of not very large values of the parameter  $\gamma_R \geq 1$  by assuming that the variations of the electrostatic potential over the spherical zone are small and, therefore, counterions are distributed almost uniformly in the spherical zone with the average concentration

$$c(R_{\text{cell}}) \approx \frac{f_R N}{V_{\text{out}}} \approx \frac{\gamma_R L}{l_B V_{\text{out}}} \quad (2.64)$$

where  $V_{\text{out}}$  is the volume of the outside (spherical) zone. Using this approximation, we can write the following expression for the osmotic coefficient of the

two-zone model

$$\phi_{\text{dilute}}^{\text{osm}} \approx \frac{c(R_{\text{cell}})V}{fN} = \frac{\gamma_{\text{R}}}{\gamma_0} \left( 1 + \frac{\pi L^3}{4V_{\text{out}}} \right) \quad (2.65)$$

Eq. (2.65) implies that in dilute solutions ( $V_{\text{out}} > L^3$ ) the osmotic coefficient is proportional to the fraction of counterions that are outside the cylindrical zone  $\gamma_{\text{R}}/\gamma_0$ . At infinite dilution, the osmotic coefficient  $\phi^{\text{osm}}$  approaches unity indicating that almost all counterions are outside the cylindrical zone and  $\gamma_{\text{R}} \approx \gamma_0$ .

Fig. 14 shows the osmotic coefficient of rod-like (Fig. 14(a)) and flexible fully charged (Fig. 14(b)) polyelectrolytes in dilute salt-free solutions [61]. The solid lines in Fig. 14(a) are the predictions of the zero-order approximation two-zone model (Eq. (2.65)) without any adjustable parameters. These figures show a decrease in the osmotic coefficient  $\phi^{\text{osm}}$  with increasing polymer concentration  $c$ . This behaviour is not only in good qualitative agreement, but for some data, even in good quantitative agreement with the predictions of the two-zone model. To verify the predictions of Eq. (2.65) for the osmotic coefficient, Fig. 15 shows a universal plot of the reduced osmotic coefficient  $\gamma_0 \phi^{\text{osm}}/\gamma_{\text{R}}$  as a function of the normalized polymer concentration  $c/c^*$ .

For the rod-like chains, we define the overlap concentration  $c^*$  as monomer concentration in the cylindrical zone  $4N/(\pi L^3)$ . All points collapse onto the universal curve as predicted by Eq. (2.65) for rod-like polyelectrolyte solutions (see Fig. 15(a)). However, the size  $R_c$  of flexible chains is a function of polymer concentration because polyelectrolytes contract with increasing concentration. To collapse all points into one universal curve and to take into account the chain contraction in Fig. 15(b), the reduced osmotic coefficient  $\gamma_0 \phi^{\text{osm}}/\gamma_{\text{R}}$  is plotted versus the ratio of polymer concentration  $c$  to monomer concentration within a cylindrical region  $c\pi[R_c(c)]^3/(4N)$ . All points once again collapse into one universal curve, proving that the two-zone model adequately describes simulation results for flexible chains as well.

The Poisson–Boltzmann approach to description of electrostatic potential near macroions fails when there are strong correlations between counterions.

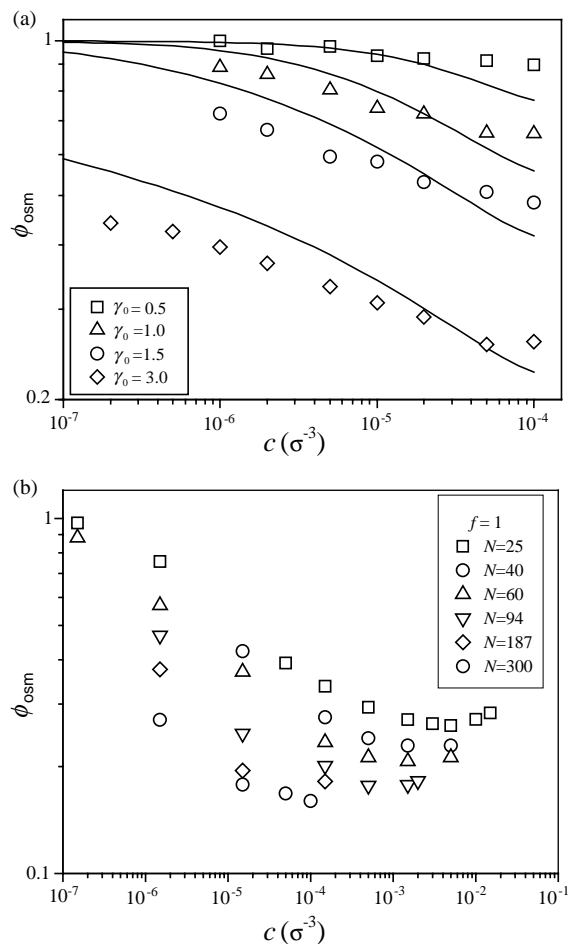


Fig. 14. (a) Dependence of the osmotic coefficient of rod-like polyions on polymer concentration in dilute solutions. Open symbols are simulation results. The lines are predictions of zero-order approximation of the two-zone model. From top to bottom, the parameter  $\gamma_0$  is 0.5, 1.0, 1.5, and 3.0, respectively. (b) Dependence of the osmotic coefficient of flexible polyions on polymer concentration in dilute solutions of strongly charged polyelectrolyte chains ( $f=1$ ). Reproduced with permission from Liao, Q., Dobrynin, A.V., & Rubinstein, M. *Macromolecules* 36, 3399–3410 (2003). [61] Copyright 2003, American Chemical Society.

This takes place either in the system with multivalent counterions or in the case of large values of the Bjerrum length  $l_{\text{B}}$ . We refer readers to Refs. [62–64] for the detailed discussion of this subject.

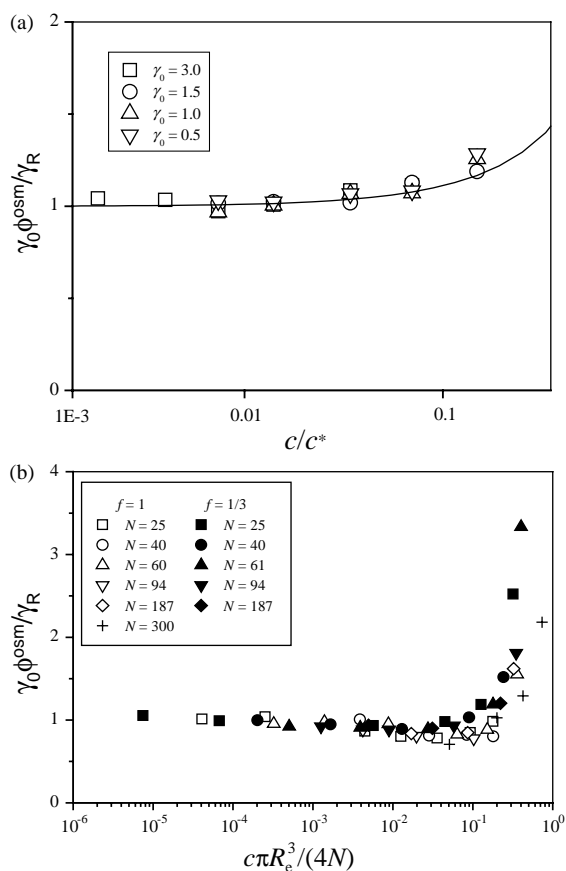


Fig. 15. Universal plots of the reduced osmotic coefficient  $\gamma_0 \phi / \gamma_R$  as a function of normalized polymer concentration (a) rigid and (b) flexible chains. The solid line corresponds to prediction of zero-order approximation of the two-zone model (Eq. (2.65)). Reproduced with permission from Liao, Q., Dobrynin, A.V., & Rubinstein, M. *Macromolecules* 36, 3399–3410 (2003). [61] Copyright 2003, American Chemical Society.

### 2.4.3. Ion-binding and ion localization models for counterion condensation

The ion-binding model was originally developed to describe the ionization equilibrium in polyelectrolytes [48,54,65]. This model also separates counterions into two different classes: bound and free counterions. The bound counterions are complexed with oppositely charged groups on the polymer backbone, forming dipoles, while free counterions can move freely through the solution. Under these assumptions, the chemical potentials of both bound and free counterions are calculated.

The chemical potential of bound counterions has the following contributions:

- (i) An entropic contribution due to redistribution of bound counterions between different charged groups along the polymer backbone. For polyelectrolyte chain with  $fN$  monomers carrying ionic groups and having  $(1-\beta)fN$  of these groups ionized this contribution is

$$\mu_{\text{bind}}^{\text{entr}} = k_B T \ln \left( \frac{\beta}{1-\beta} \right) \quad (2.66)$$

- (ii) The localization of counterions within volume  $v$  near the binding site results in an additional penalty, which depends on the localization volume logarithmically

$$\mu_{\text{bind}}^{\text{local}} = -k_B T \ln(v) \quad (2.67)$$

- (iii) Formation of ion pairs also changes the local solvent structure. This contribution to the counterion chemical potential has both entropic and energetic parts. The entropic part is due to the solvent rearrangement around the ion pair and the energetic contribution is due to electrostatic interactions between solvent molecules and ions of both types. This contribution to the chemical potential of bound ions is usually measured with respect to the chemical potential in the ionized state and considered as an input parameter of the theory. We will denote this part of the bound ion chemical potential as  $\Delta\mu_{\text{bind}}$ .

The ‘free’ counterions are still free to explore the whole volume of the system. Their chemical potential has

- (i) An entropic contribution due to the translational entropy of counterions

$$\mu_{\text{free}}^{\text{trans}} \approx k_B T \ln[(1-\beta)fc] \quad (2.68)$$

- (ii) An electrostatic contribution due to interactions between ionized groups along the polymer backbone leading to the increase of chain free

energy

$$\mu_{\text{free}}^{\text{electr}} \approx \frac{k_B T}{g_0^2 f (1-\beta)} \approx k_B T u^{2/3} f^{1/3} (1-\beta)^{1/3} \quad (2.69)$$

Here, we used the scaling model of the polyelectrolyte chain in a  $\Theta$ -solvent (Eq. (2.13a)) to obtain expression (2.69) for the electrostatic part of the chemical potential of the chain.

In equilibrium, the chemical potentials of bound and free counterions are equal to each other. The fraction of bound counterions is given by the following non-linear equation

$$\frac{\beta}{(1-\beta)^2} \approx f \phi \exp \left[ u^{2/3} f^{1/3} (1-\beta)^{1/3} - \frac{\Delta\mu_{\text{bind}}}{k_B T} \right] \quad (2.70)$$

where  $\phi = cv$  is the polymer volume fraction in solutions with polymer concentration  $c$ . It follows from this equation that connecting charged monomers into chains (the first term in the square brackets) shifts ionization equilibrium towards the formation of ionic pairs (increasing  $\beta$ ) in comparison with the ionization equilibrium in a monomeric system [48]. For a polymer in a  $\Theta$ -solvent, the fraction of bound counterions increases monotonically with increasing polymer volume fraction.

The counterion binding model presented above can be extended to the poor solvent condition for polymer backbone. In this case, the expression for the chemical potential describing the interactions between ionized groups on a necklace has a qualitatively different form

$$\mu_{\text{free}}^{\text{electr}} \approx k_B T \frac{u^{1/3} |\tau|}{f^{1/3} (1-\beta)^{1/3}} \quad (2.71)$$

Taking into account this expression for the electrostatic part of the chemical potential, Eq. (2.70) can be rewritten for polyelectrolytes in poor solvents as

$$\frac{\beta}{(1-\beta)^2} \approx f \phi \exp \left[ \frac{u^{1/3} |\tau|}{f^{1/3} (1-\beta)^{1/3}} - \frac{\Delta\mu_{\text{bind}}}{k_B T} \right] \quad (2.72)$$

It follows from this equation that the electrostatic energy per charged monomer increases with increasing number of bound counterions. This induces an additional influx of counterions to compensate for the growing electrostatic energy and sets up an

avalanche-like counterion condensation and an abrupt first-order transition into a globule state [47–49].

The formation of ion pairs on the polymer backbone results in additional dipole–dipole attractive interactions. These extra attractive interactions decrease the second virial coefficient shifting the position of the  $\Theta$ -temperature. The shift of the  $\Theta$ -temperature in the case of strongly charged polyelectrolytes could be significant leading to chain collapse. A detailed analysis of counterion condensation on the chain conformations in different temperature regimes was presented by Schiessel and Pincus [66] and by Schiessel [67].

The description of counterion condensation in the counterion localization model is similar to the ion-binding model. The only difference is the treatment of condensed counterions. In the counterion localization model, the condensed counterions are free to move inside the volume of a chain (see Refs. [47,49]). Such consideration of condensed counterion changes the entropic contribution to the counterion's chemical potential. It is due to translational entropy of counterions inside the volume of the chain. The interactions of counterions with the surrounding charged background can also be included into the model (see for details Ref. [68]). These interactions lead to the effective monomer–monomer attraction and could induce chain collapse at relatively large values of the Bjerrum length.

Recently, Kramarenko et al. [55] introduced a three-state model of counterion condensation in dilute polyelectrolyte solutions. This model introduces three possible states for counterions: free counterions inside and outside the polyelectrolyte chain and bound counterions forming ionic pairs with the corresponding sites on the polymer backbone. This model has features of both ion-binding and counterion localization models. The formation of ionic pairs becomes extremely important when the polyelectrolyte chain collapses, expelling solvent molecules from the chain interior and lowering the effective local dielectric constant. The decrease of the dielectric constant promotes further ion pairing and chain collapse.

The models for counterion condensation, discussed above, assume uniform distribution of charges along the polymer backbone and neglect the effects of chain ends. In Section 2.2, we have shown that the polyelectrolyte chain is non-uniformly stretched.

The non-uniform stretching of the chain results in charge depletion in the middle of the chain and additional charge accumulation at the chain ends (see for details [28,69]). This counterion redistribution occurs because the polyelectrolyte is stronger stretched in the middle than at the chain ends leading to the increase of the effective linear charge density towards chain ends.

#### 2.4.4. Effect of counterion condensation on chain size and chain conformation

As we have shown in previous sections, the number of condensed counterions increases with increasing polymer concentration. The polyelectrolyte conformations are controlled by the fraction of ionized groups. Thus, counterion condensation leads to weakening of electrostatic interactions and promotes shrinkage of polyelectrolyte chains. The decrease of chain size with increasing polymer concentration is supported by the results of computer simulations [26,70–73]. Fig. 16 shows the variation in chain size for partially charged chains with  $f=1/3$  [26].

The strength of the electrostatic interactions is also influenced by the dielectric constant of a polyelectrolyte solution. Experimentally, dielectric constant

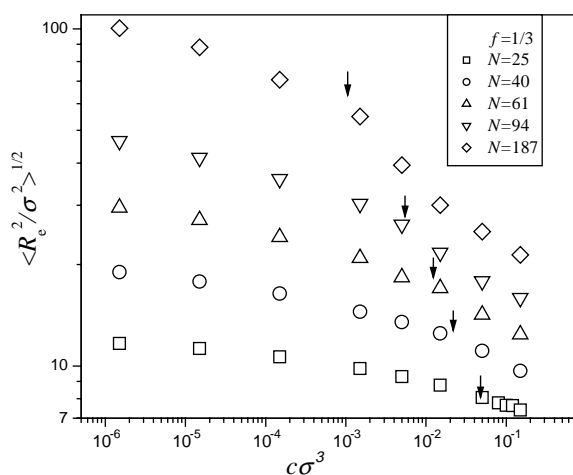


Fig. 16. Concentration dependence of the size of partially charged chains with  $f=1/3$ . The overlap concentrations are marked by arrows. Reproduced with permission from Liao, Q., Dobrynin, A.V., & Rubinstein, M. *Macromolecules* 36, 3386–3398 (2003). [26] Copyright 2003, American Chemical Society.

can be continuously changed by using mixed solvents. At constant polymer concentration, the increase of the strength of the electrostatic interactions induced by the decrease of the dielectric constant first leads to stretching of the polyelectrolyte chain. In a  $\Theta$ -solvent for polymer backbone the chain size is proportional to the 1/3 power of interaction parameter  $u$ ,  $R_e \sim u^{1/3}$  (see Eq. (2.8)). However, as the strength of electrostatic interactions increases further, the counterion condensation reduces the effective charge on polyelectrolyte chains. More counterions form ionic pairs in solutions with stronger electrostatic interactions leading to the additional attraction between monomers and shrinkage of polyelectrolyte chains. Thus, the size of a polyelectrolyte chain is expected to show the non-monotonic dependence on the strength of the electrostatic interactions (the value of the Bjerrum length  $l_B$ ). Brilliantov et al. [68] have applied the one-component plasma model to describe electrostatic interactions induced by condensed counterions. This model predicts an abrupt transition between stretched and collapsed chain conformations. The predictions of the model are in reasonably good qualitative agreement with the results of molecular dynamics simulations by Winkler et al. [74]. The collapse of polymer chains can also be described by introducing renormalization of the second virial coefficient due to the dipole–dipole and the ion–dipole interactions inside polymer coils [54]. This model predicts the non-monotonic dependence of the polymer size on the interaction parameter  $u$ , but in this case the chain size varies smoothly with the interaction parameter.

A comprehensive study of the effect of the counterion condensation on the necklace formation in dilute polyelectrolyte solutions was performed by Limbach and Holm [75]. They concluded that the polyelectrolyte chain adopts necklace conformation only in the narrow range of the interaction parameter. At finite polymer concentrations, the necklace stability region is strongly influenced by the counterion condensation. A similar trend was observed in Monte Carlo simulations of titration of hydrophobic polyelectrolytes by Ulrich et al. [76]. Depending on the solvent quality for the polymer backbone and the  $\text{pH}-\text{p}K_0$  value, polyelectrolyte chains were found in five different conformation states: coil, collapsed spherical globule, necklace globule, sausage-like aggregate and fully stretched chain.

### 2.5. Effects of added salt on chain conformations and electrostatic persistence length

The electrostatic interactions between charged monomers in solutions with finite salt concentrations are screened by salt ions and their strength decreases exponentially with the distance between charges (see Eq. (2.1)). However, the charges still interact through the unscreened Coulomb potential at distances much smaller than the Debye screening length  $r_D$ . A polyelectrolyte chain does not feel the presence of salt if the Debye screening length is much larger than the chain size  $R_c$ . At high salt concentrations such that the Debye screening length  $r_D$  is smaller than the electrostatic blob size  $D_e^0$ , the electrostatic interactions can be viewed as the short-range ones with the effective monomeric second virial coefficient  $B_{e1}$  proportional to  $f^2 l_B r_D^2$ . At these salt concentrations, a polyelectrolyte chain has the same structure as a neutral polymer in a good solvent.

It was proposed by Odijk [77] and by Skolnick and Fixman [78] (OSF) that at intermediate salt concentrations,  $D_e^0 < r_D < R_c$ , the intrachain electrostatic interactions induce additional chain stiffening beyond the Debye screening length  $r_D$ . Thus, a polyelectrolyte chain in salt solutions behaves as a semiflexible polymer with salt-concentration-dependent persistence length.

The original derivation of the electrostatic persistence length is based on the evaluation of the change of the electrostatic energy as polymer conformation deviates from a straight line. Let us consider a

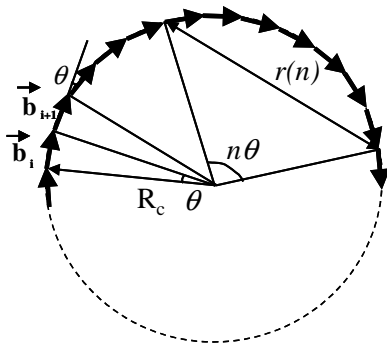


Fig. 17. Schematic representation of the conformation of a polyelectrolyte chain for calculation of the OSF electrostatic persistence length.

variation in the electrostatic energy of a fully charged polyelectrolyte chain ( $f=1$ ) with bond length  $b$  by bending the chain into a circle with radius  $R_c = b/[2 \sin(\theta/2)]$  (see Fig. 17). The distance between two monomers separated by  $n$  bonds along the polymer backbone in such conformation is equal to

$$r(n) = 2R_c \sin(n\theta/2) \\ = \frac{b \sin(n\theta/2)}{\sin(\theta/2)} \approx_{\theta \ll 1} bn(1 - n^2\theta^2/24) \quad (2.73)$$

The difference between the electrostatic energy per monomer in the circular and rod-like conformations is

$$\frac{\Delta U_{\text{electr}}(\theta)}{k_B T} \\ \approx l_B \sum_{n=1}^{\infty} \left( \frac{\exp(-\kappa r(n))}{r(n)} - \frac{\exp(-\kappa bn)}{bn} \right) \approx_{\kappa b \ll 1} \frac{l_B}{8\kappa^2 b^3} \theta^2 \quad (2.74)$$

The expression (2.74) was obtained [22] by substituting expression for  $r(n)$  (Eq. (2.73)) into the right-hand side of Eq. (2.74) and expanding it into the power series over  $\theta$ . A chain in the circular configuration makes a complete turn after  $n_p \propto \theta^{-1}$  steps leading to the persistence length  $b\theta^{-1}$ .

In the OSF derivation of the electrostatic persistence length [77,78], it was assumed that such bending of a chain can be induced by thermal fluctuations if the change in the electrostatic energy per persistence length  $n_p \Delta U_{\text{electr}}(\theta)$  is on the order of the thermal energy  $k_B T$ . This leads to the typical values of the bending angle  $\theta_{\text{OSF}} \approx \kappa^2 b^3 / l_B$  and the OSF electrostatic persistence length equal to

$$l_p^{\text{OSF}} \approx \frac{b}{\theta_{\text{OSF}}} \approx \frac{l_B r_D^2}{4b^2} \quad (2.75a)$$

The original OSF derivation [77,78] was done for intrinsically rigid chains for which the total persistence length is the sum of the electrostatic contribution given by Eq. (2.75a) and of the bare persistence length  $l_p^0$ .

Odijk [79] applied Eq. (2.75a) to describe solution properties of flexible strongly charged polyelectrolytes with the electrostatic interaction parameter  $u f^2 \approx 1$ . In this case, the electrostatic contribution to the chain persistence length  $l_p^{\text{OSF}}$  is the main factor

controlling the bending rigidity of the polyelectrolyte. The additional chain stiffening of these polyelectrolytes could occur at distances substantially larger than the Debye screening length  $r_D$ . The Odijk result was extended to flexible weakly charged polyelectrolytes with  $uf^2 \ll 1$  by Khokhlov and Khachaturian [24] by considering electrostatic blobs of size  $D_e^0$  [23] as new effective monomers

$$l_p^{KK} \approx \frac{r_D^2}{D_e^0} \quad (2.75b)$$

This result for weakly charged chains was rederived in the framework of the variational approach by several authors [80–82].

Since 1977, there were series of attempts to confirm or disprove the OSF result for electrostatic persistence length [80–85]. Schmidt [85] used a variation of the Flory approach to calculate the chain size and persistence length. In this approach, the electrostatic energy of the chain was evaluated using the worm-like chain distribution function for the average mean-square distance between monomers. The numerical minimization displays weaker than  $r_D^2$  dependence without pure scaling regime. The electrostatic persistence length at high salt concentrations appears to asymptotically approach  $r_D$ . Barrat and Joanny [86] used a variational approach with the trial function describing the chain under tension. They found a linear dependence of the electrostatic persistence length on the Debye length. In a series of papers [81,87], Ha and Thirumalai applied the Edwards and Singh variational principle [88], minimizing the error in the chain mean-square end-to-end distance between the trial chain and the actual polymer chain. The results of this minimization procedure depend on the value of the parameter  $uf^2$ . For weakly charged chains with  $uf^2 \ll 1$ , the electrostatic persistence length is proportional to  $r_D^2$ . However, in the limit  $uf^2 \rightarrow 1$ , the linear  $r_D$  dependence of the electrostatic persistence length was reproduced. Manghi and Netz [82] have recently argued that Ha and Thirumalai's prediction [81,87] for  $r_D$  dependence of the electrostatic persistence length is a result of the incorrect elimination of the divergence in the expression for chain entropy. The linear  $r_D$  dependence of the electrostatic persistence length was also derived by Muthukumar et al. [89,90].

Netz and Orland [80] and Manghi and Netz [82] have applied Gaussian variational principle considering electrostatic persistence length as an adjustable parameter. This approach leads to  $r_D^2$  dependence of the electrostatic persistence length reproducing Khokhlov–Khachaturian's result [24] for weakly charged chains.

The linear dependence of the electrostatic persistence length on the Debye screening length  $r_D$  is supported by computer simulations of weakly charged polyelectrolyte chains [91–97] and some experiments [98–104]. The recent computer simulations [105–107] have shown that in order to distinguish between the two limiting cases of the salt concentration dependence of the electrostatic persistence length, one has to go to very long chains ( $N > 512$ ). For shorter chains, the difference between quadratic and linear dependence of the electrostatic persistence length on the Debye screening length  $r_D$  is not numerically significant. However, for longer chains with  $N > 1024$ , there is a deviation from the linear dependence but not sufficient enough to rule it out completely. However, the analysis of the data was done by assuming two pure asymptotic regimes for electrostatic persistence length  $l_p \sim r_D^2$  and  $r_D$  neglecting logarithmic corrections to both results. These logarithmic corrections are due to local chain stretching and could be important for longer chains with a degree of polymerization  $N > 1024$  as we described in Section 2.2 on non-uniform chain stretching in dilute salt-free solutions.

In order to describe the possible origin of different dependence of the electrostatic persistence length on the Debye screening length, consider a freely rotating polyelectrolyte chain with adjustable, but uniform

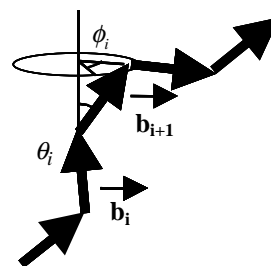


Fig. 18. Conformation of a polyelectrolyte chain with the arbitrary distribution of torsion angles  $\phi_i$  and bond angles  $\theta_i$ .

(same for all bonds) value of the bond angle  $\theta$  (see Fig. 18) [10]. While the values of the bond angles are fixed, the torsion angles can assume any values from the interval  $-\pi \leq \phi_i \leq \pi$ . In this approach, we assume that the electrostatic repulsion between charged monomers imposes constraints on the bond angles in comparison with those for freely jointed (neutral) polymer chain. The optimal value of the bond angle is then found by minimizing the sum of electrostatic and entropic (conformational) contributions to the free energy of the chain with respect to the bond angle  $\theta$ . In the limit of small bond angles, the freely rotating chain model reduces to the worm-like chain model with the orientational memory between two vectors  $\mathbf{b}_i$  and  $\mathbf{b}_{i+n}$  decaying exponentially with the number of bonds  $n$  between them [10]

$$\begin{aligned} \langle (\mathbf{b}_i \cdot \mathbf{b}_{i+n}) \rangle_\phi &= b^2 \langle \cos(\theta(n)) \rangle_\phi \approx b^2 \langle \cos(\theta) \rangle^n \\ &\approx b^2 \exp(-n\theta^2/2) \end{aligned} \quad (2.76)$$

where brackets  $\langle \rangle_\phi$  denote the average over torsion angles  $\phi_i$ . The characteristic length of orientational correlations [10] is equal to  $2/\theta^2$ . The square of the angle  $\theta(n)$  between any two bond vectors separated by  $n$  bonds along the polymer backbone is equal to  $n\theta^2$  ( $\langle \theta(n)^2 \rangle \approx n\theta^2$ ), which is a direct result of the randomness in the torsion angles distribution.

The mean-square average distance between two monomers of this chain separated by  $n$  bonds is equal to [10]

$$\langle \mathbf{r}(n)^2 \rangle_\phi \approx \frac{8b^2}{\theta^4} \left( \exp\left(-\frac{n\theta^2}{2}\right) + \frac{n\theta^2}{2} - 1 \right) \quad (2.77)$$

(In the derivation of Eq. (2.77), it is assumed that the typical values of the angle  $\theta$  are small so that  $\cos(\theta)$  can be approximated  $\cos(\theta) \approx 1 - \theta^2/2$ . At short distances along the polymer backbone,  $n\theta^2 \ll 1$ , the conformation of the chain is close to the rod-like with the average mean-square distance  $\langle \mathbf{r}(n)^2 \rangle_\phi \approx b^2 n^2$ . At larger distances along the polymer backbone,  $n\theta^2 \gg 1$  the orientational memory is lost and the chain behaves as an ideal chain with the persistence length

$$l_p \approx 2b/\theta^2 \quad (2.78)$$

and the mean-square distance between two monomers varies linearly with the number of bonds  $n$  between them,  $\langle \mathbf{r}(n)^2 \rangle_\phi \approx 4b^2 \theta^{-2} n$ . The difference of the

electrostatic energy per monomer between a freely rotating chain with bond angle  $\theta$  and a rigid rod is equal to

$$\begin{aligned} &\frac{\langle \Delta U_{\text{electr}}(\theta) \rangle_\phi}{k_B T} \\ &\approx l_B \sum_{n=1}^{\infty} \left( \frac{\exp(-\kappa \sqrt{\langle \mathbf{r}(n)^2 \rangle_\phi})}{\sqrt{\langle \mathbf{r}(n)^2 \rangle_\phi}} - \frac{\exp(-\kappa b n)}{b n} \right) \Big|_{\kappa b \ll 1} \approx \frac{l_B \theta^2}{\kappa b^2} \end{aligned} \quad (2.79)$$

In the derivation of Eq. (2.79) we use the following expansion for

$$\sqrt{\langle \mathbf{r}(n)^2 \rangle_\phi} \Big|_{n\theta^2 \ll 1} \approx b n \left( 1 - \frac{n\theta^2}{12} \right) \quad (2.80)$$

By imposing the angular constraint one changes the number of available states in bond orientational space. For a freely rotating chain with the fixed bond angle  $\theta_i = \theta$  and unrestricted torsion angles  $\phi_i$  each bond vector is localized on a circle of radius  $b \sin(\theta)$  (see Fig. 18). The number of states  $\Omega(\theta)$  available to a bond vector is proportional to the circumference  $2\pi b \sin(\theta)$ , which for small values of the bond angle is proportional to angle  $\theta$ ,  $\Omega(\theta) \propto \theta$ . Thus, for a chain with the bare persistence length  $b$  the entropy change due to imposed angular constraint depends logarithmically on the value of the bond angle  $\theta$

$$\Delta S(\theta) \approx k_B \ln(\Omega(\theta)) \approx k_B \ln(\theta) \quad (2.81)$$

The free energy change per bond of a chain with electrostatic interactions is equal to the sum of entropic Eq. (2.81) and energetic Eq. (2.79) contributions

$$\frac{F(\theta)}{k_B T} \approx -\ln(\theta) + \frac{l_B \theta^2}{\kappa b^2} + \text{const} \quad (2.82)$$

Minimization of this expression with respect to angle  $\theta$  leads to the optimal angle value  $\theta$  to be on the order of  $\sqrt{\kappa b^2 / l_B}$ . This results in the linear dependence of the electrostatic persistence length on the Debye screening length  $r_D$

$$l_p^{\text{WLC}} \approx 2b/\theta^2 \approx \kappa r_D \quad (2.83)$$

Thus, minimization of Eq. (2.82) with respect to angle  $\theta$  corresponds to optimization of the chain persistence length. There is very simple interpretation of the electrostatic contribution to the chain persistence length.

It is proportional to the energy of electrostatic interactions between two chain segments with length on the order of the Debye screening length  $r_D$  carrying  $r_D/b$  charged monomers and separated by a distance  $r_D$ ,  $\tilde{\epsilon}_{\text{elect}} \approx k_B T l_B (r_D/b)^2 / r_D \approx k_B T u r_D / b$ .

There are two important differences between the result of OSF and of the free energy minimization based on the freely rotating chain model. In the OSF calculations it is assumed that the main deformation mode of the chain is the circular mode. However, this deformation mode has a stronger dependence of the electrostatic energy on the Debye screening length (see Eq. (2.74)) than in the case of the freely rotating chain model with the average electrostatic energy given by Eq. (2.79). Therefore, for similar bond angles  $\theta$  the circular mode has a larger value for the electrostatic energy. To offset this fast increase in the electrostatic energy as a function of the angle  $\theta$  in the circular conformation one needs smaller values for the bond angles. This increases the bond alignment and polyelectrolyte persistence length. The weaker dependence of the average electrostatic energy on the Debye screening length (see Eq. (2.79)) indicates that there are other softer deformation modes that have lower electrostatic energies and provide dominant contributions to the chain partition function. Thus, by allowing fluctuations of the torsion angles one increases the separation between ionic groups and therefore lowers the electrostatic energy of the chain. Another important difference between the OSF approach and the free energy minimization approach is the entropic penalty for bond orientation. In the free energy minimization approach, this penalty is on the order of the thermal energy  $k_B T$  per oriented bond (for the freely rotating chain model the entropy change due to imposed angular constraint depends logarithmically on the value of the angle  $\theta$  ( $\Delta S(\theta) \approx k_B \ln(\theta)$ ) while in the OSF approach it is  $k_B T$  per persistence length. The bond orientational entropy prevents the extreme alignments of the bonds into rod-like conformation, which would otherwise be energetically favourable. Thus, the decrease in the chain bending energy occurs at the expense of the bond orientational entropy. It is worth mentioning that the optimization of the free energy (Eq. (2.82)) of the freely rotating chain with respect to the bond angle is similar to the Flory-like approach to the optimization of the polyelectrolyte chain size described in Section 2.1.

### 3. Semidilute polyelectrolyte solutions

#### 3.1. Overlap concentration

Polyelectrolyte chains begin to overlap when the distance between them becomes on the order of their size. For non-uniformly stretched chains, the relation between the number of monomers  $N$  and chain size  $R_e^F$  in salt-free solutions is given by Eq. (2.8). Thus, the overlap concentration  $c^*$  can be estimated as

$$c^* \approx \frac{N}{(R_e^F)^3} \approx b^{-3} u^{-1} f^{-2} N^{-2} \ln^{-1}(N/g_e) \quad (3.1)$$

In order to verify this modified scaling prediction with logarithmic correction, the dependence of the overlap concentration  $c^*$  on the degree of polymerization  $N$  for partially  $f=1/3$  (circles) and fully  $f=1$  (squares) charged chains is presented in Fig. 19(a) [26]. The solid and dashed lines correspond to Eq. (3.1) for different values of  $f$ . The dependence of the overlap concentration  $c^*$  on the degree of polymerization  $N$  follows the modified scaling predictions given by Eq. (3.1) for the longer chains but deviates from it for shorter ones. This deviation from the scaling law can be attributed to the finite size effect. Short chains are not stretched enough to satisfy the strong stretching approximation in the evaluation of their sizes. It follows from Fig. 19(a) that the simulation curves for both charge densities  $f=1$  and  $f=1/3$  have similar shapes. In Fig. 19(b), the simulation results are collapsed onto one universal curve. The numerical factor for this transformation is equal to 0.4. According to the scaling theory this factor should be inversely proportional to the square of the ratio of the effective charge densities on the chains  $[f_*(1/3)/f_*(1)]^2 = 0.4$ . For weakly charged chains with bare charge density  $f=1/3$ , this conversion factor is equal to  $[1/3/(1)]^2 = 0.11$ . This discrepancy between 0.11 and 0.4 can be explained by the counterion condensation. The ratio of the effective charge fractions on the two chains obtained from the osmotic coefficient is  $f_*(1/3)/f_*(1) = 0.69$  (see Ref. [61]), which is close to the expected value  $f_*(1/3)/f_*(1) = \sqrt{0.4} \approx 0.63$ . Thus, effective charge densities  $f_*$  rather than the bare ones have to be used for the evaluation of the conversion factor. Below we will use  $f_*$  to describe the effective charge density on

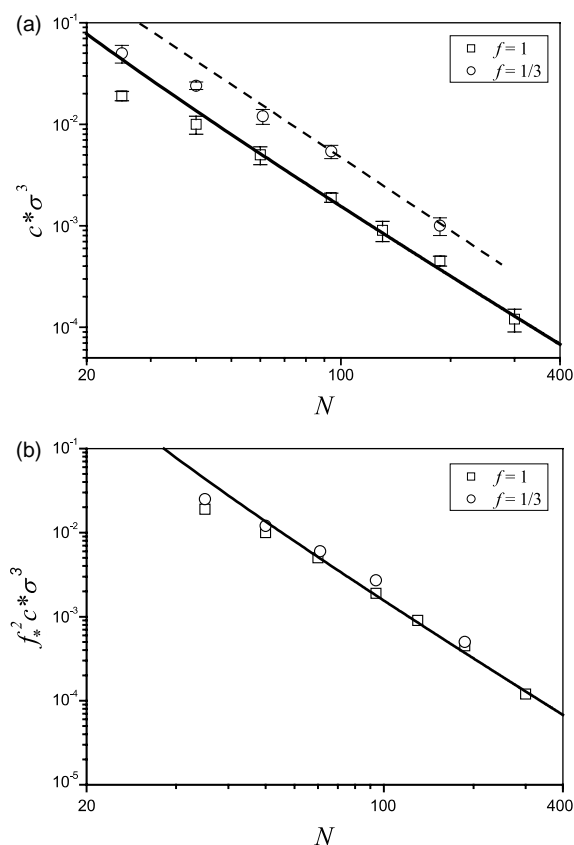


Fig. 19. (a) Dependence of the overlap concentration on the number of monomers for partially  $f=1/3$  (circles) and fully  $f=1$  (squares) charged chains. Lines are predictions of Eq. (3.1). (b) Universal curve for the dependence of the overlap concentration on the number of monomers. The solid line is given by  $c^* f^2 \sim N^{-2}/\ln N$ . Reproduced with permission from Liao, Q., Dobrynin, A.V., & Rubinstein, M. *Macromolecules* 36, 3386–3398 (2003). [26] Copyright 2003, American Chemical Society.

the polymer backbone rather than its bare value  $f$  and consider it as an adjustable parameter. Experimentally this value can be evaluated from conductivity [108, 109] or from the osmotic pressure measurements.

### 3.2. Scaling model of semidilute polyelectrolyte solutions

#### 3.2.1. Correlation length

The important length scale above the overlap concentration,  $c > c^*$ , is the correlation length  $\xi$ —

the average mesh size of the semidilute polyelectrolyte solution. The average charge of the correlation volume  $\xi^3$  is equal to zero because the charge on the section of the chain with  $g_\xi$  monomers within the correlation length  $\xi$  is compensated by counterions. The interactions between correlation volumes can be ignored in the zero order approximation, and the electrostatic blob size and stretching of a chain can be estimated by taking into account only electrostatic interactions within the correlation volume  $\xi^3$ . In fact, the multipole expansion of electrostatic interactions between correlation volumes starts with quadrupole–quadrupole terms due to cylindrical symmetry inside the correlation volume. Thus, each charged monomer experiences electrostatic repulsion from all other charged monomers within the correlation volume and electrostatic attraction to the counterion background. This corresponds to the well-known Katchalsky's cell model approximation (see Section 2.4.2) [3,56,58,59]. Electrostatic interactions within a correlation cell with radius  $\xi/2$  and length  $\xi$  can be estimated by assuming that the cell has cylindrical symmetry with the polyelectrolyte chain located along the axis of the cylinder (see Fig. 20).

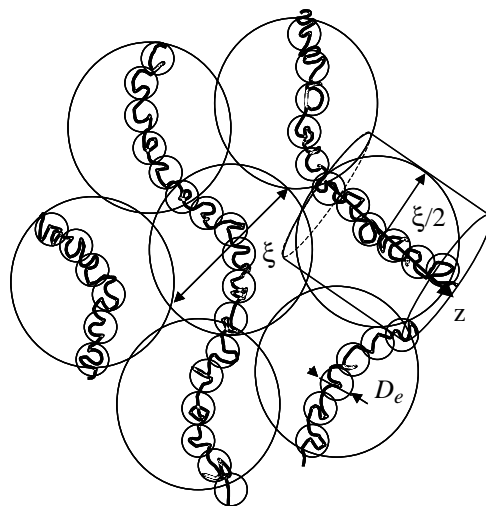


Fig. 20. Schematic representation of a semidilute polyelectrolyte solution.

The electrostatic interactions per monomer located at point  $z_m$  along the chain axis are

$$\begin{aligned} \frac{U_{el}}{k_B T} = & 2l_B f_*^2 \int_{D_e(z_m)/2}^{\xi/2} \frac{g_e(z)}{D_e(z)} \frac{dz}{z} + \frac{l_B f_*^2 g_e(z_m)}{D_e(z_m)} \\ & - 2\pi l_B f_* \int_{-\xi/2}^{\xi/2} dz \int_0^{-\xi/2} \frac{c_{count}(r)r dr}{\sqrt{z^2 + r^2}} \end{aligned} \quad (3.2)$$

where  $c_{count}(r)$  is the counterion density profile. The first two terms in Eq. (3.2) describe the intrachain electrostatic interactions between a charged monomer and the chain section within correlation length  $\xi$  (see Eq. (2.17b)). The last term in this equation corresponds to the attraction of the charged monomer to the counterion background. Since each monomer on the polyelectrolyte chain experiences on average the same electrostatic interactions, except for the monomers that are close to chain ends, we can assume that chains are uniformly stretched so that  $g_e(z)/D_e(z) = g_e/D_e = \text{const}$ . In this case, the first integral over  $z$  in Eq. (3.2) can be easily evaluated. The last integral can also be evaluated if the counterion density profile around the polyelectrolyte chain is known. However, in order to obtain scaling relations between correlation length  $\xi$  and polymer concentration, one can assume a uniform counterion density profile  $c_{count}(r) = f_* c$ . This leads to the following expression for the electrostatic interaction energy per monomer

$$\frac{U_{el}}{k_B T} \approx \frac{l_B f_*^2 g_e}{D_e} \ln\left(\frac{\xi}{D_e}\right) - l_B f_*^2 c \xi^2 \quad (3.3)$$

The total interaction energy per monomer consists of the electrostatic part  $U_{el}$  and the elastic contribution due to stretching of the polyelectrolyte chain  $k_B T D_e^2 / (b^2 g_e)$  per electrostatic blob containing  $g_e$  monomers. Therefore, the interaction part of the monomer chemical potential can be written as

$$\frac{\mu}{k_B T} \approx \frac{D_e^2}{b^2 g_e^2} + \frac{l_B f_*^2 g_e}{D_e} \ln\left(\frac{\xi}{D_e}\right) - l_B f_*^2 c \xi^2 \quad (3.4)$$

This expression has to be minimized with respect to the correlation length  $\xi$  and the electrostatic blob size  $D_e$  by taking into account the relation between the number of monomers in the electrostatic blob  $g_e$  and its size ( $D_e^2 \propto b^2 g_e$ ). This minimization leads to the following

expression for the correlation length

$$\xi \ln^{1/6}\left(\frac{e\xi}{D_e^*}\right) \approx \left(\frac{D_e^*}{cb^2}\right)^{1/2} \quad (3.5)$$

and the electrostatic blob size

$$D_e \approx D_e^* \ln^{-1/3}\left(\frac{e\xi}{D_e^*}\right) \quad (3.6)$$

where we have introduced the electrostatic blob size  $D_e^* \approx b(uf_*^2)^{-1/3}$  for the effective charge fraction  $f_*$  (cf. Eq. (2.13b)). The electrostatic blob size  $D_e$  (Eq. (3.6)) increases logarithmically with polymer concentration. The correlation length of semidilute polyelectrolyte solution (see Eq. (3.5)) has only minor logarithmic corrections to the well-known scaling form [2,23,25,110,111]  $\xi \propto c^{-1/2}$

$$\xi \propto c^{-1/2} \ln^{-1/6}\left(\frac{ec_b}{c}\right) \propto c^{-1/2} \quad (3.7)$$

The concentration dependence of the number of monomers in a correlation volume  $\xi$  can be obtained by imposing the close-packing condition for chain sections of size  $\xi$ ,  $c \approx g_e/\xi^3$ . This leads to the following concentration dependence of the number of monomers within a correlation volume [2,23,25,110,111]

$$\begin{aligned} g_\xi & \propto c \xi^3 \propto c^{-1/2} \ln^{-1/2}\left(\frac{e}{c D_e^* b^2}\right) \\ & \approx c^{-1/2} \ln^{-1/2}\left(\frac{ec_b}{c}\right) \end{aligned} \quad (3.8)$$

where  $c_b$  is the polymer concentration at which electrostatic blobs begin to overlap.

Fig. 21 displays the results of MD simulations for concentration dependence of the correlation length  $\xi$  for several chain lengths (open symbols) [26] and results of scattering experiments (filled symbols) [112,113] in the semidilute salt-free polyelectrolyte solutions. For the fixed chain length  $N$ , simulations show that the slope of the correlation length approaches the scaling value  $-1/2$  in the semidilute regime. However, for the same polymer concentrations, the correlation length increases with increasing number of monomers  $N$  and, finally, saturates for longer chains. This saturation of the correlation length indicates that the  $N$ -dependence of the correlation length is due to the finite size effects. For shorter chains there are not enough correlation blobs per

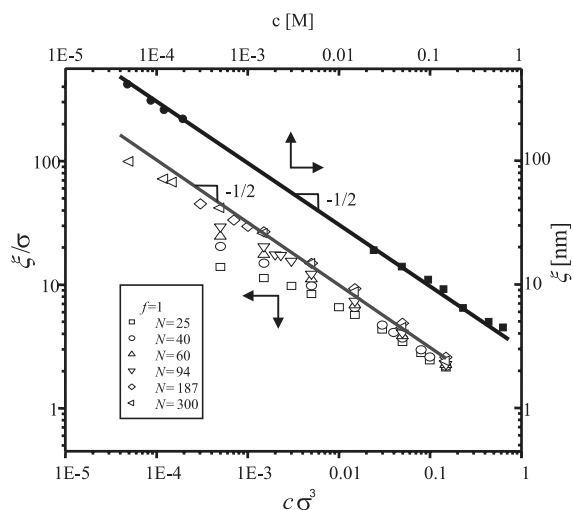


Fig. 21. Concentration dependence of the correlation length  $\xi$  in salt-free polyelectrolyte solutions. Filled symbols corresponds to the SANS data (circles) (Nierlich, M. et al. *J. Phys. (Paris)* 40, 701 (1979)) and light scattering data (squares) (Drifford, M., Dalbiez, J.P. *J. Phys. Chem.* 88, 5368 (1984)) in solutions of NaPSS. Open symbols represent results of the molecular dynamics simulations [26]. The lines with slope  $-1/2$  are shown to guide the eye.

chain to completely suppress the contributions from chain ends. Scattering experiments in the semidilute solutions [112,113] find the correlation length varying reciprocally with square root of polymer concentration,  $\xi \sim c^{-1/2}$ . Light scattering [112] and neutron scattering [113] data were combined to cover four orders of magnitude in concentration of salt-free solutions of polystyrene sulfonate sodium salt:  $5 \times 10^{-5} < c < 5 \times 10^{-1}$  M. (see filled symbols in Fig. 21).

A plot of  $R(c^*)/\xi$  as a function of  $c/c^*$  (Fig. 22) provides an estimate (with the logarithmic accuracy) of the number of blobs per chain. All simulation data collapse onto a single universal curve. The y-axis of this plot is proportional (up to a logarithmic correction) to the number of correlation blobs per chain. The number of blobs per chain  $R(c^*)/\xi$  in the semidilute solution increases with polymer concentration as  $c^{1/2}$  as predicted by the scaling theory. It follows from this plot that for short chains the number of correlation blobs per chain does not exceed 10 throughout the entire semidilute regime. Finite size effects dominate chain properties of such short chains. However, for longer chains far from the overlap

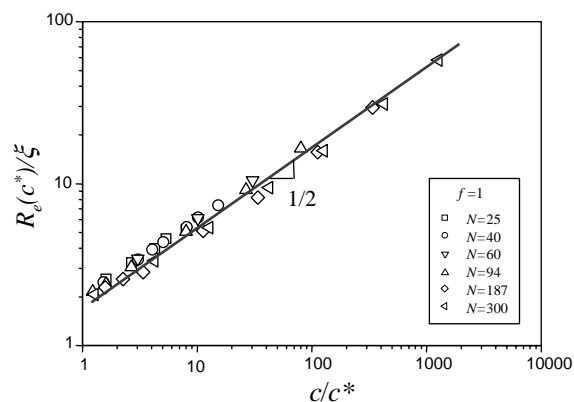


Fig. 22. Normalized chain size  $R_c(c^*)/\xi$  as a function of reduced concentration  $c/c^*$ . The line with slope  $1/2$  is shown to guide the eye. Reproduced with permission from Liao, Q., Dobrynin, A.V., & Rubinstein, M. *Macromolecules* 36, 3386–3398 (2003). [26] Copyright 2003, American Chemical Society.

concentration, the number of blobs approaches 100, and finite size effects are suppressed.

### 3.2.2. Persistence length and chain size

The scaling model of a polyelectrolyte chain in semidilute solutions is based on the assumption of the existence of a single length scale—the correlation length  $\xi$ . On length scales larger than the correlation length  $\xi$ , the conformations of a polyelectrolyte chain in semidilute solutions are assumed to be Gaussian. Thus, the polyelectrolyte chain is assumed to be flexible at length scales on the order of the correlation length  $\xi$ . MD simulations are the optimal tool to check the assumptions of the scaling theory. The persistence length  $l_p$  (chain section containing  $k_p$  bonds) can be calculated from the decay rate of the bond angle correlation function along the chain contour

$$\langle \cos \theta_k \rangle = \frac{\vec{b}_s \cdot \vec{b}_{s+k}}{|\vec{b}_s| |\vec{b}_{s+k}|} \propto \exp\left(-\frac{k}{k_p}\right) \quad (3.9)$$

Here,  $\vec{b}_s$  and  $\vec{b}_{s+k}$  are the bond vectors of  $s$ th and  $s+k$ th bonds. The persistence length  $l_p$  is estimated as the square-root of the mean-square end-to-end distance of the chain section containing  $k_p$  bonds. The brackets  $\langle \rangle$  denote the averaging over different chain conformations. The averaging over different possible positions of  $s$ th bond vector along the

chain ( $s=0, \dots, N-k$ ) is performed by keeping the number of bonds  $k$  between the two vectors constant.

Fig. 23 shows the bond angle correlation function of a fully charged ( $f=1$ ) polyelectrolyte chain with the number of monomers  $N=300$  at different polymer concentrations in semidilute solutions. The bond angle correlation function has two regimes. At small distances within the electrostatic blob, it decays very fast because the electrostatic interactions are too weak to orient the bonds. At the intermediate  $k$  values, the decay is much slower due to the electrostatic interactions. The persistence length  $l_p$  in simulations was estimated from the exponential decay of the bond angle correlation function in the intermediate region [70]. Fig. 24 shows the results for the concentration dependence of the electrostatic persistence length  $l_p(c)$  and the correlation length  $\xi(c)$  in semidilute polyelectrolyte solutions. As one can see from this plot, both length scales are proportional (in fact very close) to each other. These results support the hypothesis of a single length scale in semidilute polyelectrolyte solutions.

At length scales larger than the correlation length  $\xi$ , other chains and counterions screen electrostatic interactions, and the statistics of the chain are those of a Gaussian chain with the effective persistence length

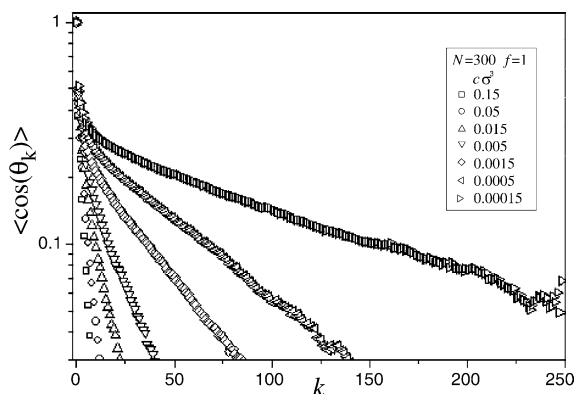


Fig. 23. Dependence of the bond angle correlation function on the distance  $k$  along the chain for polyelectrolytes with  $N=300$  and  $f=1$  at different polymer concentrations. Semilogarithmic scales. Reproduced with permission from Liao, Q., Dobrynin, A.V., & Rubinstein, M. *Macromolecules* 36, 3386–3398 (2003). [26] Copyright 2003, American Chemical Society.

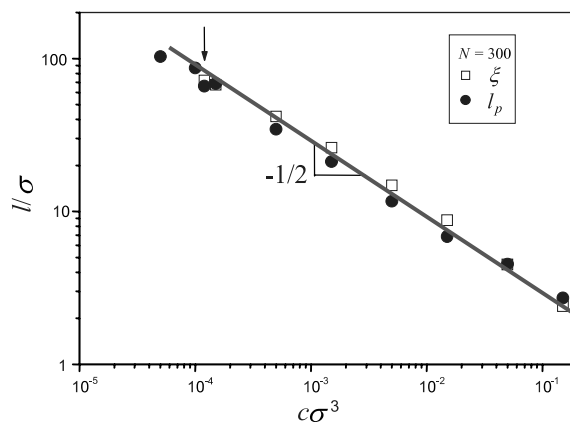


Fig. 24. Concentration dependence of the persistence length  $l_p$  (filled circles) and the correlation length  $\xi$  (open squares) for chains with  $N=300$  and  $f=1$ . The arrow marks the location of the overlap concentration. Reproduced with permission from Liao, Q., Dobrynin, A.V., & Rubinstein, M. *Macromolecules* 36, 3386–3398 (2003). [26] Copyright 2003, American Chemical Society.

on the order of the correlation length  $\xi$ . Thus, according to the scaling model, a chain in the semidilute salt-free polyelectrolyte solution is a random walk of correlation blobs [2,23,25,110,111] with size

$$R_e \approx \xi \left( \frac{N}{g\xi} \right)^{1/2} \propto N^{1/2} c^{-1/4} \ln^{1/2} \left( \frac{ec_b}{c} \right) \propto N^{1/2} c^{-1/4} \quad (3.10)$$

To verify the scaling hypothesis for the chain size, the plot of the normalized chain size  $R_e/\xi$  as a function of the number of correlation blobs per chain  $N/g\xi$  is shown in Fig. 25. All points for chains with different degrees of polymerization, different fractions of charged monomers, and at different polymer concentrations collapse onto one universal line, with the slope 1/2 as expected for Gaussian chains with  $N/g\xi$  correlation blobs.

Fig. 26 shows the results of molecular dynamics simulations for the end-to-end distance of chains as a function of reduced concentration  $c/c^*$  in semidilute solutions for polyelectrolytes with different number of monomers. The results show that the concentration dependence of the chain size can be described by the power law  $R \sim c^{-\nu}$ ; however, the exponent  $\nu$  is  $N$ -dependent. The simulation results clearly show the crossover from the weak concentration dependence

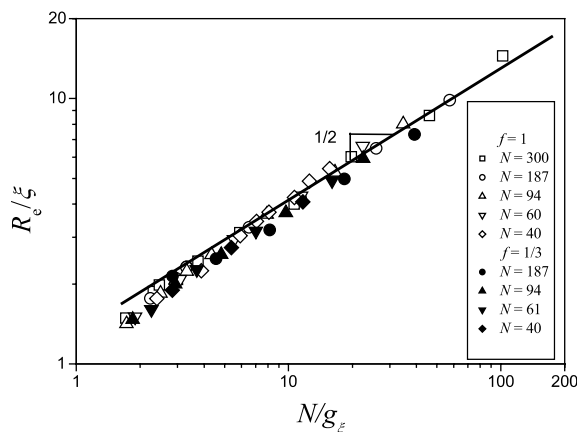


Fig. 25. Dependence of the reduced chain size  $R_e/\xi$  on the number of correlation blobs  $N/g\xi$  for chains with different degrees of polymerization, fractions of charged monomers, and at different polymer concentrations. Thin solid line has slope 1/2. Reproduced with permission from Liao, Q., Dobrynin, A.V., & Rubinstein, M. *Macromolecules* 36, 3386–3398 (2003). [26] Copyright 2003, American Chemical Society.

of end-to-end distance of polyelectrolyte chain,  $R_e \sim c^{-0.094}$  for  $N=25$ , to a stronger concentration dependence,  $R_e \sim c^{-0.22}$  for  $N=300$ . The concentration dependence of the chain size for the longest chains

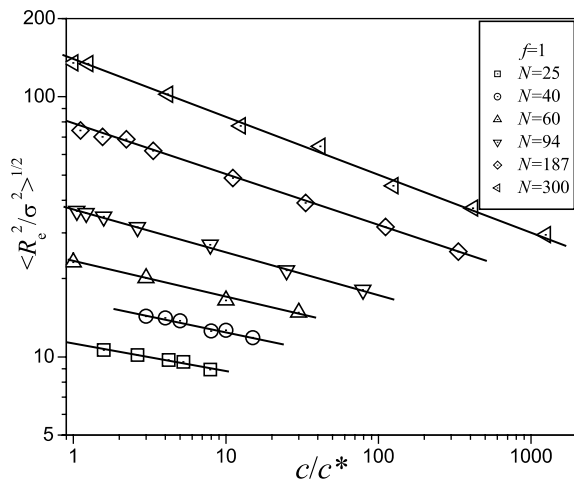


Fig. 26. Dependence of the root-mean-square end-to-end distance for chains with the fraction of charged monomers  $f=1$  on the reduced polymer concentration  $c/c^*$ . Reproduced with permission from Liao, Q., Dobrynin, A.V., & Rubinstein, M. *Macromolecules* 36, 3386–3398 (2003). [26] Copyright 2003, American Chemical Society.

approaches the predicted value of the scaling exponent of  $-1/4$ .

The chain size of NaPSS in aqueous semidilute solutions with no added salt was found [114] to scale with concentration as  $R_e \sim c^{-1/4}$  in agreement with Eq. (3.10).

### 3.2.3. Semidilute polyelectrolyte solutions with added salt [25]

The electrostatic interactions in salt-free solutions are screened at length scales on the order of the correlation length  $\xi$ . The reason for such screening is that the Debye screening length due to counterions alone  $\kappa^{-1} = (4\pi l_B f_* c)^{-1/2}$  is always larger than the correlation length  $\xi$  as long as the system is below the counterion condensation threshold. The counterion condensation in a  $\Theta$ -solvent takes place for strongly charged polyelectrolytes for which the parameter  $uf^{1/2}$  is larger than unity. For weakly charged polyelectrolytes, the parameter  $uf^{1/2}$  is smaller than unity and counterion condensation can be neglected (see Section 2.4.1). In this case, one has to include the sections of the chains inside the Debye screening length into the screening of electrostatic interactions. In order to calculate the contribution of sections of the chains into the Debye screening length, each chain is divided into subsections of size  $\kappa^{-1}$ . The charges on each of these subsections are strongly interacting and contribute coherently to the screening as one big charge  $Z$

$$Z \approx \frac{f_* g_e \kappa^{-1}}{D_e} \approx \left(\frac{f_*}{u}\right)^{1/3} \frac{1}{\kappa b} \quad (3.11)$$

The concentration of these sections is equal to

$$c_Z \approx \frac{cf_*}{Z} \quad (3.12)$$

By assuming that each section contributes to screening independently, one can use the expression for the Debye screening length for multivalent ions to estimate the electrostatic screening length

$$\kappa^{-1} = [4\pi l_B (f_* c + c_Z Z^2)]^{-1/2} \approx (4\pi l_B c f_* Z)^{-1/2} \quad (3.13)$$

Notice that for  $Z \gg 1$ , the sections of the chain provide the main contribution to the screening. The screening length can be determined self-consistently

from Eq. (3.13) by substituting expression (3.11) for the section valence  $Z$  [25]

$$\kappa^{-1} = \left(4\pi l_B f_*^2 \frac{c g_e}{D_e}\right)^{-1/3} \approx (u f_*^2)^{-2/9} c^{-1/3} \quad (3.14)$$

The Debye screening length due to chain sections  $\kappa(Z)^{-1}$  is smaller than the solution correlation length  $\xi$ . This means that there is less than one polyion section inside a Debye volume  $c_Z \kappa(Z)^{-3} \ll 1$  contradicting the assumption of the Debye–Huckel theory. In semidilute solutions, the Debye screening length  $\kappa^{-1}$  due to counterions alone is larger than the correlation length of the solution  $\xi$ , while the screening length due to sections of the chain is smaller than  $\xi$ . Therefore one can conclude that in this case when the counterion screening is too weak, but screening due to sections of the chains is too strong, the electrostatic screening length is on the order of the distance between chains  $\xi$ . Thus, the electrostatic screening length  $r_{\text{scr}}$  in the solutions of multivalent ions with valence  $Z$  can be found self-consistently by assuming that the number of counterions and salt ions inside the volume with radius on the order of the electrostatic screening length is equal to the charge valence  $Z$

$$c_{\text{ion}} r_{\text{scr}}^3 \approx (c f_* + 2c_s) r_{\text{scr}}^3 \approx Z \quad (3.15)$$

It is important to point out that this is the minimal conjecture: it is conceivable that the electrostatic screening length expands even more, but it must expand at least up to  $r_{\text{scr}}$  to compensate for the charge with valence  $Z$ .

For semidilute polyelectrolyte solutions, the effective charge on a chain section inside the electrostatic screening length  $r_{\text{scr}}$  is equal to (see Eq. (3.11))

$$Z \approx \frac{f_* g_e r_{\text{scr}}}{D_e} \approx \left(\frac{f_*}{u}\right)^{1/3} \frac{r_{\text{scr}}}{b} \quad (3.16)$$

Substituting expression (3.16) into Eq. (3.15) one can find the relation between the electrostatic screening length and the ion concentration

$$\begin{aligned} r_{\text{scr}} &\approx \left(\frac{f_*}{u}\right)^{1/6} b^{-1/2} (c f_* + 2c_s)^{-1/2} \\ &\approx \xi_0(c) \left(1 + \frac{2c_s}{f_* c}\right)^{-1/2} \end{aligned} \quad (3.17)$$

where

$$\xi_0(c) \approx b(u f_*^2)^{-1/6} (c b^3)^{-1/2}$$

is the correlation length of the salt-free polyelectrolyte solution.

Using this assumption about the electrostatic screening length, one can calculate the correlation length of a semidilute polyelectrolyte solution in the presence of added salt. The calculation of the correlation length in polyelectrolyte solutions with added salt is based on the assumption that the chain conformation at the length scales smaller than the screening length is that of a rod-like chain consisting of  $g_{\text{scr}} = g_e r_{\text{scr}} / D_e$  monomers, while at the length scales larger than the screening length  $r_{\text{scr}}$ , but smaller than correlation length  $\xi$ , the sections of the chain of length  $r_{\text{scr}}$  obey self-avoiding walk statistics. On length scales longer than correlation length  $\xi$  the chain is ideal. (Note that this assumption disagrees with the OSF result (see Section 2.5) but it is consistent with the result  $l_p \approx r_{\text{scr}}$  (see Fig. 24)). This leads to the following expression for the correlation length of a polyelectrolyte solution in the presence of added salt

$$\begin{aligned} \xi(c) &\approx r_{\text{scr}} \left(\frac{g_\xi}{g_{\text{scr}}}\right)^{3/5} \approx r_{\text{scr}} \left(\frac{D_e g_\xi}{r_{\text{scr}} g_e}\right)^{3/5} \\ &\approx b(c b^3)^{-1/2} (u f_*^2)^{-1/6} \left(1 + \frac{2c_s}{c f_*}\right)^{1/4} \\ &\approx \xi_0(c) \left(1 + \frac{2c_s}{c f_*}\right)^{1/4} \end{aligned} \quad (3.18)$$

where  $g_\xi$  is the number of monomers in a correlation volume. The concentration dependence of the correlation length  $\xi$  in the high salt concentration regime ( $c_s \gg c f_*$ ) is similar to that in solutions of uncharged polymers  $\xi \propto c^{-3/4}$ . At low salt concentrations, Eq. (3.18) reproduces salt-free result  $\xi \propto c^{-1/2}$ . Thus, any quantity  $X$  of the polyelectrolyte solution with salt concentration  $c_s$  can be expressed in terms of the same property  $X_0$  in a salt-free solution as

$$X = X_0 \left(1 + \frac{2c_s}{f_* c}\right)^\alpha \quad (3.19)$$

The results for static properties of semidilute polyelectrolyte solutions with added salt are summarized in Table 1 (see Section 3.2.5).

Table 1

Scaling relations for semidilute solutions of polyelectrolytes in a  $\Theta$ -solvent for polymer backbone [25]

	$R \approx bN^{1/2}B^{-1/4}(cb^3)^{-1/4}y^{-1/8}$ ; $\xi \approx bB^{1/2}(cb^3)^{-1/2}y^{1/4}$	
	Unentangled	Entangled
$\tau$	$(\eta_s b^3/k_B T)B^{-3/2}N^2(cb^3)^{-1/2}y^{-3/4}$	$(\eta_s b^3/k_B T)N^3n^{-2}B^{-3}y^{-3/2}$
$G$	$k_B Tc/N$	$(k_B T/b^3)n^{-2}B^{-3/2}(cb^3)^{3/2}y^{-3/4}$
$\eta$	$\eta_s NB^{-3/2}(cb^3)^{1/2}y^{-3/4}$	$\eta_s(N^3/n^4)B^{-9/2}(cb^3)^{3/2}y^{-9/4}$
$D_{\text{self}}$	$(k_B T/\eta_s b)N^{-1}By^{1/2}$	$(k_B T/\eta_s b)n^2N^{-2}B^{5/2}(cb^3)^{-1/2}y^{5/4}$

where  $y = 1 + 2c_s/cf_*$ , and the parameter  $B \approx (uf_*^2)^{-1/3}$ .

### 3.2.4. Osmotic pressure and scattering function

Donnan equilibrium [5] in ionic systems requires charge neutrality on both sides of the membrane across which the osmotic pressure  $\pi$  is measured. The electroneutrality condition leads to the partitioning of salt ions between the reservoir and the polyelectrolyte solution region

$$c_s^+ = c_s^- + f_* c \quad (3.20)$$

where  $c_s^+$  and  $c_s^-$  are the average concentrations of positively and negatively charged salt ions in the polyelectrolyte solution. Here it is assumed that counterions are positively charged and macroions are negatively charged.

The local ion concentration  $c_s^+(r)$  or  $c_s^-(r)$  in polyelectrolyte solutions is related to the local value of the reduced electrostatic potential  $\varphi(r)$  by the Boltzmann distribution

$$\begin{aligned} c_s^+(r) &= c_s^+ \exp[\varphi(r)] \\ c_s^-(r) &= c_s^- \exp[-\varphi(r)] \end{aligned} \quad (3.21)$$

where the reduced electrostatic potential  $\varphi(r)$  is defined as  $\varphi(r) = e\Psi(r)/k_B T$ . Thus, the product of the concentrations of salt ions stays constant at each point of the solution. Since salt ions can penetrate through the membrane, the chemical equilibrium on both sides of the membrane requires that this product stays constant in the reservoir as well. This leads to

$$c_s^+ c_s^- = c_s^2 \quad (3.22)$$

where  $c_s$  is the average salt concentration in the reservoir. By solving Eq. (3.20) with Eq. (3.22) one can find the average concentrations of positively and negatively charged salt ions in the polyelectrolyte solution as functions of the average salt concentration

$c_s$  and polymer concentration  $c$ . The ionic contribution to the osmotic pressure is equal to the difference between the ideal gas pressure of salt ions in the polyelectrolyte solution and in the reservoir [5].

$$\begin{aligned} \frac{\pi_{\text{ion}}}{k_B T} &= c_s^+ + c_s^- - 2c_s \\ &= \sqrt{(f_* c)^2 + 4c_s^2} - 2c_s \end{aligned} \quad (3.23)$$

In the limit of low salt concentrations,  $c_s \ll f_* c$ , the difference is proportional to the pressure from the ideal gas of counterions. At higher salt concentrations,  $c_s \gg f_* c$ , the ionic part of the osmotic pressure is equal to

$$\frac{\pi_{\text{ion}}}{k_B T} \approx \frac{(f_* c)^2}{4c_s} = \frac{2\pi l_B (f_* c)^2}{\kappa^2} \quad (3.24)$$

and can be considered as the result of the effective excluded volume interactions between charged monomers on the polyelectrolyte backbone with excluded volume  $l_B r_D^2$ . (At high salt concentrations ( $c_s \gg f_* c$ ), the concentrations of salt ions  $c_s^+$  and  $c_s^-$  in a polyelectrolyte solution are almost equal to those in reservoir  $c_s$ .)

In addition to the ionic contribution, polyelectrolyte solutions have the polymeric contribution to their osmotic pressure. In semidilute solutions, the polymeric contribution is essentially  $k_B T$  per correlation volume [10,22]

$$\frac{\pi_{\text{pol}}}{k_B T} \approx \xi^{-3} \quad (3.25)$$

The total osmotic pressure of polyelectrolyte solutions can be approximated as the sum of the

ionic and polymeric contributions

$$\frac{\pi}{k_B T} = \frac{\pi_{\text{ion}}}{k_B T} + \frac{\pi_{\text{pol}}}{k_B T} \approx \sqrt{(f_* c)^2 + 4c_s^2} - 2c_s + \xi^{-3} \quad (3.26)$$

At low salt concentrations,  $c_s \ll f_* c$ , the ionic contribution to the osmotic pressure  $f_* c$  dominates over the polymeric contribution throughout the entire semidilute regime. At high salt concentrations,  $c_s \gg f_* c$ , both ionic and polymeric contributions are much smaller than those at low salt concentrations. However, for the vast majority of the systems studied so far [115–123], the ionic contribution dominates the osmotic pressure of polyelectrolyte solutions. Therefore, Eq. (3.26) is a good approximation of the osmotic pressure of polyelectrolyte solutions.

To illustrate this point, Fig. (27) shows the total osmotic pressure  $\pi$  obtained from the MD simulations [61] of semidilute polyelectrolyte solutions of fully charged chains with  $N=300$  (squares), together with the polymeric contribution to the osmotic pressure (circles). The polymeric contribution is estimated as  $k_B T / \xi^3$ . As one can see, the polymeric contribution to the osmotic pressure is negligible at lower concentrations. It becomes on the same order of magnitude as the total osmotic pressure at polymer concentrations on the order of  $100c^*$ . Thus, the osmotic pressure of semidilute polyelectrolyte solutions is dominated by

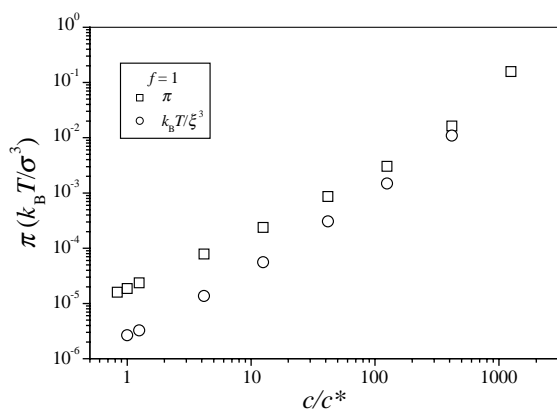


Fig. 27. Comparison of the total osmotic pressure  $\pi$  in semidilute polyelectrolyte solutions with the polymeric contribution estimated as  $k_B T / \xi^3$  for fully charged ( $f=1$ ) flexible chains with  $N=300$ . Reproduced with permission from Liao, Q., Dobrynin, A.V., & Rubinstein, M. *Macromolecules* 36, 3399–3410 (2003). [61] Copyright 2003, American Chemical Society.

the pure counterion contribution over a wide range of polymer concentrations.

The ionic part of the osmotic pressure in semidilute polyelectrolyte solutions can be calculated by using the Katchalsky's cell model [3,56]. In the frameworks of this model, a semidilute polyelectrolyte solution is represented as a periodic array of chains separated by the distance  $R = \sqrt{g_\xi / (\pi \xi c)}$ , where  $\xi$  and  $g_\xi$  are the correlation length and the number of monomers within the correlation length, respectively. The osmotic coefficient predicted by the Katchalsky's cell model [3,56] is given in Eq. (2.63). To evaluate the osmotic coefficient, we have to know two parameters  $\alpha$  and  $\gamma_0$ . The evaluation of the parameter  $\gamma_0$  is straightforward, using the number of monomers  $g_\xi$  within the correlation length  $\xi$ . In the case of pure complex values of the parameter  $\alpha$ , it satisfies the following non-linear equation obtained from the boundary conditions (Eq. (2.57))

$$|\alpha| \ln \left( \frac{R}{\sigma} \right) = \arctan \left( \frac{1}{|\alpha|} \right) + \arctan \left( \frac{\gamma_0 - 1}{|\alpha|} \right) \quad (3.27)$$

where the radius of the cylinder is set to be equal to  $\sigma$ . The osmotic coefficient predicted by the Katchalsky's cell model [3,56] is compared with the results of the computer simulations in Fig. 28.

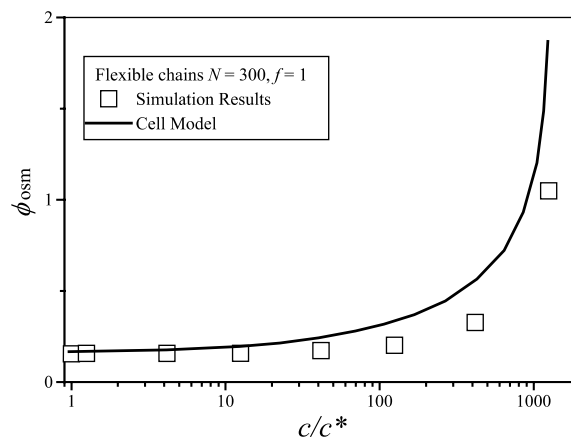


Fig. 28. Comparison of the osmotic coefficient obtained in MD simulations of semidilute polyelectrolyte solutions (open squares) with the predictions of the Katchalsky's cell model (solid line). Reproduced with permission from Liao, Q., Dobrynin, A.V., & Rubinstein, M. *Macromolecules* 36, 3399–3410 (2003). [61] Copyright 2003, American Chemical Society.

The predictions of the cell model agree reasonably well with simulation results for  $c < 100c^*$ . Nevertheless, the cell model systematically overestimates the osmotic coefficient, and the largest deviations are observed in the concentration interval where the polymeric contribution to the osmotic pressure becomes comparable to the one due to counterions. The comparison of the experimental data with the predictions of the cell model was done by Hansen et al. [119]. They found that the predictions of the Katchalsky's cell model for the osmotic coefficient are in surprisingly good agreement with all available experimental finding over a wide range of DNA concentrations.

The experimental data for the osmotic pressure of semidilute solutions of NaPSS obtained by Koene et al. [122] and the salt-free data of Takahashi et al. [123] are shown in Fig. 29. While Takahashi et al. did

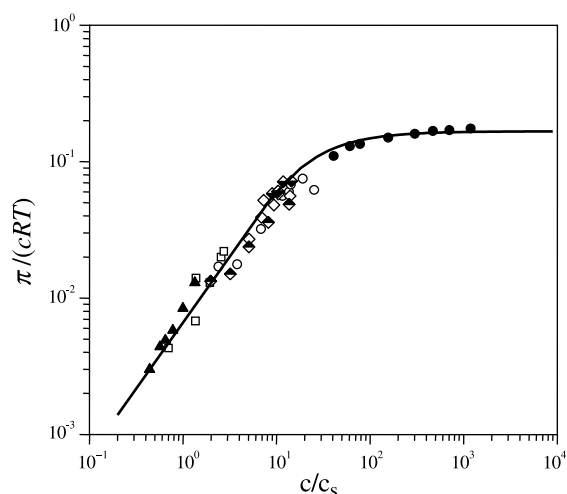


Fig. 29. Osmotic pressure of semidilute NaPSS solutions as a function of polymer and salt concentration. Filled circles are data of Takahashi et al. [123] for  $M_w = 4.3 \times 10^5$  Da with no added salt and apparent salt concentration  $c_s = 3 \times 10^{-5}$  M. Other symbols are data of Koene et al. [122] for molecular weight  $M_w = 6.5 \times 10^5$  Da and salt concentrations  $c_s = 5 \times 10^{-3}$  M (open circles),  $c_s = 5 \times 10^{-2}$  M (open squares),  $c_s = 1 \times 10^{-2}$  M (open diamonds), and  $c_s = 1 \times 10^{-1}$  M (filled triangles); for  $M_w = 4 \times 10^5$  Da and  $c_s = 1 \times 10^{-2}$  M (bottom-filled diamonds); and for  $M_w = 12 \times 10^5$  Da and  $c_s = 1 \times 10^{-2}$  M (top-filled diamonds). The solid curve is Eq. (3.23) with  $f_* = 0.16$ . Reproduced with permission from Dobrynin, A.V., Colby, R.H., & Rubinstein, M. *Macromolecules* 28, 1859–1871 (1995). [25] Copyright 1995, American Chemical Society.

not report the salt concentration of their ‘salt-free’ solutions, the data clearly indicate a low level of salt (see Fig. 1 of Ref. [123]) and we estimated it from their data. Data at high salt concentrations from Ref. [123] were not used in Fig. 29 because they correspond to a dilute solution regime. The solid curve in Fig. 29 is the prediction of Eq. (3.23) with the effective fraction of free counterions  $f_*$  equal to 0.2. The agreement between the scaling theory and the experimental data is very good over a wide range of polymer and salt concentrations.

The high osmotic pressure of salt-free polyelectrolyte solutions has important consequences for the scattering function  $S(q)$ . The osmotic compressibility is related to the scattering at zero wavelength

$$S(0) = k_B T \frac{\partial c}{\partial \pi} \quad (3.28)$$

At low salt concentrations, the osmotic pressure is controlled by the concentration of free counterions. This leads to the scattering function  $S(0)$  inversely proportional to the fraction of free counterions

$$S(0) \approx 1/f_* \quad (3.29)$$

The counterion pressure causes  $S(0)$  to be much smaller than its value at the correlation length  $S(2\pi\xi^{-1})$ . The fluctuations of polymer density on the length scales larger than the electrostatic screening length are governed by the electroneutrality condition. However, these fluctuations are  $f_* g_\xi$  times larger than thermal fluctuations of counterion density and would result in a prohibitively large loss of counterion entropy. Therefore, the extremely high counterion pressure suppresses density fluctuations on length scales larger than the correlation length  $\xi$ . For  $q > 2\pi\xi^{-1}$ , the scattering function  $S(q)$  decreases with  $q$  as in the case of neutral polymers. This suggests that there is a maximum in the scattering function  $S(q)$  of salt-free polyelectrolyte solutions at the wave vector  $q$  on the order of  $2\pi\xi^{-1}$ .

The maximum in the scattering function  $S(q)$  disappears at high salt concentrations. When the salt concentration  $c_s$  is on the order of  $cg_\xi^2$ , the polymer density fluctuations on the length scales larger than the correlation length  $\xi$  are no longer suppressed ( $S(0) \sim g_\xi$ ). In this high salt concentration regime, the scattering function is similar to that in solutions of neutral polymers.

### 3.2.5. Dynamics of polyelectrolyte solutions [25,111]

**3.2.5.1. Unentangled regime ( $c^* < c < c_e$ ).** The hydrodynamic interactions between sections of a chain in semidilute solutions are screened on the length scales larger than the correlation length  $\xi$  [8–10]. Inside the correlation blob the motion of different chain sections are strongly hydrodynamically coupled just as in dilute solutions. The relaxation time of the section of a polyelectrolyte chain with  $g_\xi$  monomers inside the correlation blob is Zimm-like (proportional to the volume pervaded by the section) [8,10]

$$\tau_\xi \approx \eta_s \xi^3 / (k_B T) \quad (3.30)$$

Each chain consists of  $N/g_\xi$  correlation blobs. The hydrodynamic interactions between these blobs are screened and therefore their motion can be described by Rouse dynamics [8,10]

$$\tau_{\text{Rouse}} \approx \tau_\xi (N/g_\xi)^2 \approx \frac{\eta_s b^3}{k_B T} (uf_*^2)^{1/2} (cb^3)^{-1/2} N^2 \quad (3.31)$$

$$c^* < c < c_e$$

(Here we consider salt-free polyelectrolyte solutions.) The chain relaxation time in this unentangled semidilute regime decreases with increasing polymer concentration as  $\tau_{\text{Rouse}} \sim c^{-1/2}$ . This decrease of solution relaxation time with increasing polymer concentration is unique for unentangled polyelectrolyte solutions. Relaxation time of ‘normal’ polymer solutions increases with increasing polymer concentration. The reason for such unusual dependence is that the chain size decreases with increasing polymer concentration while their friction coefficient (proportional to contour length) does not change. This leads to the concentration-independent self-diffusion coefficient

$$D_{\text{self}} \approx R^2 / \tau_{\text{Rouse}} \approx \frac{k_B T}{\eta_s b} (uf_*^2)^{-1/3} N^{-1} \quad (3.32)$$

$$c^* < c < c_e$$

that is inversely proportional to the degree of polymerization,  $N$ . The terminal modulus  $G$  of a solution in the Rouse model for unentangled polymers is  $k_B T$  per chain [8,10]. The viscosity of

polyelectrolyte solutions in this regime is

$$\eta \approx G \tau_{\text{Rouse}} \approx \eta_s (uf_*^2)^{1/2} (cb^3)^{1/2} N \quad (3.33)$$

$$c^* < c < c_e$$

In the salt-free solution, the viscosity grows as the square root of concentration  $\eta \sim c^{1/2}$ . Thus, the scaling model of polyelectrolyte solutions recovers the well-known phenomenological Fuoss law [11].

**3.2.5.2. Entanglement criterion.** The unentangled semidilute regime of neutral polymer chains exists above the chain overlap concentration  $c^*$  within the polymer concentration range  $c^* < c < c_e$ , where  $c_e$  is polymer concentration corresponding to the onset of entanglements. The physical reason for the unentangled semidilute regime is that the topological constraints between polymers require significant chain overlap. This leads to the diameter of the topological tube constraining transversal motion of the chain to be larger than the correlation length. It was established experimentally that at the entanglement onset, each chain has to overlap with  $n$  other chains (see for discussion Refs. [10,124–126]), with  $5 < n < 10$ . To estimate the entanglement concentration  $c_e$  for polyelectrolytes, we will assume that it is necessary to have  $n$  chains within the volume occupied by a polyelectrolyte chain to topologically constrain its motion. Thus, the monomer concentration required for chain entanglement is

$$\begin{aligned} c_e &\approx \frac{nN}{R_e^3(c_e)} \approx c^* \frac{nR_e^3(c^*)}{R_e^3(c_e)} \approx n(c^*)^{1/4} c_e^{3/4} \\ &\approx n^4 c^* \end{aligned} \quad (3.34)$$

where we use the following relation between the chain size at entanglement concentration  $c_e$  and that at overlap concentration  $c^*$ ,  $R(c_e) \approx R(c^*)(c^*/c_e)^{1/4}$ .

Thus, the unentangled semidilute regime in salt-free solutions could be 3–4 decades wide ( $10^3 < c_e/c^* < 10^4$ ) [25,111]. The physical reason for this unusually wide unentangled regime is the strong concentration dependence of the chain size ( $R_e \sim c^{-1/4}$ ). It is only slightly weaker than the concentration dependence of the distance between centers of mass of neighboring chains ( $R_{\text{cm}} \sim c^{-1/3}$ ). Therefore, the number of chains overlapping with a selected chain has very weak

concentration dependence  $[(R_e/R_{cm})^3 \approx (c/c^*)^{1/4}]$ . The viscosity at the entanglement concentration  $c_e$  is  $\eta(c_e) \approx n^2 \eta_s \approx 50 \eta_s$ , as in the case of neutral polymers.

**3.2.5.3. Semidilute-entangled regime ( $c > c_e$ ).** Entanglements are characterized by the tube diameter  $\mathbf{a}$  (the mesh size of the temporary entanglement network) (see Fig. 30). The polymer strand between entanglements is a random walk of  $N_e/g\xi \approx (\mathbf{a}/\xi)^2$  correlation blobs, where  $N_e$  is the number of monomers in an entanglement strand. There are  $n$  such strands inside the volume  $\mathbf{a}^3$ , so that  $(\mathbf{a}/\xi)^3 \approx nN_e/g\xi$  leading to  $n = \mathbf{a}/\xi$ . Thus, the tube diameter  $\mathbf{a}$  is proportional to the correlation length. The longest relaxation time of a polymer chain can be calculated using the reptation theory [8,10]. By assuming that the dynamics of the chain at the length scales smaller than a correlation blob size is Zimm-like, and the relaxation of a polymer strand between entanglements is Rouse-like, the longest relaxation time of the chain is concentration-independent

$$\tau_{\text{rep}} \approx \tau_{\xi} \left( \frac{N_e}{g\xi} \right)^2 \left( \frac{N}{N_e} \right)^3 \approx \frac{\eta_s b^3}{k_B T} u f_*^2 n^{-2} N^3 \quad (3.35)$$

The plateau modulus in this regime is  $G \approx \nu_e k_B T$ , where  $\nu_e$  is the number density of entanglement strands. The volume per entanglement strand is  $\xi^3 N_e/g\xi \approx \xi \mathbf{a}^2$ . The scaling model predicts the plateau

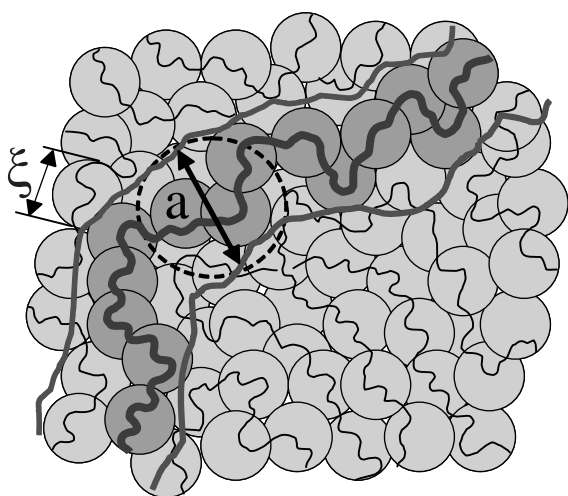


Fig. 30. Schematic representation of an entangled polyelectrolyte solution.

modulus

$$G \approx \frac{k_B T}{\xi \mathbf{a}^2} \approx \frac{k_B T}{b^3} n^{-2} (u f_*^2)^{1/2} (c b^3)^{3/2} \quad (3.36)$$

and the solution viscosity in the semidilute-entangled regime

$$\eta \approx \tau_{\text{rep}} G \approx \eta_s n^{-4} N^3 (u f_*^2)^{3/2} (c b^3)^{3/2} \quad (3.37)$$

In salt-free entangled polyelectrolyte solutions, the viscosity is predicted to grow faster than linearly with polymer concentration  $c$ .

The diffusion coefficient in the entangled regime decreases as  $c^{-1/2}$  with increasing polymer concentration

$$D_{\text{self}} \approx \frac{R_e^2}{\tau_{\text{rep}}} \approx \frac{k_B T}{\eta_s b} n^2 N^{-2} (u f_*^2)^{-5/6} (c b^3)^{-1/2} \quad (3.38)$$

Any dynamic property  $X$  of a polyelectrolyte solution with added salt can be expressed in terms of the same property  $X_0$  in salt-free solutions as

$$X = X_0 (1 + 2c_s/f_* c)^\alpha \quad (3.39)$$

by analogy with the similar relation for static properties (see Eq. (3.19)). The results for dynamic properties of semidilute solutions are summarized in Table 1.

**3.2.5.4. Comparisons with experiments.** Fig. 31 demonstrates dependence of the overlap concentration,  $c^*$ , on the chain degree of polymerization,  $N$ , for salt-free solutions of NaPSS [127]. It is in excellent agreement with the prediction of the scaling model  $c^* \sim N^{-2}$ . The overlap concentration for shorter polymers was obtained from X-ray scattering data (squares), while for longer polymers it is determined from viscosity data (circles). The overlap concentration  $c^*$  is predicted to decrease with the fraction  $f$  of charged monomers as  $c^* \sim f^{-2}$  for polyelectrolytes in a  $\Theta$ -solvent for polymer backbone (Eq. (3.1)) and as  $c^* \sim f^{-12/7}$  for polyelectrolytes in a good solvent. Fig. 32 confirms this scaling prediction for ethylene glycol solutions of  $N$ -methyl-2-vinyl pyridinium chloride random copolymers with fraction of quaternized monomers up to 10 mol%. At higher fraction of quaternized monomers one reaches the Manning counterion condensation limit of one charge per Bjerrum length ( $l_B = 15 \text{ \AA}$  in ethylene glycole) and

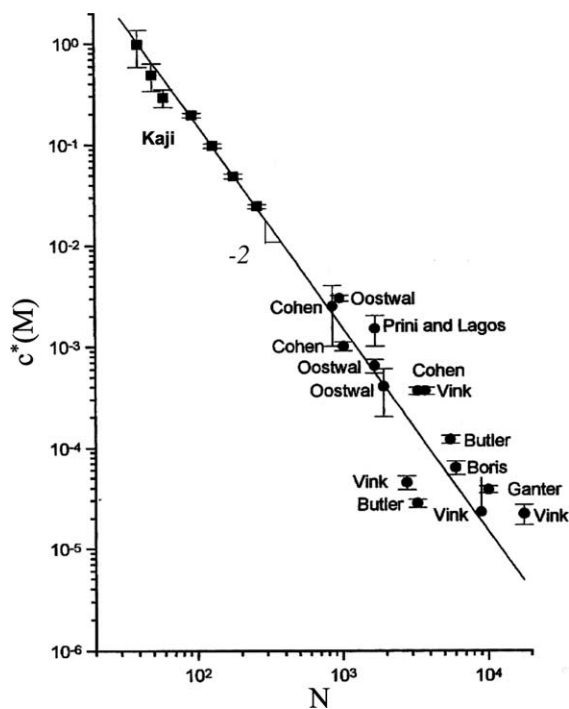


Fig. 31. Dependence of the overlap concentration,  $c^*$ , on chain degree of polymerization,  $N$ , in salt-free polyelectrolyte solutions of NaPSS. Data obtained from X-ray scattering (squares) and from viscosity (circles). Reproduced with permission from Boris, D.C., & Colby, R.H. *Macromolecules* 31, 5746–5755 (1998). [127] Copyright 1998, American Chemical Society.

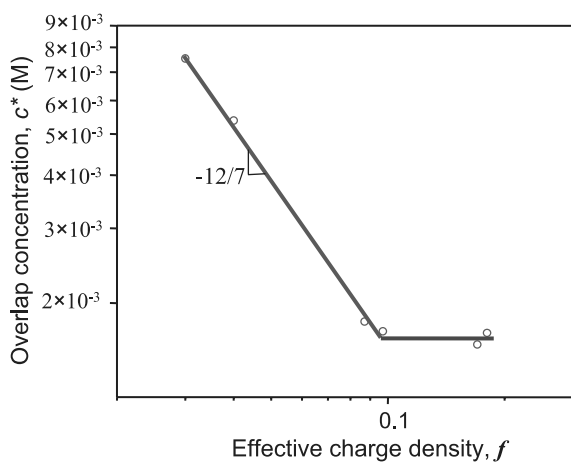


Fig. 32. Dependence of the overlap concentration,  $c^*$ , on the effective charge density,  $f$ , for 2-vinyl pyridine and *N*-methyl-2-vinyl pyridinium chloride random copolymer in ethylene glycol solvent of the at 25 °C. Data provided by Dou, S. and Colby, R. H.

the overlap concentration  $c^*$  becomes independent of charge density  $f$  (saturates at  $f_*$ ).

Fig. 33 shows the dependence of the specific viscosity of salt-free solutions of 2-vinyl pyridinium chloride and *N*-methyl-2-vinyl pyridinium chloride random copolymers on the ratio of polymer concentration  $c$  to the overlap concentration  $c^*$ . These data clearly indicate linear concentration dependence of specific viscosity in dilute solutions ( $\eta_{sp} \approx c/c^*$  for  $c < c^*$ ) as well as concentration regimes corresponding to unentangled solutions with  $\eta_{sp} \sim c^{1/2}$  and entangled solutions with  $\eta_{sp} \sim c^{3/2}$ . There is indeed a wide range of polymer concentrations (two orders of magnitude for chains with higher charged fractions) where solution viscosity follows the Rouse dynamics (Eq. (3.33)) manifested by the Fouss law [11],  $\eta_{sp} \sim c^{1/2}$ . This regime of unentangled semidilute polyelectrolyte solutions has much wider concentration range than similar regime in solutions of neutral polymers (open circles in Fig. 33). This concentration dependence of specific viscosity is general for salt-free polyelectrolyte solutions [127].

The crossover at concentration  $c_e$  to the entangled regime is also seen in the specific viscosity data (Fig. 33). According to the Kavassalis–Noolandi

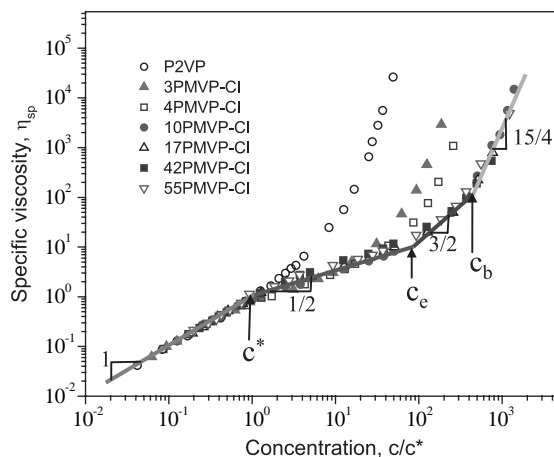


Fig. 33. Reduced concentration,  $c/c^*$ , dependence of the specific viscosity,  $\eta_{sp}$ , at 25 °C in ethylene glycol solvent of the random copolymer 2-vinyl pyridine and *N*-methyl-2-vinyl pyridinium chloride (PMVP-Cl) with various charge densities [numbers in the legend correspond to the extent (mole %) of quaternization] and the uncharged neutral parent poly(2-vinyl pyridine) (P2VP) of  $M_w = 364\,000$  Da (open circles). Data provided by Dou, S. and Colby, R. H.

conjecture [124–126], the crossover to the entangled regime occurs when there is a universal number  $n$  of overlapping chains to form an entanglement. Experimental data indicate that the Kavassalis–Noolandi conjecture [124–126] for entanglements used in the scaling model requires some modification [127]. It is possible that the properties of the confining tube for charged polymers changes with concentration leading to the concentration-dependent parameter  $n$ .

The correlation length  $\xi$  becomes smaller than electrostatic blob size  $D_e$  at concentrations higher than  $c_b$ . Electrostatic interactions are not important in polyelectrolyte solutions with concentration  $c$  above  $c_b$  and specific viscosity is expected to have concentration dependence similar to that in solutions of entangled neutral polymers,  $\eta_{sp} \sim c^{1.5/4}$ . This quasi-neutral regime of polyelectrolyte solutions at high polymer concentrations  $c > c_b$  is confirmed by the data in Fig. 33.

Fig. 34 shows the concentration dependence of the terminal modulus. The terminal modulus is  $k_B T$  per chain ( $G \sim k_B T c / N$ ) in the unentangled regime. The modulus at polymer concentrations above entanglement onset  $c_e$  increases rapidly with increasing

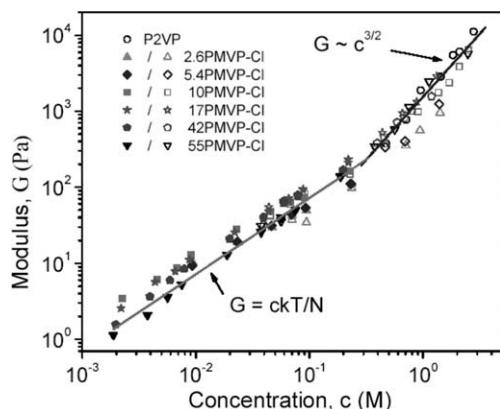


Fig. 34. Concentration dependence of the terminal modulus calculated from steady shear relaxation time (filled symbols) and from the oscillatory shear relaxation time (open symbols) at 25 °C in ethylene glycol solvent of random copolymer 2-vinyl pyridine and *N*-methyl-2-vinyl pyridinium chloride (PMVP-Cl) with various charge densities [numbers in the legend correspond to the extent (mole %) of quaternization] and the uncharged neutral parent poly(2-vinyl pyridine) (P2VP) of  $M_w = 364\,000$  Da (open circles). Data provided by Dou, S. and Colby, R. H.

concentration in the way expected by the scaling model  $G \sim c^{3/2}$ .

The concentration dependence of the self-diffusion coefficient of sodium poly(styrene sulfonate) with molecular weight in the range ( $16\,000 < M < 350\,000$  Da) in the salt-free aqueous solution measured by the pulse field gradient NMR [128, 129] presents further evidence of the validity of the Rouse model. The self-diffusion coefficient is concentration-independent in semidilute unentangled regime in agreement with the prediction of the scaling model (Eq. (3.32)). The molecular weight dependence of the self-diffusion coefficient  $D_{self} \sim M^{-1}$  is in excellent agreement with the prediction of the scaling model for the unentangled salt-free solutions (Eq. (3.32)).

### 3.2.6. Semidilute polyelectrolyte solutions in a poor solvent for polymer backbone

Polyelectrolyte chains in a poor solvent for the polymer backbone adopt necklace-like conformations. There are three different length scales in the necklace globule: the string length  $l_{str}$ , the bead size  $D_b$  and the thermal blob size  $\xi_T$  determining the length scale of density fluctuations inside beads. Thus, all three different length scales will determine the properties of semidilute polyelectrolyte solutions in a poor solvent for the polymer backbone [49, 130].

The crossover from dilute to semidilute solutions takes place when the size of the necklace becomes comparable to the distance between chains

$$c^* \approx \frac{N}{L_{nec}^3} \approx b^{-3} N^{-2} \left( \frac{|\tau|}{u f_*^2} \right)^{3/2} \approx \frac{m_b^{3/2}}{b^3 N^2} \quad (3.40)$$

where we have neglected the logarithmic correction to the chain size.

In a semidilute solution ( $c > c^*$ ), the configuration of the chain on length scales shorter than the correlation length  $\xi$  is similar to that in dilute solutions. On length scales longer than the correlation length  $\xi$ , the chain is assumed to be a random walk of correlation segments  $\xi$ . The correlation length at the overlap concentration  $\xi(c^*)$  is equal to the necklace size  $L_{nec}$ . In the semidilute regime ( $c > c^*$ ) the correlation length is independent of the degree of polymerization.

$$\begin{aligned}\xi &\approx L_{\text{nec}} \left( \frac{c^*}{c} \right)^{1/2} \approx b \left( \frac{|\tau|}{uf_*^2} \right)^{1/4} (cb^3)^{-1/2} \\ &\approx bm_b^{1/4} (cb^3)^{-1/2}\end{aligned}\quad (3.41)$$

The correlation length is inversely proportional to the square root of polymer concentration. In the case of the necklace-like chain, the number of monomers in the correlation volume is

$$g_\xi \approx c\xi^3 \approx m_b^{3/4} (cb^3)^{-1/2}\quad (3.42)$$

The normal dependence of the correlation length  $\xi$  on polymer concentration (see Eq. (3.7)) continues while  $\xi$  is larger than the length of the string  $l_{\text{str}}$  between neighboring beads. These two lengths become of the same order of magnitude ( $\xi \sim l_{\text{str}}$ ) at polymer concentration [49,130]

$$c_{\text{Bead}} \approx b^{-3} \left( \frac{uf_*^2}{|\tau|} \right)^{1/2} \approx b^{-3} m_b^{-1/2}\quad (3.43)$$

For higher polymer concentrations  $c > c_{\text{Bead}}$ , the electrostatic interaction between beads is screened, and there is one bead per every correlation volume  $\xi^3$ . The correlation volumes are space filling  $c \approx g_\xi \xi^{-3}$ . The number of monomers inside the correlation volume for  $c > c_{\text{Bead}}$  is

$$g_\xi \approx c\xi^3 \approx m_b\quad (3.44)$$

since we have assumed that most of the polymer mass is in beads ( $m_b/m_{\text{str}} \gg 1$ ). Therefore, the correlation length decreases inversely proportional to the one-third power of polymer concentration

$$\xi \approx \left( \frac{|\tau|}{uf_*^2} \right)^{1/3} c^{-1/3} \approx \left( \frac{c}{m_b} \right)^{-1/3}\quad (3.45)$$

This concentration dependence of the correlation length  $\xi$  is unusual for semidilute solutions of polymers and is more typical for the distance between chains in dilute solutions (the system behaves as a dilute solution of beads). The main difference between  $c^{-1/3}$  concentration dependence of Eq. (3.45) and similar concentration dependence of the correlation length in dilute polyelectrolyte solutions is that correlation length in semidilute solutions (Eq. (3.45)) is  $N$ -independent, while in dilute polyelectrolyte solutions  $\xi \approx (c/N)^{-1/3}$

Since the electrostatic interactions are screened on the length scales longer than the correlation length  $\xi$ , the configuration of a polyelectrolyte chain is that of a random walk of size  $\xi$

$$\begin{aligned}R_e &\approx \xi \left( \frac{N}{g_\xi} \right)^{1/2} \\ &\approx bN^{1/2} \begin{cases} (c_{\text{Bead}}/c)^{1/4}, & \text{for } c^* < c < c_{\text{Bead}} \\ (c_{\text{Bead}}/c)^{1/3}, & \text{for } c_{\text{Bead}} < c < c_b \end{cases}\end{aligned}\quad (3.46)$$

where  $c_b$  is the polymer concentrations at which the beads start to overlap. This crossover concentration is on the order of the concentration inside the beads  $c_b \approx b^{-3} |\tau|$ . It is important to point out that at the crossover concentration between string-controlled and bead-controlled regimes, the chain size is approximately equal to the Gaussian chain size  $bN^{1/2}$ , but its conformation is far from that of an ideal chain. In the bead-controlled regime, the chain size is smaller than the Gaussian chain size. However, above the bead overlap concentration, the chain size is once again on the order of the Gaussian chain size. But now the chain configuration is that of an ideal chain because at these high polymer concentrations the electrostatic interactions are almost completely screened. Thus, the existence of three different length scales is manifested in non-monotonic dependence of the chain size on polymer concentration [49]. This chain size dependence on polymer concentration is reflected in the dynamic properties of polyelectrolyte solutions and is expected to lead to a dramatic increase in the solution viscosity close to bead overlap concentration. The scaling predictions of the dynamic properties of polyelectrolyte solutions in poor solvent for polymer backbone are summarized in Table 2.

The existence of different concentration regimes in semidilute polyelectrolyte solutions was confirmed by the experiments of Essafi et al. [131] and Spitteri et al. [132,133] on partially sulfonated poly(styrene sulfonate) in water. It was reported by Essafi et al. [131] that the exponent of the concentration dependence of the correlation length  $\xi(c)$  depends on the degree of sulfonation. For example, this exponent is  $-0.38$  for 40% sulfonation throughout the whole semidilute regime while it is close to its classical value  $-0.5$  for the fully

Table 2

Scaling relations for semidilute solutions of polyelectrolytes in a poor solvent for the polymer backbone

String-controlled regime: $R \approx bN^{1/2}m_b^{-1/8}(cb^3)^{-1/4}y^{-1/8}$ ; $\xi \approx bm_b^{1/4}(cb^3)^{-1/2}y^{1/4}$		Bead-controlled regime: $R \approx bN^{1/2}m_b^{-1/6}(cb^3)^{-1/3}y^{-5/24}$ ; $\xi \approx bm_b^{1/3}(cb^3)^{-1/3}y^{5/12}$		
Unentangled	Entangled	Unentangled	Entangled	
$\tau$	$(\eta_s b^3/k_B T)N^2 m_b^{-3/4}(cb^3)^{-1/2}y^{-3/4}$	$(\eta_s b^3/k_B T)N^3 n^{-2}m_b^{-3/2}y^{-3/2}$	$(\eta_s/k_B T)N^2 m_b^{-1}c^{-1}y^{-5/4}$	$(\eta_s b^3/k_B T)N^3 n^{-2}m_b^{-2}y^{-5/2}c^{-1}$
$G$	$k_B Tc/N$	$(k_B T/b^3)n^{-2}m_b^{-3/4}(cb^3)^{3/2}y^{-3/4}$	$k_B Tc/N$	$(k_B T/n^2)m_b^{-1}cy^{-5/4}$
$\eta$	$\eta_s N m_b^{-3/4}(cb^3)^{1/2}y^{-3/4}$	$\eta_s (N^3/n^4)m_b^{-9/4}(cb^3)^{3/2}y^{-9/4}$	$\eta_s N m_b^{-1}y^{-5/4}$	$\eta_s (N^3/n^4)m_b^{-3}y^{-15/4}$

where  $y = (1 + 2c_s/cf_*)$ , and  $m_b \approx |\tau|/uf_*^2$  is the number of monomers in a bead. Reproduced with permission from Dobrynin, A.V. and Rubinstein, M. *Macromolecules* 32, 915–922 (1999). [130] Copyright 1999, American Chemical Society.

sulfonated samples. Similar observations were reported by Heitz et al. [134] for poly(methacrylic acid) in water as a function of its neutralization. The exponent of concentration dependence of the correlation length  $\xi(c)$  was found to change from  $-0.43$  to  $-0.31$  as the neutralization decreased from 0.95 to 0.09. Evidence of the intrachain correlation peak associated with the presence of beads was observed in the Kratky plot of the data obtained in the small angle neutron scattering experiments by Spitteri et al. [132,133]. The evolution of the polyelectrolyte solution with increasing polymer concentration in solvophobic polyelectrolytes in a series of polar organic solvents [135] shows that the scaling exponent of  $\xi(c)$  changes from  $-0.45$  to  $-0.13$ . Similar behavior was reported for partially sulfonated polystyrene by the Williams group [136,137]. This concentration dependence of the correlation length is in qualitative agreement with the predictions of the necklace model for the crossover to the bead-controlled regime.

The small angle neutron scattering (SANS) spectra [138] measured in dilute solutions of water/acetone mixtures of poly(methacryloylethyltrimethylammonium methyl sulfate) can be analyzed using the necklace model of polyelectrolyte chains. According to the results of these experiments, each polyelectrolyte chain consists of a sequence of dense beads connected by regions of loose polymer. The radius of these dense beads is about 28 nm. Each molecule has about 3–4 dense beads with the volume fraction of polymer inside these globular sections close to 8%.

Recent nuclear magnetic resonance (NMR) studies [139] of semidilute solutions of poly(styrenesulfonic acid) (PSS), poly(methacrylic acid) (PMA), and

poly(acrylic acid) (PAA) in water/methanol mixtures are consistent with the necklace-like structure of polyelectrolytes in poor solvent conditions. These observations indicate that, while parts of polyelectrolyte chains have compact globule-like conformation, the segments of the chains connecting these compact globules retain flexibility similar to those observed in  $\Theta$  and good solvents. The fraction of the mass of polyelectrolytes in compact globules varies from 27 to 32% depending on the polymeric system.

Atomic force microscopy (AFM) images of necklace globules of poly(2-vinylpyridine) and poly(methacryloyloxyethyl dimethylbenzylammonium chloride) adsorbed at mica surface were reported by Kiriya et al. [140] and by Minko et al. [141]. These images clearly show an abrupt conformational transition from elongated chains to compact globules through the intermediate necklace-like globule conformations with increasing ionic strength of the solution.

Molecular dynamics simulations of partially charged polyelectrolytes in poor solvent conditions were performed by the German group [46,71,72] and by Liao et al. [142]. These simulations have confirmed that polyelectrolyte chains at low polymer concentrations form necklaces of beads connected by strings (see Fig. 35). As the polymer concentration increases, the fraction of condensed counterions on the chain increases and chains shrink by decreasing the length of strings and the number of beads per chain. At higher polymer concentrations, polymer chains interpenetrate leading to a concentrated polyelectrolyte solution. In this range of polymer concentrations the chain size is observed to increase towards its Gaussian value. The non-monotonic dependence of the chain size on polymer concentration shown in Fig. 35 is in a

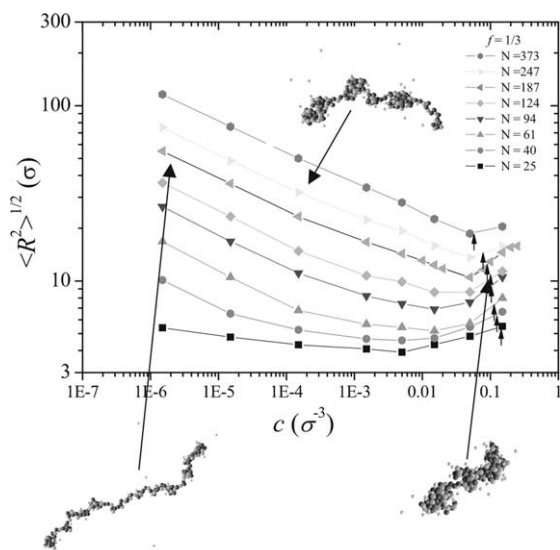


Fig. 35. Concentration dependence of the chain size for partially charged chains with fraction of charged monomers  $f=1/3$  in poor solvent [142] with interaction parameters  $l_B=3\sigma$ ,  $\varepsilon_{LJ}=3/2k_B T$ . Different color symbols and lines correspond to the different number of monomers per chain, as indicated in the figure. The positions of the overlap concentration  $c^*$  are marked by the arrows. Inserts show typical chain conformations.

qualitative agreement with the scaling model described above [130].

### 3.3. Phase separation in polyelectrolyte solutions

#### 3.3.1. Mean-field approach

It is well known that below  $\Theta$ -temperature the solution of uncharged polymers is unstable with respect to phase separation into concentrated and dilute polymeric phases. This phenomenon is driven by the minimization of the number of unfavourable polymer–solvent contacts and the relatively small entropic penalty for chain partitioning between concentrated and dilute polymeric phases. For polymers, the entropic penalty is on the order of the thermal energy  $k_B T$  per chain that is much smaller than that in the mixture of similar low molecular compounds at the same concentrations. Charging polymers can significantly improve solution solubility. In the salt-free solutions, the electroneutrality condition should be satisfied in both concentrated and dilute phases in order to avoid huge electrostatic energy penalty caused by charge inhomogeneities

(Donnan equilibrium). Thus, separating polymers into concentrated and dilute phases will lead to additional entropic penalty due to the redistribution of counterions. In order to show this, consider Flory–Huggins lattice model of polyelectrolyte solution [143,144] with polymer volume fraction  $\phi = cb^3$

$$\begin{aligned} \frac{F(\phi)}{k_B T} = & \frac{V}{b^3} \left( \frac{\phi}{N} \ln(\phi) + f\phi \ln(\phi) + \frac{\tau}{2} \phi^2 + \frac{\phi^3}{6} \right) \\ & + \frac{\Delta F_{\text{ionic}}(\phi)}{k_B T} \end{aligned} \quad (3.47)$$

where  $\tau = 1 - \Theta/T$  is the effective temperature. The first two terms in Eq. (3.47) are contributions of chains and counterions to the entropy of mixing, while third and fourth terms correspond to short-range interactions between polymers and solvent. Finally, the last term describes the contribution to the solution free energy from the density fluctuations. The form of this term depends on the assumptions made about the effect of polymeric degrees of freedom on density and charge fluctuations in the system. If the polymeric effects are completely ignored, the fluctuation term is the well-known Debye–Huckel correction due to charge density fluctuations (see for details Ref. [32]). In the limit  $\kappa b \ll 1$  it reduces to the Debye–Huckel law,  $-k_B T V \kappa^3$ . The fluctuation correction has a completely different form if the effect of the connectivity of charged monomers into polymeric chain is taken into account. There are two different expressions for this term: one was derived by Borue and Erukhimovich [145] (see also Ref. [146]) and another is due to Mahdi and Olvera de la Cruz [147]. (Ermoshkin and Olvera de la Cruz [148] have recently modified Mahdi and Olvera de la Cruz's [147] approach by taking into account finite ion size and counterion condensation.) Both calculations treat polymeric and counterion density fluctuations in the framework of the random phase approximation. The expression derived by Mahdi and Olvera de la Cruz has a more general form and takes into account the finite  $N$  effects. In the limit of long polyelectrolyte chains,  $N \gg 1$ , it reproduces Borue and Erukhimovich's result [145].

The fluctuation corrections to the free energy of the solution of weakly charged polyelectrolytes with

$f \ll 1$  can be neglected and the terms in the brackets on the right-hand side of Eq (3.47) are sufficient to determine the stability region of the polyelectrolyte solution. The spinodal of the polyelectrolyte solution is given by the following equation

$$\frac{\partial^2 F(\phi)}{\partial \phi^2} = \left( f + \frac{1}{N} \right) \phi^{-1} + \tau + \phi = 0 \quad (3.48)$$

If there is more than one ionized group per chain,  $fN \gg 1$ , the  $1/N$  term can be neglected and the location of the stability region is determined by the counterion entropy and by the strength of polymer solvent interactions. In this case the critical point is located at

$$\phi_{\text{cr}} = \sqrt{f}, \quad \text{and} \quad \tau_{\text{cr}} = -2\sqrt{f} \quad (3.49)$$

At effective temperature  $\tau$  below  $\tau_{\text{cr}}$  the polyelectrolyte solutions are phase separated over some concentration range. The dependence of the spinodal line of the salt-free polyelectrolyte solution on the fraction of charged monomers  $f$  on the polymer backbone is shown in Fig. 36. With increasing fraction of charged monomers  $f$  the two-phase region moves towards lower effective temperatures and is located at lower temperatures than in solutions of neutral polymers (for neutral polymers  $\tau_{\text{cr}} \approx -2/\sqrt{N}$ ) making polyelectrolyte solutions more stable. Monte Carlo simulations [149] of the phase separation in polyelectrolyte solutions have confirmed that  $\phi_{\text{cr}}$  is independent of the degree of polymerisation  $N$ .

The addition of salt to polyelectrolyte solutions lowers the penalty due to counterion redistribution

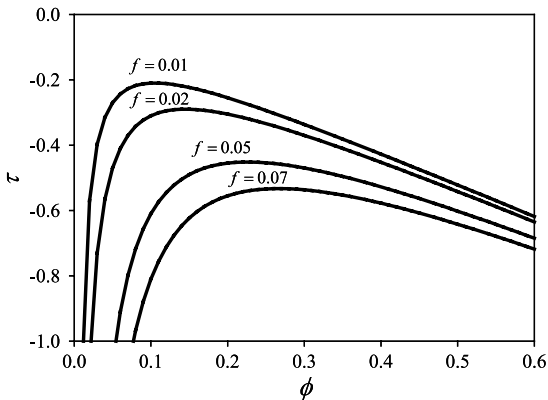


Fig. 36. Spinodal line given by Eq. (3.48) for weakly charged polyelectrolytes with the degree of polymerization  $N=1000$ .

thus promoting phase separation. At high salt concentrations, the electrostatic interactions between charged monomers are exponentially screened leading to the renormalization of the second virial coefficient between monomers. The Flory–Huggins free energy of polyelectrolyte solutions at high salt concentrations is

$$\begin{aligned} \frac{F(\phi)}{k_B T} = & \frac{V}{b^3} \left[ \frac{\phi}{N} \ln(\phi) + \left( \tau + \frac{f^2}{2c_s b^3} \right) \frac{\phi^2}{2} + \frac{\phi^3}{6} \right] \\ & + \frac{\Delta F_{\text{ionic}}(\phi)}{k_B T} \end{aligned} \quad (3.50)$$

Taking the second derivative of Eq. (3.50) with respect to polymer volume fraction  $\phi$ , we obtain the following equation for the spinodal line of the phase diagram

$$\frac{1}{N\phi} + \tau + \frac{f^2}{2c_s b^3} + \phi = 0 \quad (3.51a)$$

with the critical point located at volume fraction

$$\phi_{\text{cr}} = \frac{1}{\sqrt{N}}, \quad (3.51b)$$

and effective temperature

$$\tau_{\text{cr}} = -\frac{2}{\sqrt{N}} - \frac{f^2}{2c_s b^3} \quad (3.51c)$$

Thus, addition of salt leads to the increase of the critical temperature. The shift of the critical point is inversely proportional to the salt concentration  $c_s$  at high salt concentrations. For a recent review of experimental results of the phase separation in polyelectrolyte solutions see the paper by Volk et al. [150].

The Flory–Huggins lattice consideration of the polyelectrolyte solutions presented above incorrectly describes dilute polyelectrolyte solutions. In the Flory–Huggins approach, the monomers are uniformly distributed over the whole volume of the system leading to underestimation of the effect of short-range monomer–monomer interactions and of the intrachain electrostatic interactions. A similar problem appears in the Flory–Huggins theory of phase separation of polymer solutions (see for discussion Refs. [10,22]). This leads to the incorrect expression

for the low polymer density branch of the phase diagram.

### 3.3.2. Microphase separation

Phase separation into dilute and concentrated phases is not the only option for polyelectrolytes in a poor solvent for polymer backbone. It was shown that weakly charged polyelectrolytes could locally violate electroneutrality condition thus minimizing the entropy loss due to the redistribution of counterions. This local violation of electroneutrality leads to the formation of mesophases—alternating regions with high and low polymer densities. These mesophases appear as a result of optimization of electrostatic and short-range interactions. The possibility of this type of instability of the homogeneous phase in solutions of weakly charged polyelectrolytes was first discovered by Borue and Erukhimovich [145] and then studied in a series of papers by Joanny and Leibler [151], Vilgis and Borsali [146], and Khokhlov and Nyrkova [143].

The stability analysis of the homogeneous phase is done by investigating the correction to the free energy of homogeneous phase that is quadratic in the power of the Fourier transform of the polymer density fluctuations  $\delta\phi(\mathbf{q})$ . For weakly charged polyelectrolytes, this correction has the following form

$$\frac{\Delta F(\{\delta\phi(\mathbf{q})\})}{k_B T} = \frac{1}{2b^3} \int \frac{d\mathbf{q}}{(2\pi)^3} \left[ \frac{1}{\phi N} + \frac{\mathbf{q}^2 b^2}{12\phi} + \tau + \phi + \frac{4\pi l_B f^2}{b^3(\mathbf{q}^2 + \kappa^2)} \right] \delta\phi(\mathbf{q})\delta\phi(-\mathbf{q}) \quad (3.52)$$

where  $q$  is the wave vector of the reciprocal space. The first two terms in square brackets in Eq. (3.52) describe the effect of the connectivity of the polymer chain, the third and fourth terms correspond to the short-range interactions between monomers, while the last term describes the effect of electrostatic interactions between charge density waves formed by polymer density fluctuations. The Debye screening length,  $\kappa^{-1}$ , in Eq. (3.52) includes contributions from both counterions and salt ions,  $\kappa^2 = 4\pi l_B (fc + 2c_s)$ .

The magnitude of the mean-square fluctuations of the Fourier component of the polymer volume fraction at wavelength  $2\pi/q$  corresponds to fluctuations of the free energy, Eq. (3.52), of the order of the

thermal energy  $k_B T$  and is proportional to

$$\langle \delta\phi(\mathbf{q})\delta\phi(-\mathbf{q}) \rangle \propto \left( \frac{1}{\phi N} + \frac{\mathbf{q}^2 b^2}{12\phi} + \tau + \phi + \frac{4\pi l_B f^2}{b^3(\mathbf{q}^2 + \kappa^2)} \right)^{-1} \quad (3.53)$$

The fastest growing modes correspond to the maximum of the right-hand side of Eq. (3.53). The maximum of the expression (3.53) as a function of the absolute value of  $q$ -vector is located at

$$\mathbf{q}_{\max}^2 b^2 = (48\pi u f^2 \phi)^{1/2} - \kappa^2 b^2 \quad (3.54)$$

In salt-free polyelectrolyte solutions, the position of the maximum  $q_{\max}$  scales as one-fourth power of the polymer volume fraction  $\phi$ . This concentration dependence of the maximum in the scattering function was recently observed by Braun et al. [152]. As salt is added to the solution, the maximum shifts towards smaller  $q$  values corresponding to larger length scales. At high salt concentrations, the maximum disappears and the system behaves as a solution of neutral polymers with effective short-range interactions.

The spinodal of the homogeneous phase with respect to density fluctuations with finite value of the wavevector  $q_{\max}$  (so-called microphase separation) is

$$\frac{1}{\phi N} + \tau + \phi + \left( \frac{4\pi}{3} \frac{u f^2}{\phi} \right)^{1/2} - \frac{\kappa^2 b^2}{12\phi} = 0 \quad (3.55)$$

In salt-free solutions with  $c_s = 0$  and  $\kappa^2 = 4\pi l_B f c$  this expression becomes

$$\frac{1}{\phi N} + \tau + \phi + \left( \frac{4\pi}{3} \frac{u f^2}{\phi} \right)^{1/2} - \frac{\pi u f}{3} = 0 \quad (3.56)$$

and the critical point of the spinodal is located at

$$\phi_{\text{cr}} = \left( \frac{\pi}{3} u f^2 \right)^{1/3}, \quad \text{and} \quad (3.57)$$

$$\tau_{\text{cr}} = -(9\pi u f^2)^{1/3}$$

where we neglected  $N^{-1}$  term in Eq. (3.56). Thus, below the critical temperature the system could form mesophases. It turns out that the critical temperature for microphase separation given by Eq. (3.57) is located above the critical temperature for macrophase separation transition (see Eq. (3.49)). It indicates that upon cooling the system first forms mesophases and

then phase separates into concentrated and dilute phases.

The phase separation and mesophase formation in solutions of weakly charged polyelectrolytes in poor solvent for polymer backbone was investigated by Dormidontova et al. [153] (see Fig. 37). Using the weak-crystallization theory, they calculated a phase diagram of the system in the Flory–Huggins parameter  $\chi$ —volume fraction  $\phi$  plane. Dormidontova et al. found in some parts of phase diagram spherical microdomains organized into body-centered-cubic lattice (region 2), in other parts of the phase diagram cylindrical domains forming a triangular lattice (region 3), while in the third part of phase diagram they found lamellar microdomains (region 4). These mesophases can coexist with homogeneous concentrated and dilute phases (region 1). The specific feature of the phase diagram in Ref. [153] is the region of stability of the cylindrical mesophase (region 3) that separates coexistence region (5) into two parts. It should be noted that the weak-crystallization theory is only correct close to the spinodal line of the homogeneous phase, where the relative amplitudes

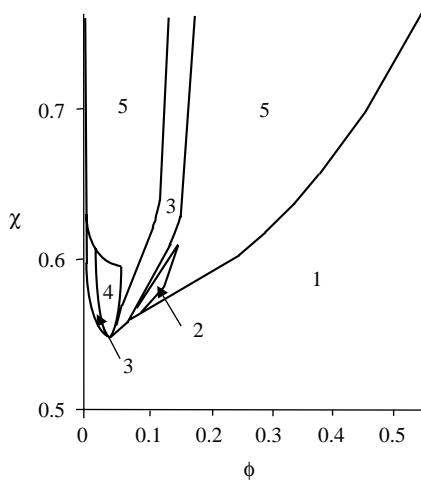


Fig. 37. Phase diagram of solutions of weakly charged polyelectrolytes in Flory–Huggins interaction parameter  $\chi$  and polymer volume fraction  $\phi$  plane [153]. The numbered regions correspond to: homogeneous phase (1), microphase separated phase with microdomains forming body-centered-cubic lattice (2), triangular microdomain phase (3), lamellar microdomain phase (4), and region of phase separation (5). Reproduced with permission from Dormidontova, E.E., Erukhimovich, I.Y., & Khokhlov, A.R. *Macromolecular Theory and Simulations* 3, 661–675 (1994). [153] Copyright 1994, Wiley–VCH.

of the density waves, corresponding to the formation of the microdomains, are smaller than unity. Furthermore, in the strong segregation limit with well-defined interface between regions of dense and very dilute polymer solutions, the cylindrical microdomains are unstable with respect to capillary waves that lead to the formation of the necklace-like structure of beads (spherical microdomains) connected by strings of polymeric strands. A similar effect causes a cylindrical polyelectrolyte globule [47] to transform into a necklace-like globule [34] (see Section 2.3).

The weak-crystallization theory of microphase separation in polyelectrolyte solutions has another shortcoming. It assumes that the effect of electrostatic interactions on the chain conformation is very weak allowing one to utilize the ideal chain statistics in describing the effect of chain connectivity on polymer density fluctuations. This approximation is only correct at high polymer concentrations such that  $\phi > |\tau|$ . Thus, the description of the semidilute and dilute polymer solution regions of the phase diagram in Ref. [153] could only be qualitatively correct.

### 3.3.3. Necklace model of phase separation

A different approach to the phase separation in polyelectrolyte solutions was proposed by Dobrynin and Rubinstein [49]. They used a two-zone model to describe counterion condensation inside beads of the necklace-like globules in dilute solutions. Within this approximation, the free energy of the dilute solution of necklaces is

$$\frac{F_{\text{neck}}(\phi)}{k_B T} \approx \frac{V}{b^3} \left( \frac{\phi}{N} \ln(\phi) + \phi f \ln(f\beta|\tau|) + \phi f \frac{(1-\beta)^{2/3}}{3} \left( \frac{u}{f} \right)^{1/3} |\tau| - \phi \tau^2 \right) \quad (3.58)$$

where  $\beta$  is the fraction of condensed counterions. The first term on the right-hand side of Eq. (3.58) describes polymer contribution to the entropy of mixing, the second term is the entropy of counterions localized inside beads, the third term is the free energy of the beads, and, finally, the last term is the contribution to the necklace free energy due to the short-range monomer–monomer interactions inside beads. The dense polymeric phase was described by adopting the virial expansion of the Flory–Huggins free energy

(see Eq. (3.47)). The phase diagram was calculated by comparing the chemical potential of chains and the osmotic pressure in dilute and concentrated phases. Fig. 38 shows the resultant phase diagram of salt-free polyelectrolyte solutions at poor solvent conditions for the polymer backbone. The shaded area corresponds to the two-phase region. Above the critical temperature (for the values of the parameter  $|\tau| < (f/u)^{1/3}$ ), the polyelectrolyte solution is stable with respect to phase separation. In regime I of the phase diagram (Fig. 38), the thermal blob size  $\xi_r \approx b/|\tau|$  is larger than the bead size  $D_b \approx b(uf^2)^{-1/3}$ . For the range of the effective temperatures  $|\tau| < (uf^2)^{1/3}$  the polymer–solvent interactions are not strong enough to collapse chains, and they adopt the conformations similar to the ones for polyelectrolytes in a  $\Theta$ -solvent (regime I). In regime II, the polymer–solvent interactions dominate at small length scales and polyelectrolytes form necklace globules. The chains can either be in a dilute regime for polymer concentration below the overlap concentration  $c^*$  (see Eq. (3.40)) or in a semidilute regime for  $c > c^*$ . In the semidilute regime, the correlation length  $\xi$  decreases with increasing polymer concentration  $c$  (see Eq. (3.41)). The correlation length  $\xi$  becomes on the order of the length of a string  $l_{\text{str}}$  connecting two neighboring beads at polymer concentration  $c \approx c_{\text{Bread}}$  (see Eq. (3.43)). At this polymer concentration the

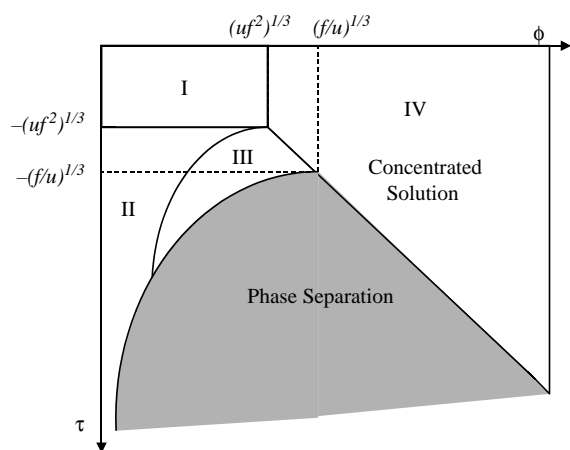


Fig. 38. Phase diagram of polyelectrolytes in a poor solvent. Logarithmic scales. Reproduced with permission from Dobrynin, A.V. & Rubinstein, M. *Macromolecules* 34, 1964–1972 (2001). [49] Copyright 2001, American Chemical Society.

system crosses over into the so-called bead-controlled regime in which there is one bead per every correlation volume  $\xi^3$  and polyelectrolyte solution can be viewed as a strongly correlated charged colloidal liquid of beads (regime III). It is interesting to point out that the upper crossover point of the regime III has the same dependence on the parameters  $u$  and  $f$  as the critical point of the spinodal of the microphase separation transition (see Eq. (3.57)). The structure of the polyelectrolyte solution in the bead-controlled regime resembles that of microphase separated one with beads forming polymer-rich spherical domains that are surrounded by a solution of strings with the excess of the solvent.

For the effective temperature  $|\tau| \approx (f/u)^{1/3}$ , the correlation length  $\xi$  becomes on the order of the size of a bead  $D_b$  at polymer concentration  $cb^3 \approx |\tau|$ . At higher polymer concentrations, the system crosses over into the concentrated polyelectrolyte solution (regime IV). However, if the value of the parameter  $|\tau|$  is larger than  $(f/u)^{1/3}$  the system will phase separate into a concentrated polymer solution and a solution of necklaces. The left boundary of the two-phase region is

$$\phi_{\text{dil}} \approx |\tau| \exp\left(-\left(\frac{u}{f}\right)^{1/3} |\tau|\right) \quad (3.59)$$

while the right boundary of the two-phase region is

$$\phi_{\text{con}} \approx |\tau| \quad (3.60)$$

Thus, the polymer volume fraction in the concentrated phase at the two-phase boundary is the same as inside beads of the necklace globule in the dilute phase. Two lines given by Eqs. (3.59) and (3.60) intersect at  $\phi_{\text{cr}} \approx (f/u)^{1/3}$  and  $\tau_{\text{cr}} \approx -(f/u)^{1/3}$ .

The phase separation in solutions of hydrophobic polyelectrolyte was observed in MD simulations of Chang and Yethiraj [154]. They have found that solutions of necklaces phase separate with increasing polymer concentration. Polyelectrolytes in the dense phase form spherical, cylindrical, and lamellar structures depending on polymer concentration.

### 3.4. PRISM and self-consistent field methods

The self-consistent integral equation approach to polyelectrolyte solutions [155–157] is an extension of

the polymer–reference-interacting site model (PRISM) to charged systems introduced by Curro and Schweizer [158]. In this approach a multi-chain system is approximated by a single chain in the effective medium. Monomers on the polymer chain in this medium interact via the bare potential  $V(r)$  and the medium-induced interaction potential  $W(r)$ . The theory self-consistently determines relations between the total correlation function  $h(r)$ , direct correlation function  $c(r)$ , and the single chain structure factor  $\omega(r)$ . In the Fourier space these equations are

$$\hat{h}(q) = \hat{\omega}(q)\hat{c}(q)\hat{S}(q) \quad (3.61)$$

where the carets denote the Fourier transforms

$$\hat{h}(q) = \int dr \exp(i\mathbf{q}\mathbf{r})h(r) \quad (3.62)$$

$\hat{S}(q)$  is the static structure factor

$$\hat{S}(q) = \hat{\omega}(q) + \rho\hat{h}(q) \quad (3.63)$$

and  $\rho$  is the average monomer–monomer density. The single chain structure factor  $\omega(r)$  is defined as

$$\omega(r) = N^{-1} \sum_{\gamma,\delta} \omega_{\gamma\delta}(r) \quad (3.64)$$

where  $\omega_{\gamma\delta}(r)$  is the probability distribution function that two monomers  $\gamma$  and  $\delta$  are separated by distance  $r$ , and  $N$  is the chain degree of polymerization. The PRISM equations can be solved providing the closure relation between the direct,  $c(r)$ , and the total correlation function,  $h(r)$ . For charged systems the Laria–Wu–Chandler (LWC) closure [159]

$$\omega * c * \omega(r) = \omega * \left( -\frac{V(r)}{k_B T} \right) * \omega(r) + h(r) - \ln g(r) \quad (3.65)$$

achieves a better agreement between simulations and analytical results for static properties of polyelectrolyte solutions. In Eq. (3.65), the asterisks denote convolution integrals and  $g(r)$  is the pair correlation function,  $g(r) = 1 + h(r)$ . In this closure, the direct correlation between two molecules is approximated by the sum of the pairwise interaction and the reaction field induced by many-body correlations.

The medium-induced interaction potential is obtained from the pair correlation functions using the mean pair approximation. In the hypernated chain

approximation, the medium-induced potential is given by

$$\frac{\hat{W}(q)}{k_B T} = -\rho\hat{c}(q)\hat{S}(q)\hat{c}(q) \quad (3.66)$$

The chain structure factor  $\omega(r)$  is then self-consistently calculated either from the minimization of a chain free energy in the effective medium calculated in the Gaussian approximation [80] or from the Edwards–Singh approach [88] which minimizes an error in the perturbation series expansion of the mean-square average end-to-end distance of polymers. The PRISM equations and the equation for the chain structure factor are solved iteratively with the initial guess for the medium-induced interaction  $W(r) = 0$ . The procedure is repeated until the required accuracy is achieved.

Fig. 39 shows comparison of the results of PRISM calculations for the concentration dependence of the chain size in the solution of polyelectrolyte chains interacting via Yukawa potential to the results of computer simulations [70]. The PRISM theory underestimates the chain size in both dilute and semidilute solutions. The agreement with the simulation results can be improved if instead of using variational approach in calculating single chain properties, one

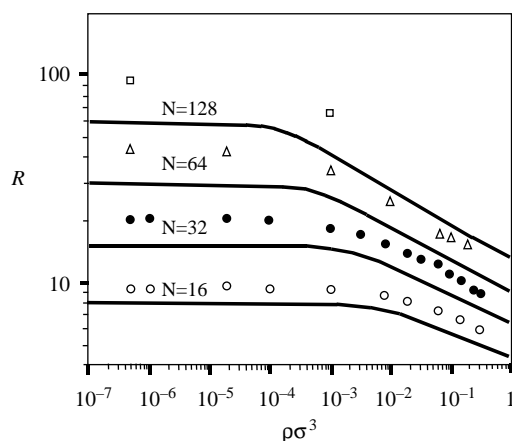


Fig. 39. Comparison of concentration dependence of the root-mean-square end-to-end distance obtained by PRISM method [166] (solid lines) to those obtained in molecular dynamics simulations by Stevens and Kremer (*Journal of Chemical Physics* 103, 1669–1690 (1995)) (symbols). Reprinted with permission from Yethiraj, A. *Journal of Chemical Physics*, 108, 1184 (1998). Copyright 1998, American Institute of Physics.

performs Monte–Carlo simulations of a chain with the effective interaction potential at each iteration step. The PRISM theory predicts scaling exponents for the position of the maximum in the structure factor  $\hat{S}(q)$  in both dilute,  $q_{\max} \sim \rho^{1/3}$ , and semidilute,  $q_{\max} \sim \rho^{1/2}$ , solution regimes, as well as polymer and salt concentration dependence of the chain size in dilute and semidilute regimes similar to those obtained in the framework of the scaling theories described in Section 3.2.

This approach was successfully applied by Yethiraj [155,156] to describe solutions of flexible polyelectrolytes interacting via the Yukawa potential. During the last few years this approach was utilized to obtain solution properties of rod-like [160–162] and semiflexible [163–166] polyelectrolyte chains in a wide concentration range.

The field theoretical approach to polyelectrolyte solution was pioneered by Muthukumar [167]. This approach also reduces a multi-chain problem of strongly interacting polyelectrolytes to a single-chain problem in the effective medium potential. This is achieved by performing Hubbard–Stratonovich transformation that reduces the pairwise interactions to the effective external field (effective medium field) acting on each monomer. As in the PRISM approach, the effective medium properties and chain structure factor are found in a self-consistent manner. This approach allows calculations of the limiting scaling laws in semidilute and concentrated polyelectrolyte solutions as well as analytical interpolation formulas for the correlation length, chain persistence length, and the average chain size at various polymer and salt concentrations.

The computationally efficient realization of the field theoretical method in concentrated polyelectrolyte systems was recently developed by Wang et al. [168]. In this approach, the electrostatic interactions are described by the non-linear Poisson–Boltzmann equation with space-dependent dielectric constant that accounts for the large differences in dielectric constants of pure solvent and regions filled with polymers. The solution of the non-linear Poisson–Boltzmann equation at a given polymer density profile provides the distribution of the electrostatic potential over the system volume. The polymer density distribution is then re-calculated by solving the diffusion equation for the monomer probability

distribution function in the effective external potential. This distribution function is used to obtain a new polymer density profile, which is used as the input parameter for the Poisson–Boltzmann equation. The iterative procedure continues until the required accuracy is achieved. This method was applied to the phase separated polyelectrolyte solutions in a poor solvent, to the lamellar structured system of the symmetric diblock polyelectrolytes, and to the polyelectrolyte blends. This method provides a quantitative agreement with results of computer simulations.

## 4. Adsorption of polyelectrolytes

### 4.1. A brief historic overview of theoretical models of polyelectrolyte adsorption

Adsorption of charged polymers on charged surfaces and interfaces is a classical problem of polymer physics and has been under extensive theoretical and experimental studies for the last four decades [63,169–173]. Interest in this problem is stimulated by its tremendous importance for different areas of natural sciences ranging from materials science to physics of disordered systems and biophysics.

One of the first analytical calculations of the polyelectrolyte adsorption at a charged surface was performed by Wiegel [174,175]. Assuming the Gaussian statistics of a polyelectrolyte chain, he calculated the adsorption threshold and the thickness of the adsorbed chain as a function of salt concentration. The binding of flexible macromolecules to the oppositely charged cylinder was treated by Odijk in a similar way [176]. The interaction between the charged monomers on the chain was taken into account by Muthukumar [177], who considered a general case of the adsorption of a polyelectrolyte chain that can take any conformation between those of a self-avoiding walk and a rod, depending on the ionic strength of the solution. This theory was later extended to polyelectrolyte adsorption on charged patterned surfaces [178] and validated by Monte Carlo simulations [178–180]. The scaling theory of the conformations of a weakly charged polyelectrolyte chain near a charged surface was

proposed by Borisov et al. [181]. There are different stages of adsorption of a polyion corresponding to the rearrangement of chain conformations on different length scales. The predictions of the theory were confirmed by computer simulations [182]. The detailed interfacial properties of a lattice model for adsorption of a single polyelectrolyte chain were studied by Beltran et al. [183] using Monte Carlo simulations. It was demonstrated that polyelectrolyte chains flatten out forming long trains of loops upon increase in the surface charge density or in the fraction of the charged monomers on the chain.

The Hoeve's theory [184,185] for adsorption of uncharged polymers was generalized by Hesselink [186], who incorporated the electrostatic contribution into Hoeve's partition function of an uncharged adsorbed polymer and considered the total free energy of a system as a sum of electrostatic and non-electrostatic terms. Assuming a step-like polymer density distribution in the adsorbed layer, Hesselink calculated the adsorption isotherm and polymer surface coverage as a function of salt concentration. The adsorbed amount rises very steeply and levels off at the saturation value in solutions with extremely low polymer concentrations. Hesselink's theory predicts an increase of polymer adsorbed amount with increasing salt concentration.

The significant fraction of theoretical works dealing with multi-chain polyelectrolyte adsorption at a charged surface was carried out within the framework of the self-consistent field (SCF) method [170,187,188]. The polymer density distribution is coupled in these theories to the local electrostatic potential through the combination of the Poisson–Boltzmann equation and the Edwards equation describing polymer conformations in the effective external potential. This approach was first applied by van der Schee and Lyklema [189] and Evers et al. [190]. They have showed that strong repulsion between charged monomers leads to very thin adsorbed layers. The adsorbed amount increases and the adsorbed layer becomes thicker, if this repulsion is screened by adding salt. The extension of the Van der Schee and Lyklema theory to the case of weak polyelectrolytes was done by Bohmer et al. [191]. The charge on adsorbed weak polyelectrolytes is determined by the pH and salt concentration in the local environment of ionizable groups [172,191–193].

Polyelectrolyte adsorption was also studied using the ground-state dominance approximation of the SCF method [194–198]. Linearized solution of the Poisson–Boltzmann and of Edwards' equations was obtained by Varoqui et al. [194]. They considered conformations of weakly charged polyelectrolytes at a liquid–solid interface and calculated the adsorption isotherm and the concentration profile of these polyelectrolytes near the charged interface. These calculations show that the thickness of the adsorbed layer  $D$  increases with increasing the surface number charge density  $\sigma$  as  $D \propto \sigma^{1/3}$ . The numerical solution of the non-linear Poisson–Boltzmann equation was presented by Borukhov et al. [197,199]. These authors also calculated the concentration profile of weakly charged polyelectrolytes between two charged surfaces and the effective interactions between charged surfaces [199–201]. Protective polyelectrolyte layers lead to additional repulsive interactions between surfaces. The analytical results for the polymer density profiles within the framework of linear response approximation were obtained by Chatellier and Joanny [198]. It was demonstrated that the concentration profile at low ionic strength shows damped oscillations. The microscopic theory in the framework of integral equation approach for the interaction forces between hydrophobic surfaces immersed in salt-free polyelectrolyte solutions have been developed by Yethiraj [202]. The theory predicts oscillatory forces between surfaces with the period of oscillation proportional to the correlation length of polyelectrolyte solution. This theory is in good qualitative agreement with computer simulations by Carignano and Dan [203].

The attempt to describe the irreversible nature of polyelectrolyte adsorption was made by Barford et al. [204,205]. They proposed a model of the sequential adsorption in which the polymer density profile is built-up by the adsorption of incremental concentrations of polymers. Once each increment was adsorbed, its surface concentration remains constant, but the bulk profile equilibrates as more polymers are adsorbed. This scheme was implemented in the framework of the ground-state dominance approximation for the SCF method for which authors derived the integro-differential equation for the polymer density profile in the adsorbed layer. This model predicts that less polymer can be adsorbed and that the

polymer density profile is more extended for irreversible adsorption in comparison with the case of equilibrium adsorption.

The kinetics of polyelectrolyte adsorption was investigated theoretically by Stuart et al. [206]. The authors develop a Kramer's rate theory model that is based on the electrostatic origin of the barrier that polyelectrolytes encounter in their motion toward adsorbing surface. The height of the barrier was calculated within a self-consistent field model [170]. The model predicts that the equilibrium in adsorption is attained at high and moderate salt concentrations. However, for low salt concentrations the equilibrium cannot be reached during the time of a typical experiment.

Recent rejuvenation of the theoretical interest in the problem of polyelectrolyte adsorption [207–217] is due, in part, to the importance of this problem for understanding the formation of polyelectrolyte multilayers formed by the successive deposition of positively and negatively charged polyelectrolytes on charged surfaces from aqueous solutions [12–17]. It is now possible to produce a sequence of hundreds of alternating polyelectrolyte layers. These experiments raised an important fundamental question about the charge inversion in the adsorbed polyelectrolytes that is responsible for the successful build-up of alternating polymer layers. A model for the charge inversion in the adsorbed layer of flexible polyelectrolytes was proposed by Joanny [215]. Following the traditional route using the Edwards mean-field equation for a polyelectrolyte chain in the effective external potential together with the Poisson–Boltzmann equation he showed that the overcharging is proportional to the layer thickness and is inversely proportional to the Debye screening length.

However, the self-consistent field approach fails to describe two-dimensional semidilute and dilute adsorbed layers where polyelectrolyte chains form a strongly correlated liquid [218–221]. A good approximation in this case is to divide the adsorbed layer into Wigner–Seitz cells surrounding each polyelectrolyte chain in dilute adsorbed layer and sections of a chain in a semidilute layer [207–216]. In the framework of this approach the surface overcharging depends on the size of the Wigner–Seitz cell and can be much larger than the bare surface charge density. The Wigner–Seitz cell description of polyelectrolyte adsorption is

similar to the Katchalsky's cell model described in Section 2.4.2.

#### 4.2. Why self-consistent field method based on Poisson–Boltzmann approach does not work for polyelectrolyte adsorption

Consider adsorption of polyelectrolyte chains with the degree of polymerisation  $N$  and with fraction of charged monomers  $f$  from a dilute solution onto an oppositely charged surface with the charge number density  $\sigma$ . At very low surface charge density  $\sigma$  (below adsorption threshold) polyelectrolyte chains replace surface counterions and screen the surface charge. The number density of polyions in this pre-adsorption regime decreases with distance  $z$  from the surface according to the Gouy–Chapman solution of the non-linear Poisson–Boltzmann equation [222]

$$c_{\text{ch}}(z) = \frac{1}{fN} \frac{\sigma \lambda_{fN}}{(z + \lambda_{fN})^2} \quad (4.1)$$

The Gouy–Chapman length  $\lambda_{fN}$  for polyions with valency  $fN$  is

$$\lambda_{fN} = (2\pi l_B fN \sigma)^{-1} \quad (4.2)$$

The density of polyelectrolyte chains,  $c_{\text{ch}} \approx l_B \sigma^2$ , is almost constant within distance  $\lambda_{fN}$  from the surface. The average distance  $R$  between neighboring polyions located within the Gouy–Chapman length from the surface can be estimated as  $R \approx c_{\text{ch}}^{-1/3} \approx l_B^{-1/3} \sigma^{-2/3}$ . This screening layer is dilute with the distance between macroions  $R$  larger than their size  $R_e$  ( $R_e < R < \lambda_{fN}$ ). The electrostatic repulsion between two polyions carrying charge  $efN$  separated by distance  $R$  is equal to

$$U_{\text{el}} \approx k_B T \frac{l_B (fN)^2}{R} \approx k_B T (\sigma / \sigma_{\text{WC}})^{2/3} \quad (4.3)$$

This electrostatic repulsion is weaker than the thermal energy  $k_B T$  when the surface charge number density  $\sigma$  is smaller than

$$\sigma_{\text{WC}} \approx l_B^{-2} f^{-3} N^{-3} \quad (4.4)$$

At low surface charge densities,  $\sigma < \sigma_{\text{WC}}$ , the classical Poisson–Boltzmann approach works well to describe distribution of polyions near charged substrates. However, at higher surface charge densities,  $\sigma > \sigma_{\text{WC}}$ , the electrostatic repulsion between polyions,

$U_{el} > k_B T$ , forces them to organize into a two-dimensional strongly correlated Wigner liquid at the charged surface (distance  $R$  between chains becomes larger than their distance  $\lambda_{fN}$  to the surface). For a polyelectrolyte chain consisting of  $N=10^2$  Kuhn monomers with 10% of these monomers charged ( $f=0.1$ ) adsorbing from the aqueous solutions with the Bjerrum length  $l_B=7$  Å the crossover surface charge density is equal to  $\sigma_{wc} \approx 2 \times 10^{-5}$  A $^{-2}$ . This is very low surface charge density, which is at the lowest end of the most experiments on polyelectrolyte adsorption on glass and mica substrates. Thus, for most experiments adsorbed polyelectrolyte chains form strongly correlated Wigner liquid [218–221].

#### 4.3. Two-dimensional adsorbed layers [209]

In this section we review the results of the cell model of polyelectrolyte adsorption from a dilute solution with salt concentration  $c_s$ . In this approach, each polyelectrolyte chain or section of a chain is localized in the center of the cell due to strong electrostatic repulsion between chains.

##### 4.3.1. Dilute regime

The distance  $R$  between chains in a dilute two-dimensional adsorbed layer is larger than their size  $R_c$ . (Here, we will use the scaling expression for the chain size in a  $\Theta$ -solvent for the polymer backbone neglecting logarithmic corrections and consider adsorption of polyelectrolyte chains driven exclusively by electrostatic interactions.) The total electrostatic energy of an adsorbed polyelectrolyte chain includes the electrostatic attraction of the chain to the charged surface with the surface charge number density  $\sigma$  (see Fig. 40)

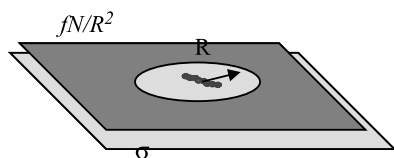


Fig. 40. Schematic sketch of an adsorbed layer in dilute 2D regime. Reproduced with permission from Dobrynin, A.V., Deshkovski, A., & Rubinstein, M. *Macromolecules* 34, 1964–1972 (2001). [209] Copyright 2001, American Chemical Society.

$$\frac{U_{att}}{k_B T} \approx -l_B f N \sigma \int_0^{\infty} dr r \exp(-r/r_D) = -l_B f N \sigma r_D \quad (4.5)$$

and repulsion from other adsorbed polyelectrolytes distributed with the effective surface charge density  $efN/R^2$ , starting at distance  $R$  from a given polyion

$$\begin{aligned} \frac{U_{rep}}{k_B T} &\approx \frac{l_B (fN)^2}{R^2} \int_R^{\infty} dr r \exp(-r/r_D) \\ &= \frac{l_B (fN)^2 r_D}{R^2} \exp(-R/r_D) \end{aligned} \quad (4.6)$$

The total electrostatic energy of the adsorbed layer with the surface area  $S$  is the sum of the contributions from all chains

$$\frac{U_{cell}}{k_B T} \approx S l_B f N r_D \left[ \frac{1}{2} \frac{fN}{R^4} \exp(-R/r_D) - \frac{\sigma}{R^2} \right] \quad (4.7)$$

The factor 1/2 in front of the first term is added to avoid double-counting the repulsive interactions between the chains. The dependence of the cell size  $R$  on the salt concentration is derived by minimizing the total electrostatic energy with respect to  $R$ . The equilibrium cell size corresponding to the minimum of the electrostatic energy (Eq. (4.7))

$$\frac{fN}{R^2} \exp(-R/r_D) \left[ 1 + \frac{R}{4r_D} \right] \approx \sigma \quad (4.8)$$

At low salt concentrations,  $r_D > \sqrt{fN/\sigma}$ , the cell size  $R$  has a very weak dependence on the Debye screening length  $r_D$ . Thus, on the scaling level, at low salt concentrations the size of the cell is

$$R \approx R_0 \approx \sqrt{fN/\sigma}, \quad \text{low salt } r_D > \sqrt{fN/\sigma} \quad (4.9)$$

In this salt concentration regime the cell is almost electroneutral. The size of the cell is inversely proportional to the square root of the surface charge number density  $\sigma$ . In this regime the left-hand side of Eq. (4.8) can be expanded in the power series of  $R/r_D$ . Within this approximation the surface overcharging by adsorbed polyelectrolyte chains is

$$\delta\sigma \approx \frac{fN}{R^2} - \sigma \approx \frac{\sqrt{fN/\sigma}}{r_D}, \quad \text{low salt } r_D > \sqrt{fN/\sigma} \quad (4.10)$$

This equation implies that the effective surface charge density at crossover between low and high salt

regimes ( $r_D \approx R_0$ ) is of the same order of magnitude as the bare surface charge density  $\sigma$ , but has opposite sign.

The adsorption energy of polyelectrolyte chain includes repulsion from other adsorbed chains and attraction to an oppositely charged background

$$\begin{aligned} \frac{\varepsilon_{\text{ads}}}{k_B T} &\approx l_B r_D f N \left( \frac{fN}{R^2} \exp(-R/r_D) - \sigma \right) \\ &\approx -\frac{l_B (fN)^2}{R} \approx -l_B \sigma^{1/2} (fN)^{3/2} \end{aligned} \quad (4.11)$$

In rewriting Eq. (4.11) we have substituted for the surface charge density  $\sigma$  its relation with the cell size  $R$  given by Eq. (4.8) and expanded exponential functions in the power series of  $R/r_D$ . Eq. (4.11) shows that at low salt concentrations each adsorbed chain effectively interacts only with its neutralizing background within a cell of size  $R$ . Using this approximation we can estimate adsorption energy of a chain with the center of mass located at distance  $z$  ( $z \ll R$ ) from adsorbing surface

$$\begin{aligned} \frac{\varepsilon_{\text{ads}}(z)}{k_B T} &\approx l_B f N \sigma \int_0^R \frac{r dr}{\sqrt{r^2 + z^2}} \\ &\approx -l_B \sigma^{1/2} (fN)^{3/2} \left( 1 - \frac{z}{R} \right) \end{aligned} \quad (4.12)$$

The polyelectrolyte chains are strongly attracted to the surface with the binding energy  $|\varepsilon_{\text{ads}}| \gg k_B T$  as long as the surface charge density  $\sigma$  is larger than the threshold value  $\sigma_{\text{WC}}$  (see Eq. (4.4)). The electrostatic attraction of a polyelectrolyte chain to a charged surface  $|\varepsilon_{\text{ads}}| \approx k_B T (N/g_e^0) R_e/R$  is weaker than the electrostatic self-energy of a chain  $k_B T (N/g_e^0)$  as long as polyelectrolyte chains in the adsorbed layer do not overlap ( $R_e < R$ ). Therefore, this attraction is not strong enough to perturb the internal chain structure determined by the repulsion between charged monomers along the polymer backbone and only influence translational and orientational degrees of freedom of the polyelectrolyte. The polyelectrolytes are localized within thickness

$$D \approx (l_B f N \sigma)^{-1} \quad (4.13)$$

inside which (for  $z < D$ ) the variations of the adsorption energy Eq. (4.12) are on the order of the

thermal energy  $k_B T$ . The probability of finding polyelectrolyte chain beyond this distance  $D$  is exponentially low. The localization length scale  $D$  is on the order of the Gouy–Chapman length  $\lambda_{fN}$ . The polyelectrolyte chains lay flat on the surface when the localization length  $D$  becomes of the order of the transversal size of the polyelectrolyte chains  $bN^{1/2}$ . This takes place at the surface charge density  $\sigma_{\text{def}}$  equal to

$$\sigma_{\text{def}} \approx b^{-1} l_B^{-1} f^{-1} N^{-3/2} \quad (4.14)$$

At higher surface charge densities  $\sigma > \sigma_{\text{def}}$ , the electrostatic attraction to the surface compresses the chain within thickness  $D$  in the direction perpendicular to the charged surface. The thickness of the polyelectrolyte chain is determined by balancing the confinement entropy of a polyelectrolyte chain  $k_B T N b^2 / D^2$  with its attraction  $\varepsilon_{\text{ads}}(D)$  to the charged surface (see Eq. (4.12)). This gives the equilibrium thickness of the chain

$$D \approx b^{2/3} (l_B f \sigma)^{-1/3} \quad (4.15)$$

that is independent on the chain degree of polymerization  $N$ . The thickness of adsorbed polyelectrolyte chains decreases with increasing the surface charge density  $\sigma$  as  $\sigma^{-1/3}$ .

When the Debye radius  $r_D$  becomes smaller than  $\sqrt{fN/\sigma}$  the adsorbed polyelectrolyte chains interact with the part of the surface within distance  $r_D$  from polyion. The cell size  $R$  that minimizes the electrostatic energy of chains in the adsorbed layer, Eq. (4.7), is equal to

$$R \approx r_D \ln \left( \frac{fN}{\sigma r_D^2} \right), \quad \text{high salt } r_D < \sqrt{fN/\sigma} \quad (4.16)$$

Thus, the cell size is proportional to the Debye radius  $r_D$  up to logarithmic corrections. The effective surface charge density in this high salt concentration regime is

$$\delta\sigma \approx \frac{fN}{R^2} - \sigma \approx \frac{fN}{r_D^2}, \quad \text{high salt } r_D < \sqrt{fN/\sigma} \quad (4.17)$$

and can be much larger than the bare surface charge density  $\sigma$ . The polymer surface coverage  $\Gamma \approx (\sigma + \delta\sigma) f$  increases with increasing the salt concentration.

Polyelectrolyte chains in the adsorbed layer begin to overlap when the cell size  $R$  becomes comparable with the size of polyelectrolyte chains  $R_e$ . At low salt

concentrations,  $r_D > \sqrt{fN/\sigma}$ , the crossover to semidilute adsorbed layer occurs at the surface charge number density equal to

$$\sigma^* \approx \frac{1}{b^2 u^{2/3} f^{1/3} N} \quad (4.18)$$

The estimated value of the crossover surface charge number density for a solution of chains consisting of  $N=10^2$  Kuhn monomers with 10% of these monomers being charged ( $f=0.1$ ) adsorbing from an aqueous solutions with the Bjerrum length  $l_B=7$  Å is  $\sigma^* \approx 10^{-3} \text{ Å}^{-2}$ . At high salt concentration regime the crossover to semidilute regime occurs at  $r_D \approx R_e$ .

Note that the dependence of the cell size and surface overcharging in two-dimensional dilute adsorbed layer is similar to the case of adsorption of multivalent ions at oppositely charged surface (see for review Ref. [63]).

#### 4.3.2. Semidilute adsorbed layers

Above the overlap surface number charge density  $\sigma^*$  the adsorbed polymers arrange themselves into a two-dimensional semidilute polyelectrolyte solution, with the spacing between neighboring chains  $\xi$  (see Fig. 41). The intrachain electrostatic repulsion leads to chain stretching along the adsorbing surface on length scales larger than electrostatic blob size  $D_e^0$ . At the length scales smaller than  $\xi$  the polyelectrolyte configuration is that of an extended array of  $g_\xi/g_e^0$  electrostatic blobs. At these length scales the chain has the same conformation as in the semidilute polyelectrolyte solution discussed in Section 3.2. The electrostatic contribution to the total energy can again be divided into the repulsive and attractive parts (see Eq. (4.7)). The electrostatic energy of the adsorbed layer is

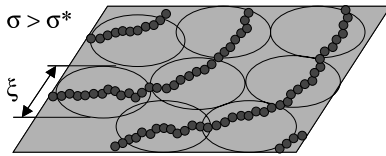


Fig. 41. Schematic sketch of an adsorbed layer in semidilute 2D regime. Reproduced with permission from Dobrynin, A.V., Deshkovski, A., & Rubinstein, M. *Macromolecules* 34, 1964–1972 (2001). [209] Copyright 2001, American Chemical Society.

$$\frac{U_{\text{cell}}}{k_B T} \approx S l_B r_D f g_\xi \left[ \frac{f g_\xi}{2 \xi^4} \exp(-\xi/r_D) - \frac{\sigma}{\xi^2} \right] \quad (4.19)$$

Minimizing this electrostatic energy with respect to the distance between chains  $\xi$  and taking into account that the number of monomers in a correlation blob is  $g_\xi \approx \xi/(bu^{1/3}f^{2/3})$  one obtains the equation (similar to the Eq. (4.8)) relating the distance between chains  $\xi$  to the Debye radius  $r_D$ , and surface charge number density  $\sigma$

$$\frac{f^{1/3}}{bu^{1/3}\xi} \left[ 1 + \frac{\xi}{2r_D} \right] \exp(-\xi/r_D) \approx \sigma \quad (4.20)$$

At low salt concentrations ( $r_D > \xi$ ) the distance between chains (the correlation length of the two-dimensional semidilute polyelectrolyte solution)

$$\xi \approx \frac{f^{1/3}}{u^{1/3}b\sigma}, \quad \text{low salt } r_D > f^{1/3}/(u^{1/3}b\sigma) \quad (4.21)$$

is inversely proportional to the surface charge number density  $\sigma$ . The surface overcharging  $\delta\sigma$  in this regime

$$\delta\sigma \approx \sigma \left( \frac{\xi}{r_D} \right) \approx \frac{f^{1/3}}{u^{1/3}b r_D}, \quad \text{low salt } r_D > f^{1/3}/(u^{1/3}b\sigma) \quad (4.22)$$

is inversely proportional to the Debye radius  $r_D$ , and is independent on the bare surface charge number density  $\sigma$ .

At higher salt concentrations the solution of Eq. (4.20) is

$$\xi \approx r_D \ln \left( \frac{f^{1/3}}{u^{1/3}\sigma r_D b} \right) \approx r_D, \quad \text{high salt } r_D < f^{1/3}/(u^{1/3}b\sigma) \quad (4.23)$$

Here, the distance between chains  $\xi$  scales linearly with the Debye screening length  $r_D$  up to logarithmic corrections. Thus, the distance between chains decreases as salt is added to the solution. The surface overcharging by adsorbed polyelectrolytes has the same functional form as the overcharging for the low salt regime, Eq. (4.22) (up to logarithmic corrections).

The thickness  $D$  of the polyelectrolyte chains in semidilute adsorbed layer follows the same scaling dependence as one derived for a dilute adsorption regime,  $D \sim \sigma^{-1/3}$  (see Eq. (4.15)).

The electrostatic blobs start to overlap at the salt concentrations for which the cell size  $\xi$  is on the order of the electrostatic blob size  $D_e^0$ . This overlap between electrostatic blobs occurs for the surface charge number density

$$\sigma_e \approx \frac{fg_e^0}{(D_e^0)^2} \approx \frac{f}{b^2} \quad (4.24)$$

For higher surface charge densities the adsorbed polyelectrolyte chains form a three-dimensional adsorbed layer. The estimated value of this crossover surface charge number density for our example is on the order of  $\sigma_e \approx 6 \times 10^{-3} \text{ A}^{-2}$ . At this crossover surface charge number density the intrachain electrostatic repulsion is on the order of the electrostatic attraction to the adsorbing surface.

The surface overcharging and the cell size dependence for the two-dimensional adsorbed layer are similar to the ones derived for rigid polyelectrolytes in Refs. [63,207]. This is due to the fact that at the length scales,  $D_e^0 < r < \xi$  a polyelectrolyte chain can be considered as rod-like. The surface overcharging and cell size are determined by the chain properties at the length scales up to the correlation length  $\xi$ .

It is interesting to point out that in the case of polyelectrolyte adsorption from poor solvent for polymer backbone [211] there are two different regimes in semidilute adsorbed layer—string-controlled and bead-controlled regimes. In the string-controlled regime the distance between chains is larger than the string length and there are many beads per each correlation area. While in the bead controlled regime there is one bead per each correlation area. This unique structural property of semidilute adsorbed layer closely resembles two regimes in semidilute solution of necklaces discussed in Section 3.2.6.

#### 4.4. Three-dimensional self-similar adsorbed layers [209]

At high surface charge densities ( $\sigma > \sigma_e$ ) the electrostatic attraction to a charged surface becomes strong enough to compress polyelectrolyte chains on the length scales smaller than the electrostatic blob size  $D_e^0$ . The polyelectrolyte chains form a concentrated polymer solution near the charged surface. In this regime, the electrostatic interactions of polyelectrolytes with the effective field created by other

polymer chains dominate over the electrostatic self-energy of the chain, therefore the polymer density distribution and the electrostatic potential can be obtained in the framework of the mean-field approximation. Within this approximation the polymer density  $c(z)$  and small ions density  $c_\alpha(z)$  depends only on the distance  $z$  from the charged surface. This approximation is correct as long as the local polymer concentration  $c(z)$  is higher than concentration inside an electrostatic blob,  $b^{-3}u^{1/3}f^{2/3}$ .

In this regime, the local polymer concentration is obtained by balancing the electrostatic attraction to the charged surface with three-body monomer–monomer repulsive interactions in a  $\Theta$ -solvent for polymer backbone

$$b^6 c(z)^3 \approx f c(z) \varphi(z) \Rightarrow c(z) \approx b^{-3} \sqrt{f \varphi(z)} \quad (4.25)$$

The concentration of the salt ions in the adsorbed layer satisfies the Boltzmann distribution

$$c_\pm(z) = c_s \exp[\mp \varphi(z)] \approx_{\varphi(z) \ll 1} c_s [1 \mp \varphi(z)] \quad (4.26)$$

where  $c_s$  is the bulk salt concentration. The electrostatic potential is given by the Poisson equation

$$\begin{aligned} \frac{d^2 \varphi(z)}{dz^2} &= 4\pi l_B [f c(z) + c_-(z) - c_+(z)] \approx \frac{\varphi(z)}{r_D^2} \\ &+ \frac{4\pi u f^{3/2}}{b^2} \sqrt{\varphi(z)} \end{aligned} \quad (4.27)$$

together with the boundary condition at the charged surface

$$\left. \frac{d\varphi(z)}{dz} \right|_{z=0} = -4\pi l_B \sigma \quad (4.28)$$

The solution of the second-order differential Eq. (4.27) leads to the following expression for polymer density profile in the adsorbed layer

$$\begin{aligned} c(z) &\approx b^{-3} \sqrt{f \varphi(z)} \\ &= \frac{16\pi}{3} \frac{u f^2 r_D^2}{b^5} \sinh^2 \left( \frac{D-z}{4r_D} \right) \end{aligned} \quad (4.29)$$

Here, the thickness  $D$  of the adsorbed layer is obtained from the boundary condition

$$\frac{64\pi}{9} \frac{u f^3 r_D^3}{b^3} \sinh^3 \left( \frac{D}{4r_D} \right) \cosh \left( \frac{D}{4r_D} \right) = \sigma b^2 \quad (4.30)$$

The equation for the polymer density profile is simplified at low salt concentrations ( $D < r_D$ )

$$c(z) \approx \frac{uf^2(D-z)^2}{b^5} \quad (4.31)$$

The polymer density profile (Eq. (4.31)) is self-similar (a power law) from the outer edge of the layer  $z=D$  inward (towards the adsorbing surface). Thus, the adsorbed layer can be considered to be built of blobs with size  $\xi(z)$  gradually increasing with distance  $z$  from the surface (see Fig. 42). The number of monomers in a concentration blob is determined from the fact that these blobs are space-filling,  $c(z) \approx g(z)/\xi(z)^3$ , and statistics of a chain inside a blob is Gaussian,  $\xi(z) \approx bg(z)^{1/2}$ . The size of the space-filling blobs in a  $\theta$ -solvent is the length scale at which three-body interaction energy is on the order of the thermal energy  $k_B T$ . These blobs are multivalent ions with valency  $fg(z)$ . Each blob interacts with the external electrostatic potential  $\varphi(z)$  with the energy  $fg(z)\varphi(z)$  on the order of the thermal energy  $k_B T$ .

In this regime the thickness  $D$  of the adsorbed layer is

$$D \approx b^{5/3} u^{-1/3} f^{-1} \sigma^{1/3} \approx D_e^0 (\sigma/\sigma_e)^{1/3} \quad (4.32)$$

The thickness of the adsorbed layer  $D$  increases with the surface charge number density as  $\sigma^{1/3}$ .

Both salt ions and polyelectrolyte chains contribute to screening of the surface charge. Inside the three-dimensional adsorbed layer the addition of salt decreases the polymer adsorbed amount, because the salt ions also take part in the screening of the surface charge. The typical excess of the salt charge density  $\delta c_s(z)$  in the adsorbed layer is

$$\delta c_s(z) \approx c_-(z) - c_+(z) \approx c_s \varphi(z) \quad (4.33)$$

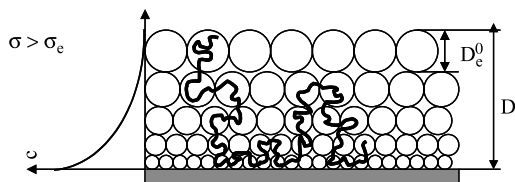


Fig. 42. Schematic sketch of the adsorbed layer in 3D regime. Reproduced with permission from Dobrynin, A.V., Deshkovski, A., & Rubinstein, M. *Macromolecules* 34, 1964–1972 (2001). [209] Copyright 2001, American Chemical Society.

A typical value of the electrostatic potential  $\varphi(z)$  in the adsorbed layer can be estimated as that of a planar capacitor with surface charge number density  $\sigma$  and distance between plates  $D$ ,  $\varphi(z) \approx l_B \sigma D$ . Multiplying the excess charge density by the layer thickness  $D$  one obtains the counterion surface excess

$$\Gamma_{\text{salt}} \approx \delta c_s D \approx l_B c_s \sigma D^2 \approx \sigma D^2 / r_D^2 \quad (4.34)$$

Thus, the fraction  $D^2/r_D^2$  of the surface charge is screened by the salt ions leaving only the fraction  $1 - D^2/r_D^2$  of the surface charge for polyelectrolytes to screen.

However, the mean-field description of the adsorbed layer is not accurate within the distance  $D_e^0$  from the outer edge of the adsorbed layer. At these distances from the outer boundary the fluctuations of the polymer density  $b^{-3}(uf^2)^{1/3}$  become larger than the average polymer density  $c(z)$  given by Eq. (4.31). This outer layer can be considered as a two-dimensional melt of electrostatic blobs with size  $D_e^0$ . The effective surface charge density  $\Delta\sigma$  experienced by the last layer of thickness  $D_e^0$  is on the order of magnitude of the threshold value  $\sigma_e$ . The surface overcharging due to this strongly fluctuating layer of electrostatic blobs is the same as in the case of semidilute adsorbed layer at the crossover surface charge density (see Eq. (4.22)). Thus, the total overcharging of the adsorbing surface by polyelectrolytes is

$$\delta\sigma \approx \frac{f^{1/3}}{u^{1/3} b r_D} - \sigma \frac{D^2}{r_D^2}, \quad \text{low salt } r_D > D \quad (4.35)$$

where the first term describes the surface overcharging by the outer layer of thickness  $D_e^0$  and the second term describes the polymeric underscreening inside the adsorbed layer (salt contribution to the surface screening). Surface overcharging  $\delta\sigma$  exhibits non-monotonic salt concentration dependence. Overcharging first increases and then decreases with increasing salt concentration (decreasing the Debye radius  $r_D$ ).

At low salt concentrations the thickness of the adsorbed layer  $D$  saturates at the surface charge number density of the order of  $\sigma_{\text{ion}} \approx b^{-2} u^{-1/2} f^{3/4}$ . Counterions start to dominate screening of the surface charge for higher surface charge number densities. In the vicinity of the substrate within the layer of

thickness  $h \approx bu^{-1/2}f^{3/4}$  the polymer concentration is almost constant and is equal to  $b^{-3}f^{4/2}$ . At this polymer concentration there is on average one charge per each correlation blob of size  $b/f^{1/2}$ . Further increase of polymer concentration will lead to increase of the monomer–monomer repulsive interactions without providing sufficient screening of the surface charge by adsorbed chains (see for details [209]).

Fig. 43 displays the dependence of the thickness of the adsorbed layer  $D$  on surface charge number density  $\sigma$  in different adsorption regimes at low salt concentrations. The layer thickness exhibits non-monotonic dependence on the surface charge density  $\sigma$ . Initially it is inversely proportional to surface charge number density  $\sigma$ . Then, it decreases with increasing the surface charge density as  $\sigma^{-1/3}$ . In this regime the thickness of the adsorbed layer is determined by the energy gain due to electrostatic attraction to the charged surface and the confinement entropy loss due to chain compression. Within the interval of the surface charge densities  $\sigma_e < \sigma < \sigma_{ion}$  the equilibrium thickness of the adsorbed layer increases with increasing surface charge density as  $\sigma^{1/3}$ . In this regime the thickness of the adsorbed layer is determined by the balance between electrostatic

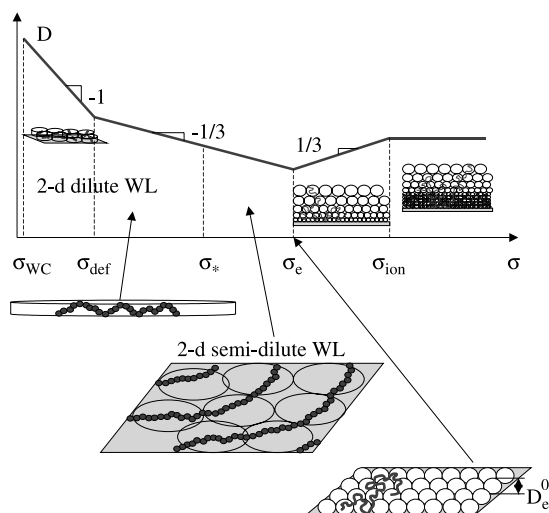


Fig. 43. Non-monotonic dependence of the thickness  $D$  of the adsorbed layer on the surface charge density. Reproduced with permission from Dobrynin, A.V., Deshkovski, A., & Rubinstein, M. *Macromolecules* 34, 1964–1972 (2001). [209] Copyright 2001, American Chemical Society.

attraction to the charged surface and monomer–monomer repulsion. Finally, the thickness of the adsorbed layer  $D$  saturates at the surface charge density  $\sigma$  on the order of  $\sigma_{ion}$ . At this high surface charge densities the surface counterions dominate screening of the surface potential.

#### 4.5. Effect of the image forces and short-range interactions on polyelectrolyte adsorption

In the description of the polyelectrolyte adsorption presented above it was assumed that the dielectric constant of the solvent  $\epsilon$  and that of the substrate  $\epsilon_1$  are the same. However, in many experimental situations, such as adsorption of polyelectrolyte chains from water onto clay, polymer latex particles or at the water/air interface, the dielectric constant of the solvent  $\epsilon$  is larger than that of the surface  $\epsilon_1$ . The presence of the charge in the medium with dielectric constant  $\epsilon$  near the surface with the dielectric constant  $\epsilon_1$  causes polarization of both media. The result is the appearance of the image charge at the symmetric positions with respect to the dielectric boundary with magnitude [21]

$$q' = \left( \frac{\epsilon - \epsilon_1}{\epsilon + \epsilon_1} \right) q \quad (4.36)$$

If the dielectric constant of the substrate is much smaller than the dielectric constant of the solvent  $\epsilon_1 \ll \epsilon$  which is usually the case for the adsorption of polyelectrolytes from aqueous solution onto polymeric substrates, the magnitude of the image charge  $q'$  is almost equal to the valence of charge  $q$  (see Fig. 44(a)). This leads to the effective repulsion of the test charge from the dielectric boundary. However, if the dielectric constant of the adsorbing substrate is larger than the dielectric constant of the solvent the valence of the image charge is opposite to the test charge creating an additional attraction to the adsorbing surface (see Fig. 44(b)). The example of this is the adsorption of polyelectrolytes at metallic surface with infinite dielectric constant,  $\epsilon_1 = \infty$ .

The electrostatic interaction between two charges located at points  $\mathbf{r}_1$  and  $\mathbf{r}_2$  above the dielectric

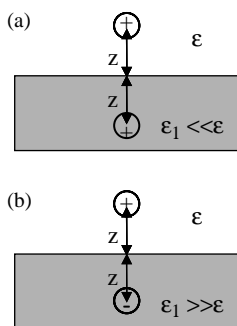


Fig. 44. A test charge near a dielectric boundary.

boundary in a salt solution can be approximated as

$$\frac{U_{\text{electr}}}{k_B T} \approx q_1 q_2 \left( \frac{l_B \exp(-|\mathbf{r}_1 - \mathbf{r}_2|/r_D)}{|\mathbf{r}_1 - \mathbf{r}_2|} + \left( \frac{\varepsilon - \varepsilon_1}{\varepsilon + \varepsilon_1} \right) \frac{l_B \exp(-\sqrt{(\mathbf{r}_1 - \mathbf{r}_2)^2 + 4z_1 z_2}/r_D)}{\sqrt{(\mathbf{r}_1 - \mathbf{r}_2)^2 + 4z_1 z_2}} \right) \quad (4.37)$$

where the first term describes the direct electrostatic interaction between charges  $q_1$  and  $q_2$  while the second term represents interaction between a charge and the image of other charge (see for details [223]). The electrostatic potential energy given by Eq. (4.37) does not take into account the self-interaction between charges and their own images. Thus, each charge near the adsorbing charged substrate with the dielectric constant different from that of the solvent, does not only interact with the ‘real’ charges but also with their images. If there are ionized groups at dielectric boundary (a charged substrate), the dielectric interface also creates an image charge for each ionized surface group. In this case, the total electrostatic interaction between a test charge with valence  $q$  located at distance  $z$  from the oppositely charged substrate with surface charge density  $\sigma$  can be written in the following form

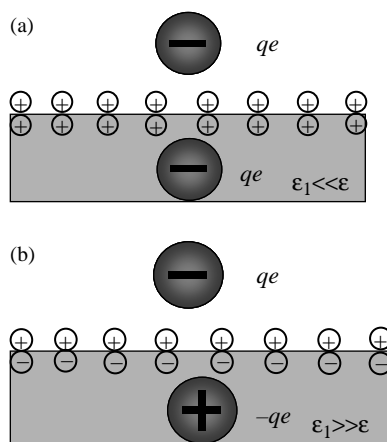
$$\frac{U_{\text{subs}}(z)}{k_B T} \approx -\frac{4\pi l_B \varepsilon \sigma r_D}{(\varepsilon + \varepsilon_1)} \exp(-z/r_D) + \frac{l_B}{4z} \left( \frac{\varepsilon - \varepsilon_1}{\varepsilon + \varepsilon_1} \right) \exp(-2z/r_D) \quad (4.38)$$

where the first term describes the interaction between the test charge and the charged substrate (including the substrate charge image) while the second term

corresponds to the electrostatic interaction between the test charge and its image. In the case when the dielectric constant of the substrate is much lower than the dielectric constant of the solvent,  $\varepsilon_1 < \varepsilon$  the image charges double the surface charge density (see Fig. 45(a)).

However, if the opposite inequality holds  $\varepsilon_1 \gg \varepsilon$  (metallic substrate) the first term in Eq. (4.38) disappears and the interaction of a test charge with the surface is controlled by attraction to its image. The disappearance of the first term should not be surprising because for each surface charge there is an image charge of the opposite sign located below the surface boundary (see Fig. 45(b)). Thus, approaching test charge ‘sees’ an array of dipoles. Electrostatic interaction of a charge with an array of dipoles is weaker than interaction with a charged surface.

Let us now describe the adsorption of polyelectrolyte chains at a charged dielectric substrate with  $\varepsilon_1 < \varepsilon$ . In this case each adsorbed polyelectrolyte chain will have a similarly charged image chain. This will lead to doubling of the electrostatic repulsion between adsorbed polyelectrolyte chains given by Eq. (4.6) and doubling of the electrostatic attraction of a chain to the charged surface given by Eq. (4.5). However, in addition to these two terms there is another contribution to the layer electrostatic energy, which is due to the interaction of a chain with its own image.

Fig. 45. Schematic representation of a test charge  $qe$  near a charged boundary with dielectric constant (a)  $\varepsilon_1 \ll \varepsilon$  and (b)  $\varepsilon_1 \gg \varepsilon$  (metallic boundary).

This interaction can be estimated as electrostatic interaction between two charged rods of similar charge separated by a distance  $2d$ , where  $d$  is the distance between the adsorbed chain and the substrate. The interaction of the polyelectrolyte chain with its image in the low salt concentration regime ( $R_e < r_D$ ) is

$$\frac{U_{\text{image}}}{k_B T} \approx \frac{l_B (fN)^2}{R_e} \ln \left( \frac{R_e}{2d} \right) \approx \frac{N}{g_e^0} \quad (4.39)$$

Neglecting the logarithmic term, the interaction of the polyelectrolyte chain with its image is on the order of the chain's self-energy. Thus, the presence of a dielectric boundary is reduced to the additional short-range repulsive interaction between charged monomers and the substrate.

The electrostatic energy of the dilute adsorbed layer (Eq. (4.7)) can be rewritten by taking into account all three contributions (electrostatic repulsion from the adsorbed chains, attraction to the charged substrate, and repulsion from the image chain)

$$\frac{U_{\text{cell}}}{k_B T} \approx Sl_B r_D fN \left[ \frac{fN}{R^4} \exp(-R/r_D) - \frac{2\sigma}{R^2} \right] + \frac{SN}{g_e^0 R^2} \quad (4.40)$$

The equilibrium distance  $R$  between adsorbed chains is obtained by minimizing Eq. (4.40) with respect to  $R$

$$\frac{fN}{R^2} \exp(-R/r_D) \left( 1 + \frac{R}{4r_D} \right) \approx \sigma - \left( \frac{f}{u} \right)^{1/3} \frac{1}{2br_D} \quad (4.41)$$

The electrostatic repulsion from the image chain (the last term on the right-hand side of the Eq. (4.41)) reduces the effective surface charge number density  $\sigma$ . The solution of Eq. (4.41) disappears if the expression on the right-hand side becomes negative. This corresponds to the chain desorption taking place at the values of the Debye radius  $r_D$  smaller than  $r_D^{\text{des}}$

$$r_D < r_D^{\text{des}} \approx \left( \frac{f}{u} \right)^{1/3} \sigma^{-1} \quad (4.42)$$

This eliminates a part of the dilute adsorption regime in comparison with the case of equal dielectric constants of both media,  $\varepsilon = \varepsilon_1$  (see Section 4.3.1). However, in the interval of the Debye radius and surface charge densities  $\sigma$  such

that  $r_D > r_D^{\text{des}}$  the scaling relations between the ionic strength dependence of the cell size, polymer surface coverage and surface number charge density  $\sigma$  and the Debye radius  $r_D$  have the same power laws as the scaling relations derived in Section 4.3.1. Note that in the case of  $\varepsilon_1 < \varepsilon$  the surface is undercharged by adsorbed polyelectrolytes. This undercharging is due to strong additional repulsion between adsorbed chain and its image

$$\begin{aligned} \delta\sigma &\approx \frac{fN}{R^2} - \sigma \approx \frac{1}{l_B r_D fN} \left( \frac{3}{4} \frac{(fN)^2}{R} - \frac{N}{2g_e^0} \right) \\ &\approx - \left( \frac{f}{u} \right)^{1/3} \frac{1}{r_D b}, \quad \text{low salt} \end{aligned} \quad (4.43)$$

In the derivation of Eq. (4.43) we have used Eq. (4.42) by expanding the left-hand side of this equation into the power series of  $R/r_D$ .

The adsorption energy of a polyelectrolyte chain at a charged dielectric substrate with  $\varepsilon_1 < \varepsilon$  includes electrostatic repulsion from the adsorbed chains, attraction to the charged substrate, and repulsion from the image chain

$$\frac{\varepsilon_{\text{ads}}}{k_B T} \approx l_B r_D fN \left( \frac{2fN}{R^2} \exp(-R/r_D) - 2\sigma \right) + \frac{N}{g_e^0} \quad (4.44)$$

The factor two in front of the first and the second terms on the right-hand side of Eq. (4.44) accounts for interaction of a chain with adsorbed chains and surface charge images. We can simplify this equation by solving Eq. (4.41) for  $\sigma$  and substituting this solution into Eq. (4.44). This leads to

$$\begin{aligned} \frac{\varepsilon_{\text{ads}}}{k_B T} &\approx - \frac{l_B (fN)^2}{2R} \exp(-R/r_D) \Big|_{R/r_D \ll 1} \approx - \frac{l_B (fN)^2}{2R} \\ &\approx - l_B (fN)^{3/2} \sigma^{1/2} \end{aligned} \quad (4.45)$$

The adsorption energy is much larger than the thermal energy  $k_B T$  for the interval of the surface charge densities  $\sigma > \sigma_{\text{WC}}$  (see Section 4.3, Eq. (4.4)).

In the semidilute adsorption regime the cell size is on the order of the two-dimensional solution correlation length  $\xi$ . The description of the semidilute adsorbed layer in the presence of the dielectric boundary is similar to the description for the dilute adsorbed layer. The dielectric boundary can be taken into account by doubling the terms on the right-hand

side of Eq. (4.17) and adding the contribution due to the interaction between a section of a chain within the correlation length  $\xi$  and its image,  $Sg\xi/(g_e^0\xi^2)$ . The equilibrium cell size in semidilute adsorption regime after these modifications is given by the following equation

$$\frac{f^{1/3}}{u^{1/3}b\xi} \exp(-\xi/r_D) \left[ 1 + \frac{\xi}{2r_D} \right] \approx \sigma - \left( \frac{f}{u} \right)^{1/3} \frac{1}{2br_D} \quad (4.46)$$

The right-hand side of Eq. (4.46) is the same as in the case of the dilute adsorbed layer (see Eq. (4.41)). Thus, the presence of the dielectric boundary simply renormalizes the surface charge number density. This renormalization of the surface charge density results in desorption of polyelectrolyte chains at high salt concentrations for which  $r_D < r_D^{\text{des}}$  (Eq. (4.42)). It is interesting to point out that the presence of the dielectric boundary will not affect the properties of the adsorbed layer in the 3D adsorption regime,  $\sigma > fb^2$ . In this regime, the electrostatic interaction between chains and the surface is always stronger than intrachain interactions (chain's electrostatic self-energy).

Monte Carlo simulations of the effect of the dielectric boundary on the adsorption of strongly charged polyelectrolytes at oppositely charged planar surface were performed by Messina [224]. These simulations have shown that image forces appearing due to the dielectric discontinuity at the adsorbing substrate lead to the decrease in polymer surface coverage which precludes the surface overcharging by adsorbed polyelectrolytes. However, the surface charge image was not taken into account in this work [224]. As we have shown in the beginning of this section the presence of the dielectric boundary also doubles the surface charge increasing the electrostatic attraction between a charged substrate and polyelectrolyte chains by the factor of two. Cheng and Lai [225] studied a single chain adsorption at the charged substrate with high dielectric constant. In the framework of the ground state dominance approximation they found that adsorption at low ionic strengths is the first order transition with the monomer density at the surface scaling linearly with the surface charge density.

The polymer surface coverage can also be changed by adjusting the affinity of the polymer backbone and

adsorbing substrate - so-called effect of the short-range interactions between adsorbing substrate and polyelectrolyte chains. These interactions can be taken into account by introducing the additional energy gain per monomer due to the contact between the polymer backbone and the surface [212]. In 2D dilute and semidilute adsorption regimes the term describing the short-range interaction between the substrate and the polymer chain is similar to the expression describing interaction of the polyelectrolyte with its image at dielectric boundary (with  $\epsilon_1 > \epsilon$  for attraction, see Eq. (4.39)). The strength of the short-range attractive interactions per monomer can be estimated as  $-kT\epsilon_{vw}^2$ , where  $-kT\epsilon_{vw}$  is the monomeric contact energy. In the case of the strong affinity between the polymer backbone and the adsorbing surface, the thickness of the two-dimensional adsorbed layer is determined by the short-range interactions and is inversely proportional to the magnitude of the contact energy  $\epsilon_{vw}$ . The polymer surface coverage in the two-dimensional adsorbed layers is controlled either by the balance between electrostatic attraction to the substrate and electrostatic repulsion between adsorbed chains at low salt concentrations or by short-range attraction and electrostatic repulsion at intermediate and high salt concentrations. The polymer surface coverage in 2D adsorption regimes is inversely proportional to the Debye radius  $r_D$ . In the three-dimensional adsorbed layer the short-range interactions change the boundary condition at the polymer–surface interface leading to the enhancement of the polyelectrolyte adsorption with increasing polymer–surface interactions (see for details [212]). The strong short-range attractive interaction between the substrate and the polymer backbone can even lead to the adsorption of polyelectrolytes at a similarly charged surface. However, this is possible when the short-range attractive interactions between the substrate and the polymer backbone are stronger than the electrostatic repulsion between similarly charged chains and the surface. The desorption transition occurs when both interactions are on the same order of magnitude.

#### 4.6. Comparison with experiments

The theory of polyelectrolyte adsorption described in Sections 4.3 and 4.4 predicts two qualitatively different regimes of polyelectrolyte adsorption [209].

At lower surface charge densities adsorbed polyelectrolyte chains form two-dimensional adsorbed layers. Electrostatic repulsion between polyelectrolytes within these layers localizes chains in the dilute regime (or sections of the chains in the semidilute regime) in the centers of the corresponding Wigner–Seitz cells (see Figs. 40 and 41). The cell size is obtained by the optimization of the electrostatic repulsion between chains and their attraction to the uniformly charged background. The electrostatic self-energy of a polyelectrolyte chain in this regime dominates over its attraction to the charged surface and over the electrostatic repulsion between chains.

The adsorbed chains form a three-dimensional adsorbed layer at higher surface charge densities. The electrostatic attraction of polyelectrolytes to the charged surface is stabilized by the short-range repulsion between monomers in this layer. Chains near the charged surface form a semidilute polyelectrolyte solution with concentration decreasing with distance from the surface (see Fig. 42). The polymer density distribution in 3D adsorbed layer is described in the framework of the mean-field approximation assuming that the electrostatic interaction of a polymer with the effective field created by the surface and other chains dominates over the electrostatic self-energy of the chain.

The screening of the electrostatic repulsion between adsorbed polyelectrolyte chains in solutions with added salt results in large overcompensation of the surface charge for two-dimensional adsorbed layers—the *screening-enhanced adsorption*. At higher salt concentrations this overcompensation of the surface charge by the 2D adsorbed layer is independent of the original surface charge and depends only on the linear charge density along the polyelectrolyte chains (fraction  $f$  of charged monomers) and increases proportional to square root of ionic strength (see Fig. 46). The polyelectrolyte surface excess in 3D adsorbed layers increases (*screening-enhanced adsorption*) at low ionic strength and decreases (*screening-reduced adsorption*) at higher ionic strength exhibiting a maximum (see Fig. 46).

Both increase and decrease of the adsorbed amount with salt concentration for polyelectrolytes with different fractions of charged monomers  $f$  was found by Durand et al. [226] for adsorption of cationic

polyacrylamides (copolymers of acrylamide and acrylate with a quaternary ammonium groups) on montmorillonite. For polyelectrolytes with fraction of charged monomers  $f=0.01$  the adsorbed amount decreases with increasing salt concentration, for  $f=0.05$  there was no salt effect, while for polyelectrolytes with  $f=0.13$  and  $f=0.2$  the adsorbed amount increases with increasing salt concentration. This trend in the dependence of the adsorbed amount on salt concentration is consistent with the predictions of the polyelectrolyte adsorption model [209]. The crossover value of the surface charge density between 2D and 3D adsorbed layers shifts into the region of high surface charge densities with increasing fraction of the charged monomers  $f$  on polymer chain. Thus, for low fraction of charged monomers  $f < 0.05$  adsorbed polyelectrolytes form 3D adsorbed layer with polymer surface excess decreasing with increasing salt concentration (screening-reduced adsorption). Polymer surface coverage is independent of salt concentration for the sample with  $f=0.05$  indicating that the surface charge density in these experiments is very close to the crossover value between 2D and 3D adsorbed layers. The adsorbed polyelectrolytes form a two-dimensional adsorbed layer at the same surface charge density for fractions of charged monomers  $f > 0.05$ . The polymer surface excess in two-dimensional adsorbed layer increases with increasing salt concentration (screening-enhanced adsorption).

The screening-reduced adsorption was also observed by other groups [226–232]. The screening-enhanced adsorption was reported by Kawaguchi

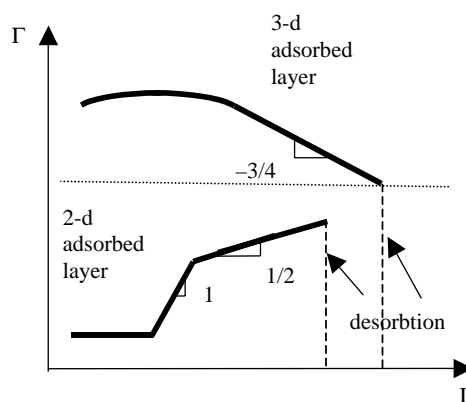


Fig. 46. Dependence of polymer surface excess on ionic strength  $I = \sum_i z_i^2 c_i$ . (logarithmic scales).

et al. [233] for adsorption of completely quaternized poly(4-vinyl-*N-n*-propylpyridinium bromide) on silica, and by Bonekamp [234] for adsorption of polylysine onto silver-iodide crystal and on glass. The linear dependence of the polymer surface excess on the square root of salt concentration was reported by Kawaguchi et al. [233] and by Marra et al. [235] for adsorption of polystyrene sulfonate on weakly charged silica at pH=2. This dependence of the polymer surface excess is in good qualitative agreement with the prediction for polyelectrolyte adsorption in 2D adsorbed layer (see Fig. 46).

The non-monotonic dependence of the polymer surface coverage on the salt concentration with weak maximum around  $10^{-1}$ – $10^{-2}$  M was observed by Bonekamp [234] for adsorption of polylysine on silica. This effect may be explained by the two opposite tendencies predicted by the model for 3D adsorbed layer (see Fig. 46): (i) the increase of the polymer surface excess due to the screening of electrostatic self-energy of adsorbed polyelectrolytes; (ii) the decrease of polymer surface excess in the 3D adsorbed layer due to the screening of the surface charge by salt ions.

The latest progress in the theory of polyelectrolyte adsorption provides an opportunity to apply these results to describe multilayer self-assembly in a wide range of salt concentrations. Unfortunately, so far, there have been only few attempts to describe polyelectrolyte multilayer formation. Solis and Olvera de la Cruz [236] developed a model of spontaneous equilibrium layering of a mixture of positively and negatively charged polymers close to a charged wall due to their chemical incompatibility. Netz and Joanny [207] proposed a scaling model of multilayer formation in semiflexible polyelectrolytes. However, this model is lacking the interdigitation and complex formation between polyelectrolyte chains in neighboring layers. Castelnovo and Joanny [237] took into account the strong interpenetration of polyelectrolyte chains in consecutive layers by incorporating the complex formation between oppositely charged polyelectrolytes into self-consistent field equations, describing polymer density profile in the adsorbed layers. The recent computer simulations of multilayer assembly [238,239] indicate the important role of ionic pairs in the stabilization of the multilayered structure and of the kinetics of deposition process.

The formation of ionic pairs between polyelectrolyte chains forming multilayers was recently taken into account by Park et al. [240] and by Lefaux et al. [241]. These models show promising results predicting correct salt concentration dependence of multilayer growth by sequential adsorption and by spin casting methods. However, the new developments in this direction are needed before the consistent theoretical model of multilayer assembly will emerge.

## 5. Conclusions and outlook

In this paper we have presented an overview of different theoretical models of polyelectrolytes in solutions and at charged substrates. In dilute salt-free polyelectrolyte solutions in a  $\Theta$ -solvent for polymer backbone the chain size is determined by the balance of chain elasticity and electrostatic repulsion between charged monomers. This leads to stronger than linear dependence of the chain size on the degree of polymerization. The chain is non-uniformly stretched experiencing stronger deformation in the middle than at its ends. Solvent quality is an important factor controlling chain's conformations. Polyelectrolytes in poor solvents have necklace-like structures of beads connected by narrow strings. This structure appears as a result of optimization of electrostatic and hydrophobic interactions between monomers. Increase of polymer concentration leads to the reduction of the polyelectrolyte effective charge and the decrease of its size due to counterion condensation. The counterion condensation phenomenon is driven by the electrostatic attraction between ionized group and counterions. For polyelectrolytes in a poor solvent, counterion condensation could occur in an avalanche-like fashion destabilizing polyelectrolyte solution and leading to its phase separation. The osmotic pressure in polyelectrolyte solutions is mainly controlled by small ions over the wide range of polymer concentrations. In semidilute solutions, the value of the osmotic coefficient could be used to estimate a fraction of free counterions. As in the case of neutral polymers, the semidilute polyelectrolyte solutions are characterized by the main length scale—the solution correlation length. In salt-free solutions, this is also a length scale of screening of electrostatic interactions. Scaling theory, PRISM, and field

theoretical models predict the same limiting scaling laws for salt and polymer concentration dependence of the solution correlation length and chain size. This agreement is assuring and confirms the existence of the single length scale controlling solution properties. The predictions of theoretical models are also in good qualitative and sometimes even quantitative agreement with experimental data and results of the computer simulations.

While there is significant progress in predicting the static properties of polyelectrolyte solutions, their dynamics is far from being completely understood. The dynamics of polyelectrolyte solution utilizes the same scaling assumption as ones used in solutions of neutral polymers. It strongly relies on the existence of the single length scale where both hydrodynamic and electrostatic interactions are screened. The screening of these interactions happens at the distances comparable with the solution correlation length. This assumption was confirmed by the effective medium calculations performed by Muthukumar [242,243] and by recent experiments [127]. The important issue that still remains unresolved is the nature of entanglements in polyelectrolyte solutions. Can we simply transfer the notion of topological constraints used in solutions of neutral polymers to polyelectrolyte solutions? There are some experimental indications that this hypothesis is violated leading to a weaker than theoretically expected  $N$ -dependence of the entanglement concentration [127]. Computer simulations of entangled polyelectrolyte solutions should be able to provide a definite answer to these questions. The non-linear dynamics of polyelectrolyte solutions was completely ignored by theoreticians. This area of research is the most valuable for polymer processing. Another interesting issue that awaits theoretical understanding is the origin of the so-called slow modes in polyelectrolyte solutions [244–248].

The new direction of the research that took off during the last 5 years is the effect of multivalent ions on complexation in solutions of charged polymers [249–253]. The interest to this problem was stimulated by the importance of this phenomenon to biological systems. Many bacteriophages use multivalent cations to package their DNA into compact and ordered forms. This phenomenon is known as DNA condensation [254]. It turns out that the DNA is not the only polyelectrolyte capable of forming complexes. Other

stiff polyelectrolytes such as F-actin and tobacco mosaic virus are capable of forming laterally ordered aggregates (bundles) in the presence of multivalent counterions. The strong salt effect on complexation supports the electrostatic nature of this process. The complexation of multivalent ions with polyelectrolytes is qualitatively different from the phenomena of counterion condensation discussed in this review. The new physical phenomenon that exists in systems with multivalent ions is the strong correlations between multivalent ions [218–221,255,256] (see for review Ref. [63]). The correlation effects can become so strong that multivalent ions invert the charge of polyelectrolyte (overcharge it) leading to effective attraction between originally similarly charged species. (This effect is similar to the surface overcharging by adsorbed polyions discussed in Section 4.2. The multivalent ions position themselves along the polymer backbone in the correlated fashion with equilibrium distance between them being determined by attraction to the oppositely charged monomers of the polymer backbone and by the repulsion from other multivalent ions.) The strong correlation between multivalent ions is the main reason for bundle formation and growth. Future progress in this area will have a significant impact on our understanding of electrostatic interactions between charged polymers and colloids, micelles, proteins, charged lipid membranes, and charged surfaces.

We have not discussed the properties of polyampholyte solutions (solutions of charged polymers carrying both positively and negatively charged groups). In these systems, the electrostatics is responsible for both attractive and repulsive interactions that lead to a variety of new and unusual phenomena. Together with R.H. Colby, we have just published the review of recent developments in this area of polymer science and recommend it to interested readers [257].

We have identified two qualitatively different regimes of polyelectrolyte adsorption. At lower surface charge densities adsorbed polyelectrolyte chains form two-dimensional adsorbed layers. The electrostatic attraction to the charged substrate and electrostatic repulsion between adsorbed chains are the leading factors controlling the structure of these layers. At higher surface charge densities the adsorbed chains form three-dimensional adsorbed layers. Here, the electrostatic attraction between polyelectrolytes

and the charged surface is stabilized by the short-range repulsion between monomers in these layers. This picture of polyelectrolyte adsorption is in good qualitative agreement with experimental data.

We hope that topics discussed in this review will help readers to understand the basics of modern theory of polyelectrolytes in solutions and at interfaces and will be useful in future studies of more complicated ionic systems such as polyelectrolyte gels [258,259], polyelectrolyte brushes [260], computer simulations of polyelectrolytes [73], and multilayer formation by charged molecules [15,16].

### Acknowledgements

We acknowledge the support of the NSF DMR-0305203 (A.V.D.), CHE-9876674 (M.R.), ECS-0103307 (M.R.) and of the donors of the Petroleum Research Fund, administered by the American Chemical Society under the grant PRF#39637-AC7 (A.V.D.). M.R. also acknowledges financial support of the NASA University Research, Engineering, and Technology Institute on Bio Inspired Materials award NCC-1-02037.

### References

- [1] Forster S, Schmidt M. Polyelectrolytes in solution. *Adv Polym Sci* 1995;120:51–133.
- [2] Barrat JL, Joanny JF. Theory of polyelectrolyte solutions. *Adv Chem Phys* 1996;94:1–66.
- [3] Schmitz KS. Macroions in solution and colloidal suspension. VCH Publishers; 1993.
- [4] Tanford C. Physical chemistry of macromolecules. New York: Wiley; 1961.
- [5] Oosawa F. Polyelectrolytes. New York: Marcel Dekker; 1971.
- [6] Polyelectrolytes. New York: Marcel Dekker; 1993.
- [7] Radeva T. Physical chemistry of polyelectrolytes. New York: Marcel Dekker; 2001.
- [8] Doi M, Edwards SF. The theory of polymer dynamics. Oxford: Clarendon Press; 1989.
- [9] de Gennes PG. Scaling concepts in polymer physics. Ithaca, NY: Cornell University Press; 1979.
- [10] Rubinstein M, Colby RH. Polymer physics. New York: Oxford University Press; 2003.
- [11] Fuoss RM. Viscosity function for polyelectrolytes. *J Polym Sci* 1948;3:603.
- [12] Decher G. Multilayer films (polyelectrolytes) In: The polymeric materials encyclopedia: synthesis, properties and applications. Boca Raton, FL: CRC Press; 1996.
- [13] Decher G. Fuzzy nanoassemblies: toward layered polymeric multicomposites. *Science* 1997;277:1232–7.
- [14] Decher G, Eckerle M, Schmitt J, Struth B. Layer-by-layer assembled multicomposite films. *Curr Opin Colloid Interface Sci* 1998;3:32–9.
- [15] Hammond PT. Recent explorations in electrostatic multilayer thin film assembly. *Curr Opin Colloid Interface Sci* 1999;4: 430–42.
- [16] Schonhoff M. Self-assembled polyelectrolyte multilayers. *Curr Opin Colloid Interface Sci* 2003;8:86–95.
- [17] Schonhoff M. Layered complexes: physics of formation and molecular properties. *J Phys Condens Matter* 2003;15: R1781–R808.
- [18] Frenkel D, Smit B. Understanding molecular simulations. San Diego: Academic Press; 2001.
- [19] Rapaport DC. The art of molecular dynamics simulation. New York: Cambridge University Press; 1995.
- [20] Kuhn W, Kunzle O, Katchalsky A. Verhalten polyvalenter fadenmolekelionen in losung. *Helv Chim Acta* 1948; 1994–2037.
- [21] Landau LD, Lifshitz EM. Electrodynamics of continuous media. Reading, MA: Addison-Wesley; 1984.
- [22] Grosberg AY, Khokhlov AR. Statistical physics of macromolecules. New York: AIP Press; 1994.
- [23] de Gennes P-G, Pincus P, Brochard F, Velasco RM. Remarks on polyelectrolyte conformation. *J Phys (France)* 1976;37: 1461–76.
- [24] Khokhlov AR, Khachaturian KA. On the theory of weakly charged polyelectrolytes. *Polymer* 1982;23:1793–802.
- [25] Dobrynin AV, Colby RH, Rubinstein M. Scaling theory of polyelectrolyte solutions. *Macromolecules* 1995;28: 1859–71.
- [26] Liao Q, Dobrynin AV, Rubinstein M. Molecular dynamics simulations of polyelectrolyte solutions: nonuniform stretching of chains and scaling behavior. *Macromolecules* 2003;36: 3386–98.
- [27] Migliorini G, Rostsiashvili V, Vilgis TA. Weak violation of universality for polyelectrolyte chain: variational theory and simulations. *Eur Phys J E* 2001;4:475–87.
- [28] Castelnovo M, Sens P, Joanny JF. Charge distribution on annealed polyelectrolytes. *Eur Phys J E* 2000;1:115–25.
- [29] Ullner M, Jonsson B, Widmark PO. Conformational properties and apparent dissociation constants of titrating polyelectrolytes: Monte Carlo simulations and scaling arguments. *J Chem Phys* 1994;100:3365–6.
- [30] Katchalsky A, Eisenberg H. Molecular weight of polyacrylic and polymethacrylic acid. *J Polym Sci* 1951;6:145–54.
- [31] Morawetz H. Revisiting some phenomena in polyelectrolyte solutions. *J Polym Sci Part B Polym Phys* 2002;40: 1080–6.
- [32] McQuarrie DA. Statistical mechanics. New York: Harper & Row; 1976.
- [33] Rayleigh L. *Philos Mag* 1882;14:184.

- [34] Dobrynin AV, Rubinstein M, Obukhov SP. Cascade of transitions of polyelectrolytes in poor solvent. *Macromolecules* 1996;29:2974–9.
- [35] Hooper HH, Beltran S, Sassi AP, Blanch HW, Prausnitz JM. Monte Carlo simulations of hydrophobic polyelectrolytes. Evidence for a structural transition in response to increasing chain ionization. *J Chem Phys* 1990;93:2715–23.
- [36] Higgs PG, Orland H. Scaling behavior of polyelectrolytes and polyampholytes: simulation by an ensemble growth method. *J Chem Phys* 1991;95:4506–18.
- [37] Chodanowski P, Stoll S. Monte Carlo simulations of hydrophobic polyelectrolytes: evidence of complex configurational transitions. *J Chem Phys* 1999;111:6069–81.
- [38] Lyulin AV, Dunweg B, Borisov OV, Darinskii AA. Computer simulation studies of a single polyelectrolyte chain in poor solvent. *Macromolecules* 1999;32:3264–78.
- [39] Solis FJ, Olvera de la Cruz M. Variational approach to necklace formation in polyelectrolytes. *Macromolecules* 1998;31:5502–6.
- [40] Balazs AC, Singh C, Zhulina E, Chern SS, Lyatskaya Y, Pickett G. Theory of polymer chains tethered at interfaces. *Prog Surf Sci* 1997;55:181–269.
- [41] Migliorini G, Lee N, Rostiashvili V, Vilgis TA. Polyelectrolyte chains in poor solvent, a variational description of necklace formation. *Eur Phys J E* 2001;6:259–70.
- [42] Tamashiro MN, Schiessel H. Stepwise unwinding of polyelectrolytes under stretching. *Macromolecules* 2000;33:5263–72.
- [43] Vilgis TA, Johner A, Joanny JF. Stretching necklaces. *Eur Phys J E* 2000;2:289–300.
- [44] Vilgis TA, Johner A, Joanny JF. Polyelectrolyte gels in poor solvent: elastic moduli. *Eur Phys J E* 2000;3:237–44.
- [45] Holm C, Joanny JF, Kremer K, Netz RR, Reineker P, Seidel C, et al. Polyelectrolyte theory. *Adv Polym Sci* 2004;166:67–111.
- [46] Limbach HJ, Holm C, Kremer K. Structure of polyelectrolytes in poor solvent. *Europhys Lett* 2002;60:566–72.
- [47] Khokhlov AR. On the collapse of weakly charged polyelectrolytes. *J Phys A* 1980;13:979–87.
- [48] Raphael E, Joanny J-F. Annealed and quenched polyelectrolytes. *Europhys Lett* 1990;13:623–8.
- [49] Dobrynin AV, Rubinstein M. Counterion condensation and phase separation in solutions of hydrophobic polyelectrolytes. *Macromolecules* 2001;34:1964–72.
- [50] Manning GS. Limiting laws and counterion condensation in polyelectrolyte solutions I. Colligative properties. *J Chem Phys* 1969;51:924–33.
- [51] Manning GS. Counterion condensation theory constructed from different models. *Physica A* 1996;231:236–53.
- [52] Manning GS. The critical onset of counterion condensation: A survey of its experimental and theoretical basis. *Ber Bunsen Ges Phys Chem Chem Phys* 1996;100:909–22.
- [53] Manning GS, Ray J. Counterion condensation revisited. *J Biomol Struct Dyn* 1998;16:461–76.
- [54] Muthukumar M. Theory of counter-ion condensation on flexible polyelectrolytes: adsorption mechanism. *J Chem Phys* 2004;120:9343–50.
- [55] Kramarenko EY, Khokhlov AR, Yoshikawa K. A three-state model for counterions in a dilute solution of weakly charged polyelectrolytes. *Macromol Theory Simul* 2000;9:249–56.
- [56] Katchalsky A, Alexandrowicz Z, Kedem O. Polyelectrolyte solutions. In: Conway BE, Barradas RG, editors. *Chemical physics of ionic solutions*. London: Wiley; 1966. p. 295–346.
- [57] Alexandrowicz Z, Katchalsky A. Colligative properties of polyelectrolyte solutions in excess of salt. *J Polym Sci Part A* 1963;1:3231–60.
- [58] Alfrey T, Berg PV, Morawetz H. The counterion distribution in solutions of rod-shaped polyelectrolytes. *J Polym Sci* 1951;7:543–51.
- [59] Fuoss RM, Katchalsky A, Lifson S. The potential of an infinite rod-like molecule and the distribution of counterions. *Proc Natl Acad Sci USA* 1951;37:579–86.
- [60] Deshkovski A, Obukhov S, Rubinstein M. Counterion phase transitions in dilute polyelectrolyte solutions. *Phys Rev Lett* 2001;86:2341–4.
- [61] Liao Q, Dobrynin AV, Rubinstein M. Molecular dynamics simulations of polyelectrolyte solutions: osmotic coefficient and counterion condensation. *Macromolecules* 2003;36:3399–410.
- [62] Netz RR, Orland H. Variational charge renormalization in charged systems. *Eur Phys J E* 2003;11:301–11.
- [63] Grosberg AY, Nguyen TT, Shklovskii BI. Colloquium: the physics of charge inversion in chemical and biological systems. *Rev Mod Phys* 2002;74:329–45.
- [64] Gonzalez-Mozuelos P, Olvera de la Cruz M. Ion condensation in salt-free dilute polyelectrolyte solutions. *J Chem Phys* 1995;103:3145–57.
- [65] Flory PJ. Molecular configuration of polyelectrolytes. *J Chem Phys* 1953;21:162–3.
- [66] Schiessel H, Pincus P. Counterion-condensation-induced collapse of highly charged polyelectrolytes. *Macromolecules* 1998;31:7953–9.
- [67] Schiessel H. Counterion condensation on flexible polyelectrolytes: dependence on ionic strength and chain concentration. *Macromolecules* 1999;32:5673–80.
- [68] Brilliantov NV, Kuznetsov DV, Klein R. Chain collapse and counterion condensation in dilute polyelectrolyte solutions. *Phys Rev Lett* 1998;81:1433–6.
- [69] Limbach HJ, Holm C. End effects of strongly charged polyelectrolytes: a molecular dynamics study. *J Chem Phys* 2001;114:9674–82.
- [70] Stevens MJ, Kremer K. The nature of flexible linear polyelectrolytes in salt-free solution—a molecular-dynamics study. *J Chem Phys* 1995;103:1669–90.
- [71] Micka U, Holm C, Kremer K. Strongly charged, flexible polyelectrolytes in poor solvents: molecular dynamics simulations. *Langmuir* 1999;15:4033–44.
- [72] Micka U, Kremer K. Strongly charged flexible polyelectrolytes in poor solvents—from stable spheres to necklace chains. *Europhys Lett* 2000;49:189–95.
- [73] Dobrynin AV. In: Kotlyanskiy M, Theodorou DN, editors. *Simulation methods for polymers*. New York: Marcel Dekker; 2004. p. 259–312.

- [74] Winkler RG, Gold M, Reineker P. Collapse of polyelectrolyte macromolecules by counterion condensation and ion pair formation: a molecular dynamics simulation study. *Phys Rev Lett* 1998;80:3731–4.
- [75] Limbach HJ, Holm C. Conformational properties of poor solvent polyelectrolytes. *Comput Phys Commun* 2002;147:321–4.
- [76] Ulrich S, Laguecir A, Stoll S. Titration of hydrophobic polyelectrolytes using Monte Carlo simulations. *J Chem Phys* 2005;122:0949111–0949119.
- [77] Odijk T. Polyelectrolytes near the rod limit. *J Polym Phys Part B Polym Phys* 1977;15:477–83.
- [78] Skolnick J, Fixman M. Electrostatic persistence length of a wormlike polyelectrolyte. *Macromolecules* 1977;10:944–8.
- [79] Odijk T. Possible scaling relations for semidilute polyelectrolyte solutions. *Macromolecules* 1979;12:658–93.
- [80] Netz RR, Orland H. Variational theory for a single polyelectrolyte chain. *Eur Phys J B* 1999;8:81–98.
- [81] Ha BY, Thirumalai D. Persistence length of flexible polyelectrolyte chains. *J Chem Phys* 1999;110:7533–41.
- [82] Manghi M, Netz RR. Variational theory for a single polyelectrolyte chain revisited. *Eur Phys J E* 2004;14:67–77.
- [83] Li H, Witten TA. Fluctuations and persistence length of charged flexible polymers. *Macromolecules* 1995;28:5921–7.
- [84] Liverpool TB, Stapper M. The scaling behaviour of screened polyelectrolytes. *Europhys Lett* 1997;40:485–90.
- [85] Schmidt M. Numerical evaluation of the electrostatic persistence length of polyelectrolytes. *Macromolecules* 1991;24:5361–4.
- [86] Barrat JL, Joanny J-F. Persistence length of polyelectrolyte chains. *Europhys Lett* 1993;24:333–9.
- [87] Ha BY, Thirumalai D. Electrostatic persistence length of a polyelectrolyte chain. *Macromolecules* 1995;28:577–81.
- [88] Edwards SF, Singh P. Size of polymer molecule in solution. *J Chem Soc Faraday Trans II* 1979;75:1001–19.
- [89] Muthukumar M. Double screening in polyelectrolyte solutions: limiting laws and crossover formulas. *J Chem Phys* 1996;105:5183–99.
- [90] Ghosh K, Carri GA, Muthukumar M. Configurational properties of a single semiflexible polyelectrolyte. *J Chem Phys* 2001;115:4367–75.
- [91] Bratko D, Dawson KA. A mean field approach to the structure of polyelectrolytes. *J Chem Phys* 1993;99:5352–64.
- [92] Reed CE, Reed WF. Monte-Carlo electrostatic persistence length compared with experiment and theory. *J Chem Phys* 1991;94:8479–86.
- [93] Seidel C. Polyelectrolyte simulation. *Ber Bunsen Ges Phys Chem Chem Phys* 1996;100:757–63.
- [94] Schafer H, Seidel C. Structure of polyelectrolytes in solutions. A Monte Carlo study. *Macromolecules* 1997;30:6658–61.
- [95] Ullner M, Jonsson B, Peterson C, Sommelius O, Soderberg B. The electrostatic persistence length calculated from Monte Carlo, variational and perturbation methods. *J Chem Phys* 1997;107:1279–87.
- [96] Micka U, Kremer K. The persistence length of polyelectrolyte chains. *J Phys Condens Matter* 1996;8:9463–70.
- [97] Micka U, Kremer K. Persistence length of the Debye-Huckel model of weakly charged flexible polyelectrolyte chains. *Phys Rev E* 1996;54:2653–62.
- [98] Tricot M. Comparison of experimental and theoretical persistence length of some polyelectrolytes at various ionic strengths. *Macromolecules* 1984;17:1698–703.
- [99] Reed CE, Reed WF. Monte-Carlo study of light-scattering by linear polyelectrolytes. *J Chem Phys* 1992;97:7766–76.
- [100] Forster S, Schmidt M, Antonietti M. Experimental and theoretical investigation of the electrostatic persistence length of flexible polyelectrolytes at various ionic strengths. *J Phys Chem* 1992;96:4008–14.
- [101] de Nooy AEJ, Besemer AC, van Bekkum H, van Dijk J, Smit JAM. TEMPO-mediated oxidation of pullulan and influence of ionic strength and linear charge density on the dimensions of the obtained polyelectrolyte chain. *Macromolecules* 1996;29:6541–7.
- [102] Nishida K, Urakawa H, Kaji K, Gabrys B, Higgins JS. Electrostatic persistence length of NaPSS polyelectrolytes determined by a zero average contrast SANS technique. *Polymer* 1997;38:6083–5.
- [103] Tanahatooe JJ. Dynamic light scattering of flexible highly charged polyelectrolytes at infinite dilution. *J Phys Chem B* 1997;101:10442–5.
- [104] Beer M, Schmidt M, Muthukumar M. The electrostatic expansion of linear polyelectrolytes: effect of gegenions, co-ions, and hydrophobicity. *Macromolecules* 1997;30:8375–85.
- [105] Nguyen TT, Shklovskii BI. Persistence length of a polyelectrolyte in salty water: Monte Carlo study. *Phys Rev E* 2002;66.
- [106] Everaers R, Milchev A, Yamakov V. The electrostatic persistence length of polymers beyond the OSF limit. *Eur Phys J E* 2002;8:3–14.
- [107] Ullner M, Woodward CE. Orientational correlation function and persistence lengths of flexible polyelectrolytes. *Macromolecules* 2002;35:1437–45.
- [108] Bordi F, Cametti C, Tan JS, Boris DC, Krause WE, Plucktaevesak N, et al. Determination of polyelectrolyte charge and interaction with water using dielectric spectroscopy. *Macromolecules* 2002;35:7031–8.
- [109] Bordi F, Colby RH, Cametti C, De Lorenzo L, Gili T. Electrical conductivity of polyelectrolyte solutions in the semidilute and concentrated regime: the role of counterion condensation. *J Phys Chem B* 2002;106:6887–93.
- [110] Pfeuty P. Conformation des polyelectrolytes ordre dans les solutions de polyelectrolytes. *J Phys France Coll* 1978;39:C2-149.
- [111] Rubinstein M, Colby RH, Dobrynin AV. Dynamics of semidilute polyelectrolyte solutions. *Phys Rev Lett* 1994;73:2776–9.
- [112] Drifford M, Dalbiez JP. Light scattering by dilute solutions of salt-free polyelectrolytes. *J Phys Chem* 1984;88:5368.
- [113] Nierlich M, Williams CE, Boue F, Cotton JP, Daoud M, Farnoux B, et al. Small angle neutron scattering by semidilute solutions of polyelectrolytes. *J Phys (Paris)* 1979;40:701.

- [114] Nierlich M, Boue F, Lapp A. Radius of gyration of a polyion in salt free polyelectrolyte solutions measured by SANS. *J Phys (Paris)* 1985;46:649–58.
- [115] Kakehashi R, Yamazoe H, Maeda H. Osmotic coefficients of vinylic polyelectrolyte solutions without added salt. *Colloid Polym Sci* 1998;276:28–33.
- [116] Kakehashi R, Maeda H. Donnan equilibria of simple electrolytes in polyelectrolyte solutions. *J Chem Soc Faraday Trans* 1996;92:3117–21.
- [117] Kakehashi R, Maeda H. Donnan equilibria of simple electrolytes in polyelectrolyte solutions. 2. Extension to polycations and the effect of charge densities. *J Chem Soc Faraday Trans* 1996;92:4441–4.
- [118] Raspaud E, de Conceicao M, Livolant F. Do free DNA counterions control the osmotic pressure? *Phys Rev Lett* 2000;84:2533–6.
- [119] Hansen PL, Podgornik R, Parsegian AV. Osmotic properties of DNA: critical evaluation of counterion condensation theory. *Phys Rev E* 1997;64:0219071–0219074.
- [120] Reddy M, Marinsky JA. A further investigation of the osmotic properties of hydrogen and sodium polystyrenesulfonate. *J Phys Chem* 1970;74:3884–91.
- [121] Wang L, Bloomfield VA. Osmotic pressure of polyelectrolytes with added salt. *Macromolecules* 1990;23:804–9.
- [122] Koene RS, Nicolai T, Mandel M. Scaling relations for aqueous polyelectrolyte-salt solutions. 3. Osmotic pressure as a function of molar mass and ionic strength in the semidilute regime. *Macromolecules* 1983;16:231–7.
- [123] Takahashi A, Kato N, Nagasawa M. The osmotic pressure of polyelectrolyte in neutral salt solutions. *J Phys Chem* 1970;74:944.
- [124] Kavassalis TA, Noolandi J. New view of entanglements in dense polymer systems. *Phys Rev Lett* 1987;59:2674–7.
- [125] Kavassalis TA, Noolandi J. A new theory of entanglements and dynamics in dense polymer systems. *Macromolecules* 1988;21:2869–79.
- [126] Kavassalis TA, Noolandi J. Entanglement scaling in polymer melts and solutions. *Macromolecules* 1989;22:2709–20.
- [127] Boris DC, Colby RH. Rheology of sulfonated polystyrene solutions. *Macromolecules* 1998;31:5746–55.
- [128] Oostwal MG, Blees MH, de Bleijser J, Leyte JC. Chain self-diffusion in aqueous salt-free solutions of sodium poly(styrenesulfonate). *Macromolecules* 1993;26:7300–8.
- [129] Oostwal MG, Odijk T. Novel dynamic scaling hypothesis for semidilute and concentrated solutions of polymers and polyelectrolytes. *Macromolecules* 1993;26:6489–97.
- [130] Dobrynin AV, Rubinstein M. Hydrophobic polyelectrolytes. *Macromolecules* 1999;32:915–22.
- [131] Essafi W. PhD Thesis, Paris; 1996.
- [132] Spiteri MN, Boue F, Lapp A, Cotton JP. Persistence length for a PSSNa polyion in semidilute solution as a function of the ionic strength. *Phys Rev Lett* 1996;77:5218–20.
- [133] Spiteri MN, Boue F, Lapp A, Cotton JP. Polyelectrolyte persistence length in semidilute solution as a function of the ionic strength. *Physica B* 1997;234:303–5.
- [134] Heitz C, Rawiso M, Francois J. X-ray scattering study of a poly(methacrylic acid) sample as a function of its neutralization degree. *Polymer* 1999;40:1637–50.
- [135] Waigh TA, Ober R, Williams CE, Galin JC. Semidilute and concentrated solutions of a solvophobic polyelectrolyte in nonaqueous solvents. *Macromolecules* 2001;34:1973–80.
- [136] Qu D, Baigl D, Williams CE, Mohwald H, Fery A. Dependence of structural forces in polyelectrolyte solutions on charge density: a combined AFM/SAXS study. *Macromolecules* 2003;36:6878–83.
- [137] Baigl D, Ober R, Qu D, Fery A, Williams CE. Correlation length of hydrophobic polyelectrolyte solutions. *Europhys Lett* 2003;62:588–94.
- [138] Aseyev VO, Klenin SI, Tenhu H, Grillo I, Geissler E. Neutron scattering studies of the structure of a polyelectrolyte globule in a water-acetone mixture. *Macromolecules* 2001;34:3706–9.
- [139] Lee MJ, Green MM, Mikes F, Morawetz H. NMR spectra of polyelectrolytes in poor solvents are consistent with the pearl necklace model of the chain molecules. *Macromolecules* 2002;35:4216–7.
- [140] Kiriya A, Gorodyska G, Minko S, Jaeger W, Stepanek P, Stamm M. Cascade of coil-globule conformational transitions of single flexible polyelectrolyte molecules in poor solvent. *J Am Chem Soc* 2002;124:13454–62.
- [141] Minko S, Kiriya A, Gorodyska G, Stamm M. Single flexible hydrophobic polyelectrolyte molecules adsorbed on solid substrate: transition between a stretched chain, necklace-like conformation and a globule. *J Am Chem Soc* 2002;124:3218–9.
- [142] Liao Q, Dobrynin AV, Rubinstein M. Molecular dynamics simulations of polyelectrolytes in poor solvent. Submitted for publication.
- [143] Khokhlov AR, Nyrkova IA. Compatibility enhancement and microdomain structuring in weakly charged polyelectrolyte mixtures. *Macromolecules* 1992;25:1493–502.
- [144] Muthukumar M. Phase diagram of polyelectrolyte solutions: weak polymer effect. *Macromolecules* 2002;35:9142–5.
- [145] Borue VY, Erukhimovich IY. A statistical theory of weakly charged polyelectrolytes: fluctuations, equation of state, and microphase separation. *Macromolecules* 1988;21:3240–9.
- [146] Vilgis TA, Borsali R. Mean-field theory of concentrated polyelectrolyte solutions. *Phys Rev A* 1991;43:6857–73.
- [147] Mahdi KK, Olvera de la Cruz M. Phase diagrams of salt-free polyelectrolyte semidilute solutions. *Macromolecules* 2000;33:7649–54.
- [148] Ermoshkin AV, Olvera de la Cruz M. Polyelectrolytes in the presence of multivalent ions: gelation versus segregation. *Phys Rev Lett* 2003;90.
- [149] Orkoulas G, Kumar SK, Panagiotopoulos AZ. Monte Carlo study of coulombic criticality in polyelectrolytes. *Phys Rev Lett* 2003;90:048303.
- [150] Volk N, Vollmer D, Schmidt M, Oppermann W, Huber K. Conformation and phase diagrams of flexible polyelectrolytes 2004.

- [151] Joanny J-F, Leibler L. Weakly charged polyelectrolytes in a poor solvent. *J Phys* 1990;51:545–57.
- [152] Braun O, Boue F, Candau F. Microphase separation in weakly charged hydrophobic polyelectrolytes. *Eur Phys J E* 2002;7:141–51.
- [153] Dormidontova EE, Erukhimovich IY, Khokhlov AR. Microphase separation in poor-solvent polyelectrolyte solutions—phase-diagram. *Macromol Theory Simul* 1994; 3:661–75.
- [154] Chang RW, Yethiraj A. Strongly charged flexible polyelectrolytes in poor solvents: molecular dynamics simulations with explicit solvent. *J Chem Phys* 2003;118:6634–47.
- [155] Yethiraj A. Conformational properties and static structure factor of polyelectrolyte solutions. *Phys Rev Lett* 1997;78: 3789–92.
- [156] Yethiraj A. Theory for chain conformations and static structure of dilute and semidilute polyelectrolyte solutions. *J Chem Phys* 1998;108:1184–92.
- [157] Yethiraj A, Shew CY. Structure of polyelectrolyte solutions. *Phys Rev Lett* 1996;77:3937–40.
- [158] Schweizer KS, Curro JG. PRISM theory of the structure, thermodynamics, and phase transitions of polymer liquids and alloys. *Adv Polym Sci* 1994;116:319–77.
- [159] Laria D, Wu D, Chandler D. Reference interaction site model polaron theory of the hydrated electron. *J Chem Phys* 1991; 95:4444–53.
- [160] Zherenkova LV, Kriksin YA, Talitskikh SK, Khalatur PG. Application of the integral equation theory to rodlike polyelectrolytes in a poor solvent. *Polym Sci Ser A* 2002; 44:791–9.
- [161] Hofmann T, Winkler RG, Reineker P. Integral equation theory approach to rodlike polyelectrolytes: counterion condensation. *J Chem Phys* 2001;114:10181–8.
- [162] Hofmann T, Winkler RG, Reineker P. Influence of salt on the structure of polyelectrolyte solutions: an integral equation theory approach. *J Chem Phys* 2003;119:2406–13.
- [163] Shew CY, Yethiraj A. Self-consistent integral equation theory for semiflexible chain polyelectrolyte solutions. *J Chem Phys* 2000;113:8841–7.
- [164] Shew CY, Yethiraj A. Integral equation theory for the structure of DNA solutions. *J Chem Phys* 2002;116:5308–14.
- [165] Zherenkova L, Khalatur P, Yoshikawa K. Self-consistent integral equation theory for semiflexible polyelectrolytes in poor solvent. *Macromol Theory Simul* 2003;12:339–53.
- [166] Hofmann T, Winkler RG, Reineker P. Self-consistent integral equation theory for solutions of finite extensible semiflexible polyelectrolyte chains. *J Chem Phys* 2003;118: 6624–33.
- [167] Muthukumar M. Double screening in polyelectrolyte solutions: limiting laws and crossover formulas. *J Chem Phys* 1996;105:5183–99.
- [168] Wang Q, Taniguchi T, Fredrickson GH. Self-consistent field theory of polyelectrolyte systems. *J Phys Chem B* 2004;108: 6733–44.
- [169] Kawaguchi M, Takahashi A. Polymer adsorption at solid liquid interfaces. *Adv Colloid Interface Sci* 1992;37: 219–317.
- [170] Flerer GJ, Cohen Stuart MA, Scheutjens JM, Gasgove T, Vincent B. *Polymer at interfaces*. London: Chapman and Hall; 1993.
- [171] Bajpai AK. Interface behaviour of ionic polymers. *Prog Polym Sci* 1997;22:523–64.
- [172] Lyklema J. *Fundamentals of interface and colloid science: solid-liquid interfaces*. London: Academic Press; 1995.
- [173] Netz RR, Andelman D. Neutral and charged polymers at interfaces. *Phys Rep Rev Sect Phys Lett* 2003;380:1–95.
- [174] Wiegand FW. Adsorption of a macromolecule to a charged surface. *J Phys Condens Matter* 1977;10:299.
- [175] Wiegand FW. In: *Phase transition and critical phenomena VII*. New York: Academic; 1983.
- [176] Odijk T. Binding of long flexible chain to a rod-like macromolecule. *Macromolecules* 1980;13:1542–6.
- [177] Muthukumar M. Adsorption of a polyelectrolyte chain to a charged surface. *J Chem Phys* 1987;86:7230–5.
- [178] Muthukumar M. Pattern-recognition by polyelectrolytes. *J Chem Phys* 1995;103:4723–31.
- [179] Kong CY, Muthukumar M. Monte Carlo study of adsorption of a polyelectrolyte onto charged surfaces. *J Chem Phys* 1998;109:1522–7.
- [180] Ellis M, Kong CY, Muthukumar M. Polyelectrolyte adsorption on heterogeneously charged surfaces. *J Chem Phys* 2000;112:8723–9.
- [181] Borisov OV, Zhulina EB, Birshtein TM. Polyelectrolyte molecule conformation near charged surface. *J Phys II* 1994; 4:913–29.
- [182] Yamakov V, Milchev A, Borisov O, Dunweg B. Adsorption of a polyelectrolyte chain on a charged surface: a Monte Carlo simulation of sealing behavior. *J Phys Condens Matter* 1999;11:9907–23.
- [183] Beltran S, Hooper H, Blanch H, Prausnitz J. Monte Carlo study of polyelectrolyte adsorption—isolated chains on a planar charged surface. *Macromolecules* 1991;24: 3178–84.
- [184] Hove CA. Theory of polymer adsorption at interfaces. *J Polym Sci* 1971;C34:1–10.
- [185] Hove CA. The general theory of polymer adsorption at a surface. *J Polym Sci* 1970;C30:361–7.
- [186] Hesselink FTH. On the theory of polyelectrolyte adsorption. The effect of adsorption behavior of the electrostatic contribution to the adsorption free energy. *J Colloid Interface Sci* 1977;60:448–66.
- [187] Scheutjens JM, Flerer GJ. Statistical theory of the adsorption of interacting chain molecules. 1. Partition function, segment density distribution, and adsorption isotherm. *J Phys Chem* 1979;83:1619–35.
- [188] Scheutjens JM, Flerer GJ. Statistical theory of the adsorption of interacting chain molecules. 2. Train, loop, and tail size distribution. *J Phys Chem* 1980;84:178–90.
- [189] van der Schee HA, Lyklema J. Lattice theory of polyelectrolyte adsorption. *J Phys Chem* 1984;88:6661–72.
- [190] Evers O, Flerer GJ, Scheutjens JM, Lyklema J. Adsorption of weak polyelectrolytes from aqueous solution. *J Colloid Interface Sci* 1986;111:446–54.

- [191] Bohmer MR, Evers O, Scheutjens JMH. Weak polyelectrolytes between two surfaces—adsorption and stabilization. *Macromolecules* 1990;23:2288–301.
- [192] Vermeer AWP, Leermakers FAM, Koopal LK. Adsorption of weak polyelectrolytes on surfaces with a variable charge. Self-consistent-field calculations. *Langmuir* 1997;13:4413–21.
- [193] Dahlgren MA, Leermakers FAM. Depletion zones in polyelectrolyte systems—polydispersity effects and colloidal stability. *Langmuir* 1995;11:2996–3006.
- [194] Varoqui R, Johnner A, Elaissari A. Conformation of weakly charged polyelectrolyte at a liquid solid interface. *J Chem Phys* 1991;94:6873–8.
- [195] Varoqui R. Structure of weakly charged polyelectrolyte at a solid-liquid interface. *J Phys II* 1993;3:1097–108.
- [196] Varoqui R. Structure and stability of weakly charged polyelectrolyte at a solid-liquid interface In: Macro-ion characterization, ACS symposium series. vol. 548 1994 p. 421–35.
- [197] Borukhov I, Andelman D, Orland H. Scaling laws of polyelectrolyte adsorption. *Macromolecules* 1998;31:1665–71.
- [198] Chatellier X, Joanny JF. Adsorption of polyelectrolyte solutions on surfaces: a Debye-Huckel theory. *J Phys II* 1996;6:1669–86.
- [199] Borukhov I, Andelman D, Orland H. Polyelectrolyte solutions between charged surfaces. *Europhys Lett* 1995;32:499–504.
- [200] Borukhov I, Andelman D, Orland H. Effect of polyelectrolyte adsorption on intercolloidal forces. *J Phys Chem B* 1999;103:5042–57.
- [201] Borukhov I. Adsorption of polyelectrolytes and intercolloidal forces. *Physica A* 1998;249:315–20.
- [202] Yethiraj A. Forces between surfaces immersed in polyelectrolyte solutions. *J Chem Phys* 1999;111:1797–800.
- [203] Carignano MA, Dan N. Density inhomogeneities of highly charged polyelectrolyte solutions confined between uncharged and nonadsorbing walls. *Langmuir* 1998;14:3475–8.
- [204] Barford W, Ball R, Nex CM. A nonequilibrium configuration theory of polyelectrolyte adsorption. *J Chem Soc Faraday Trans I* 1986;82:3233–44.
- [205] Barford W, Ball R. Towards a complete configurational theory of nonequilibrium polymer adsorption. *J Chem Soc Faraday Trans I* 1987;83:2515–23.
- [206] Stuart MAC, Hoogendam CW, deKeizer A. Kinetics of polyelectrolyte adsorption. *J Phys Condens Matter* 1997;9:7767–83.
- [207] Netz RR, Joanny JF. Adsorption of semiflexible polyelectrolytes on charged planar surfaces: charge compensation, charge reversal, and multilayer formation. *Macromolecules* 1999;32:9013–25.
- [208] Dobrynin AV, Deshkovski A, Rubinstein M. Adsorption of polyelectrolytes at an oppositely charged surface. *Phys Rev Lett* 2000;84:3101–4.
- [209] Dobrynin AV, Deshkovski A, Rubinstein M. Adsorption of polyelectrolytes at oppositely charged surfaces. *Macromolecules* 2001;34:3421–36.
- [210] Dobrynin AV. Effect of solvent quality on polyelectrolyte adsorption at an oppositely charged surface. *J Chem Phys* 2001;114:8145–53.
- [211] Dobrynin AV, Rubinstein M. Adsorption of hydrophobic polyelectrolytes at oppositely charged surfaces. *Macromolecules* 2002;35:2754–68.
- [212] Dobrynin AV, Rubinstein M. Effect of short-range interactions on polyelectrolyte adsorption at charged surfaces. *J Phys Chem B* 2003;107:8260–9.
- [213] Nguyen TT, Grosberg AY, Shklovskii BI. Screening of a charged particle by multivalent counterions in salty water: strong charge inversion. *J Chem Phys* 2000;113:1110–25.
- [214] Nguyen TT, Grosberg AY, Shklovskii BI. Macroions in salty water with multivalent ions: giant inversion of charge. *Phys Rev Lett* 2000;85:1568–71.
- [215] Joanny JF. Polyelectrolyte adsorption and charge inversion. *Eur Phys J B* 1999;9:117–22.
- [216] Joanny JF, Castelnovo M, Netz R. Adsorption of charged polymers. *J Phys Condens Matter* 2000;12:A1–A7.
- [217] Borisov OV, Hakem F, Vilgis TA, Joanny JF, Johnner A. Adsorption of hydrophobic polyelectrolytes onto oppositely charged surfaces. *Eur Phys J E* 2001;6:37–47.
- [218] Shklovskii BI. Wigner crystal model of counterion induced bundle formation of rodlike polyelectrolytes. *Phys Rev Lett* 1999;82:3268–71.
- [219] Shklovskii BI. Screening of a macroion by multivalent ions: correlation-induced inversion of charge. *Phys Rev E* 1999;60:5802–11.
- [220] Rouzina I, Bloomfield VA. Competitive electrostatic binding of charged ligands to polyelectrolytes: planar and cylindrical geometries. *J Phys Chem* 1996;100:4292–304.
- [221] Netz RR. Electrostatics of counter-ions at and between planar charged walls: from Poisson-Boltzmann to the strong-coupling theory. *Eur Phys J E* 2001;5:557–74.
- [222] Safran S. *Statistical thermodynamics of surfaces, interfaces and membranes*. Reading, MA: Addison-Wesley; 1994.
- [223] Netz RR. Debye-Huckel theory for interfacial geometries. *Phys Rev E* 1999;60:3174–82.
- [224] Messina R. Effect of image forces on polyelectrolyte adsorption. *Phys Rev E* 2004;70:0518021–0518029.
- [225] Cheng C-H, Lai P-Y. Adsorption transition of a polyelectrolyte on a high-dielectric charge substrate. *Phys Rev E* 2004;70:0618051–0618054.
- [226] Durand G, Lafuma F, Audebert R. Adsorption of cationic polyelectrolytes at clay-colloid interface in dilute aqueous suspensions—effect of the ionic strength of the medium. *Prog Colloid Polym Sci* 1988;266:278–82.
- [227] Hendrickson E, Neuman RD. Polyacrylamide adsorption from very dilute solutions. *J Colloid Interface Sci* 1986;110:243–51.
- [228] Pelton RH. Electrolyte effects in the adsorption and desorption of a cationic polyacrylamide on cellulose fibers. *J Colloid Interface Sci* 1986;111:475–85.

- [229] Durand-Piana G, Lafuma F, Audebert R. Flocculation and adsorption properties of cationic polyelectrolytes toward Namtomorillonite dilute suspensions. *J Colloid Interface Sci* 1987;119:474–80.
- [230] Wang TK, Audebert R. Adsorption of cationic copolymers of acrylamide at the silica water interface—hydrodynamic layer thickness measurements. *J Colloid Interface Sci* 1988;121:32–41.
- [231] Davies RJ, Dix LR, Toprakcioglu C. Adsorption of poly-L-lysine to mica powder. *J Colloid Interface Sci* 1989;129:145–52.
- [232] Shubin V, Linse P. Effect of electrolytes on adsorption of cationic polyacrylamide on silica—ellipsometric study and theoretical modeling. *J Phys Chem* 1995;99:1285–91.
- [233] Kawaguchi M, Kawaguchi H, Takahashi A. Competitive and displacement adsorption of polyelectrolyte and water-soluble nonionic polymer at the silica surface. *J Colloid Interface Sci* 1988;124:57–62.
- [234] Bonekamp, BC. PhD thesis, Wageningen Agricultural University, The Netherlands; 1984.
- [235] Marra J, van der Schee HA, Fleer GJ, Lyklema J. In: Ottewill R, Rochester CH, Smith AL, editors. *Adsorption in solutions*. London: Academic Press; 1983. p. 245.
- [236] Solis FJ, Olvera de la Cruz M. Surface-induced layer formation in polyelectrolytes. *J Chem Phys* 1999;110:11517–22.
- [237] Castelnuovo M, Joanny J-F. Formation of polyelectrolyte multilayers. *Langmuir* 2000;16:7524–32.
- [238] Messina R, Holm C, Kremer K. Polyelectrolyte adsorption and multilayering on charged colloidal particles. *J Polym Sci Part B Polym Phys* 2004;42:3557–70.
- [239] Panchagnula V, Jeon J, Dobrynin AV. Molecular dynamics simulations of electrostatic layer-by-layer self-assembly. *Phys Rev Lett* 2004;93:037801-1.
- [240] Park SY, Barrett CJ, Rubner MF, Mayes AM. Anomalous adsorption of polyelectrolyte layers. *Macromolecules* 2001;34:3384–8.
- [241] Lefaux CJ, Zimmerlin JA, Dobrynin AV, Mather PT. Polyelectrolyte spin assembly: influence of ionic strength on the growth of multilayered thin films. *J Polym Sci Part B Polym Phys* 2004;42:3654–66.
- [242] Muthukumar M. Theory of viscoelastic properties of polyelectrolyte solutions. *Polymer* 2001;42:5921–3.
- [243] Muthukumar M. Dynamics of polyelectrolyte solutions. *J Chem Phys* 1997;107:2619–35.
- [244] Sedlak M. Dynamic light scattering from binary mixtures of polyelectrolytes. I. Influence of mixing on the fast and slow polyelectrolyte mode behavior. *J Chem Phys* 1997;107:10799–804.
- [245] Sedlak M. Dynamic light scattering from binary mixtures of polyelectrolytes. II. Appearance of the medium polyelectrolyte mode upon mixing and comparison with experiments on binary mixtures of neutral polymers. *J Chem Phys* 1997;107:10805–15.
- [246] Sedlak M. Mechanical properties and stability of macroion domains in polyelectrolyte solutions. *J Chem Phys* 2002;116:5236–45.
- [247] Sedlak M. Long-time stability of multimacroion domains in polyelectrolyte solutions. *J Chem Phys* 2002;116:5246–55.
- [248] Sehgal A, Seery TAP. The ordinary-extraordinary transition revisited: a model polyelectrolyte in a highly polar organic solvent. *Macromolecules* 1998;31:7340–6.
- [249] Kotz J, Kosmella S, Beitz T. Self-assembled polyelectrolyte systems. *Prog Polym Sci* 2001;26:1199–232.
- [250] Huang CI, Olvera de la Cruz M. Polyelectrolytes in multivalent salt solutions: monomolecular versus multimolecular aggregation. *Macromolecules* 2002;35:976–86.
- [251] Dubois E, Boue F. Conformation of poly(styrenesulfonate) polyions in the presence of multivalent ions: small-angle neutron scattering experiments. *Macromolecules* 2001;34:3684–97.
- [252] Solis FJ, Olvera de la Cruz M. Flexible linear polyelectrolytes in multivalent salt solutions: solubility conditions. *Eur Phys J E* 2001;4:143–52.
- [253] Potemkin II, Vasilevskaya VV, Khokhlov AR. Associating polyelectrolytes: finite size cluster stabilization versus physical gel formation. *J Chem Phys* 1999;111:2809–17.
- [254] Bloomfield VA. DNA condensation by multivalent cations. *Biopolymers* 1997;44:269–82.
- [255] Rouzina I, Bloomfield VA. Macroion attraction due to electrostatic correlation between screening counterions. 1. Mobile surface-adsorbed ions and diffuse ion cloud. *J Phys Chem* 1996;100:9977–89.
- [256] Levin Y. Electrostatic correlations: from plasma to biology. *Rep Prog Phys* 2002;65:1577–632.
- [257] Dobrynin AV, Colby RH, Rubinstein M. Polyampholytes. *J Polym Sci Part B Polym Phys* 2004;42:3513–38.
- [258] Qiu Y, Park K. Environment-sensitive hydrogels for drug delivery. *Adv Drug Deliv Rev* 2001;53:321–39.
- [259] Elliott GF, Hodson SA. Cornea, and the swelling of polyelectrolyte gels of biological interest. *Rep Prog Phys* 1998;61:1325–65.
- [260] Ruhe J, Ballauff M, Biesalski M, Dziezok P, Grohn F, Johannsmann D, et al. Polyelectrolyte brushes. *Adv Polym Sci* 2004;165:79–150.